



**HAL**  
open science

# Eco-design of a dry cleaning machine by integration of a pervaporation stage for solvent dehydration

Oleksandr Dimitrov

► **To cite this version:**

Oleksandr Dimitrov. Eco-design of a dry cleaning machine by integration of a pervaporation stage for solvent dehydration. Fluids mechanics [physics.class-ph]. Ecole Centrale Marseille, 2019. English. NNT : 2019ECDM0012 . tel-03081132

**HAL Id: tel-03081132**

**<https://theses.hal.science/tel-03081132v1>**

Submitted on 18 Dec 2020

**HAL** is a multi-disciplinary open access archive for the deposit and dissemination of scientific research documents, whether they are published or not. The documents may come from teaching and research institutions in France or abroad, or from public or private research centers.

L'archive ouverte pluridisciplinaire **HAL**, est destinée au dépôt et à la diffusion de documents scientifiques de niveau recherche, publiés ou non, émanant des établissements d'enseignement et de recherche français ou étrangers, des laboratoires publics ou privés.



# ÉCOLE CENTRALE DE MARSEILLE

École doctorale n° 353: *Sciences pour l'Ingénieur: Mécanique, Physique, Micro et Nanoélectronique*

Laboratoire de Mécanique, Modélisation et Procédés Propres M2P2 UMR 7340

THÈSE DE DOCTORAT

présentée par

**OLEKSANDR DIMITROV**

soutenance prévue le 17 décembre 2019

pour obtenir le grade de docteur de l'ECM

discipline: Mécanique et Physique des Fluides

## **Eco-design of a Dry Cleaning Machine by Integration of a Pervaporation Stage for Solvent Dehydration**

*Thèse dirigée par:*

Mme Pierrette GUICHARDON

PR ECM, Marseille

Directrice de thèse

*Membres du jury:*

M Denis ROIZARD

DR CNRS, LRGP, Nancy

Rapporteur

M Boris KOSOY

PR ONAFT, Odessa

Rapporteur

Mme Ilham MOKBEL

MCF, Univ Lyon 1, Lyon

Examinatrice

Mme Isabelle RASPO

CR CNRS, M2P2, Marseille

Examinatrice

M Sylvain MARC

PhD, Arcane Ind, Gémenos

Examinateur

Mme Pierrette GUICHARDON

PR ECM, Marseille

Directrice de thèse

Mme Evelyne NEAU

PR EM, Aix-Marseille Univ, Marseille

Invitée

M Olivier BAUDOUIN

Ingénieur, PROSIM, Labège

Invité

M Jacques JOSE

PR EM, Univ Lyon 1, Lyon

Invité

M Alfred TESTA

Dirigéant, Innovaclean, Gémenos

Invité



*Oleksandr DIMITROV*

ECO-DESIGN OF A DRY CLEANING  
MACHINE BY INTEGRATION OF  
PERVAPORATION STAGE FOR  
SOLVENT DEHYDRATION

PHD THESIS

*École Centrale de Marseille, 2019*

*“... There is enough to enable everyone to have a very high standard of living with the intelligent use of technology, resources and technical personnel. When we say the use of technology, we mean technology that is not harmful to people or the environment and doesn't waste time and energy ...”*

---

JACQUE FRESCO

# ABSTRACT AND KEYWORDS

THE present Thesis covers the eco-design of a dry cleaning machine by integration of a pervaporation stage for dehydration of the ARCACLEAN solvent. This solvent was developed in order to favorably replace the perchloroethylene for the reasons of toxicity. After multiple washing cycles, the solvent is charged on dirt but also on water. When the water content in solvent becomes high (about 10%wt), the solvent becomes aggressive towards the textile and should be then imperatively dehydrated. The current dry cleaning machines are equipped with a simple batch distillation which remains a process of high energy consumption. Moreover, in our case, this distillation does not offer an excellent separation quality. In this context, INNOVACLEAN company is interested in performing the dehydration by means of an alternative process which will be able to demonstrate both high energy efficiency and excellent separation quality, being at the same time environmentally friendly. After consideration of different possibilities (such as extractive distillation, adsorption, reverse osmosis, forward osmosis), the pervaporation was chosen due to its advantages compared to distillation, such as: low energy consumption, low operational cost, high separation efficiency and a high compactness.

Firstly, we have carried out an in-depth thermodynamic study of the vapor-liquid equilibria as any data relative to ARCACLEAN solvent components were published in literature. In addition to the vapor pressure measurements of pure compounds, binary and quaternary solutions, we have developed a thermodynamic model. This model allowed to clearly understand the occurred phase equilibria and to observe the non-ideality of our solvent charged in water. To do that, the activity coefficients, varying from 1.6 to 2.1, were estimated.

Furthermore, we have demonstrated that the pervaporation offers highly favorable conditions for our solvent dehydration. Using the PERVAP4510, a poly(vinyl)alcohol cross-linked membrane, manufactured by Sultzer, we have obtained a perfect selectivity with a permeate containing only pure water. The permeate flux, measured as a function of temperature and feed water content, was in agreement with that of literature, ranging from 0.85 to 0.95 kg/(m<sup>2</sup>h) (at 10%wt and 70°C). The interpretation of the obtained results using the solution-

diffusion model has shown that the water permeance is independent of temperature but decreases when the water content in feed becomes low.

Finally, we have performed a design of the pervaporation stage to be integrated into the existing dry cleaning machine. Together with the solvent pre-treatment stage consisting of the filters and activated carbon cartridges, a membrane module having an effective area of 20 to 25 m<sup>2</sup> was chosen for solvent dehydration until 1%wt of water during a cycle of 65 minutes. Also, a heat exchanger having an exchange area of 1.32 m<sup>2</sup> was designed in order to condense the permeate.

**KEYWORDS:** dry cleaning, solvent dehydration, pervaporation, membrane separation, phase equilibria, eco-design

# RÉSUMÉ ET MOTS CLÉS

**L**A présente thèse porte sur l'éco-conception d'une machine de nettoyage à sec par intégration d'une étape de pervaporation pour déshydrater le solvant vert ARCACLEAN qui remplace avantageusement le perchloro-éthylène pour des raisons de toxicité. Après plusieurs cycles de nettoyage, le solvant est chargé en diverses salissures mais aussi en eau. Lorsque la teneur en eau du solvant devient trop grande (aux alentours de 10% massique), le solvant devient agressif vis-à-vis des textiles et il est primordial de le déshydrater. Aux machines de nettoyage actuels est intégrée un distillateur batch qui reste un procédé très énergivore et qui, dans notre cas, n'offre pas une qualité de séparation excellente. Dans ce contexte, la société INNOVACLEAN s'intéresse à réaliser la déshydratation par un procédé alternatif qui démontre une haute efficacité énergétique, ainsi qu'une excellente séparation, tout en étant écologique. Après examen de plusieurs possibilités (distillation extractive, adsorption, osmose inverse, osmose directe), la pervaporation a été choisie en raison de ses avantages par rapport à la distillation qui sont : une faible consommation énergétique, un faible coût opérationnel, une haute efficacité de séparation et une grande compacité.

Tout d'abord, nous avons réalisé une étude thermodynamique approfondie des équilibres liquide-vapeur des phases car aucune donnée n'était disponible dans la littérature. En plus des mesures expérimentales réalisées pour les corps purs, les solutions binaires et ternaires, nous avons développé un modèle thermodynamique. Ce modèle a permis de rendre compte de manière fiable des équilibres liquide-vapeur et de considérer la non-idéalité de notre solvant chargé en eau par l'estimation des coefficients d'activités qui varient suivant les conditions de 1.6 à 2.1.

Ensuite, nous avons montré que la pervaporation offre des conditions favorables à la déshydratation de notre solvant. A l'aide de la membrane PERVAP4510 en polyvinylalcool réticulé du fabricant Sulzer, nous avons obtenu une sélectivité parfaite avec un perméat formé uniquement d'eau. Les flux mesurés en fonction de la température et de la teneur en eau sont en accord avec ceux généralement observés et sont de l'ordre de 0.85 à 0.95 kg/(m<sup>2</sup>·h) (à 10%wt, 70°C). L'interprétation des résultats à l'aide du modèle de solubilisation-



diffusion a montré que la perméance ne varie pas avec la température et diminue lorsque la teneur en eau dans l'alimentation est faible.

Enfin, nous avons réalisé la conception et le dimensionnement de l'étape de pervaporation à intégrer à la machine de nettoyage à sec existante. En plus de l'étape de pré-traitement du solvant par filtres et cartouches de charbons actifs, le module membranaire d'une surface de 20 à 25 m<sup>2</sup> a été choisi pour une déshydratation du solvant jusqu'à 1%wt d'eau durant un cycle de 65 minutes. Aussi, un échangeur de chaleur d'une surface d'échange thermique de 1.32 m<sup>2</sup> a été choisi pour la condensation du perméat.

**MOTS CLÉS:** nettoyage à sec, déshydratation du solvant, pervaporation, séparation membranaire, équilibres de phases, éco-conception

# Contents

<b>ABSTRACT AND KEYWORDS</b>	<b>6</b>
<b>RÉSUMÉ ET MOTS CLÉS</b>	<b>8</b>
<b>NOMENCLATURE</b>	<b>13</b>
<b>LIST OF FIGURES</b>	<b>18</b>
<b>LIST OF TABLES</b>	<b>21</b>
<b>1 Context and problem statement</b>	<b>23</b>
1.1 A brief history of the dry cleaning . . . . .	24
1.2 The ARCACLEAN solvent . . . . .	26
1.3 Motivations and problem statement . . . . .	27
1.3.1 Current regeneration process in ARCAFLEX320 machines . . . . .	28
1.3.2 Issues and limitations of distillation . . . . .	29
1.3.3 Dry cleaning devices without distillers . . . . .	30
1.3.3.1 "IPURA" by ILSA . . . . .	31
1.3.3.2 "NEBULA" by Renzacci . . . . .	31
1.3.3.3 UNISEC . . . . .	32
1.3.4 Other classic dehydration processes . . . . .	33
1.3.4.1 The extractive distillation . . . . .	33
1.3.4.2 The adsorption . . . . .	33
1.3.4.3 Membrane processes . . . . .	34
1.4 Thesis workflow . . . . .	38
<b>2 Thermodynamics of solvents: theoretical and experimental study</b>	<b>39</b>
2.1 Experimental measurements of solvents properties . . . . .	41
2.1.1 Experimental materials and methods . . . . .	41
2.1.1.1 Materials . . . . .	41
2.1.1.2 Working principle of a static apparatus . . . . .	42

2.1.1.3	Treatment of experimental points . . . . .	44
2.1.2	Sample analysis by the gas chromatography . . . . .	45
2.1.2.1	Importance of the quantitative sample analysis . . . . .	45
2.1.2.2	Analysis performing . . . . .	46
2.1.2.3	Peaks identification and calibration . . . . .	46
2.1.3	Experimental measurements workflow . . . . .	50
2.1.3.1	Pure compounds vapor pressure . . . . .	50
2.1.3.2	VLE and VLLE of aqueous binary mixtures . . . . .	52
2.1.3.3	VLE of organic binary mixtures . . . . .	52
2.1.3.4	VLE of the quaternary mixture ARCACLEAN + water . . . . .	53
2.2	Thermodynamic modelling of phase equilibria occurring in H <sub>2</sub> O+ARCACLEAN mixtures . . . . .	54
2.2.1	Pure compounds parameters estimation . . . . .	54
2.2.1.1	Definition of the equation of state parameters . . . . .	54
2.2.1.2	Application of the Peng-Robinson EoS to glycol ethers . . . . .	55
2.2.1.3	Fitting of estimated pure compound properties . . . . .	59
2.2.2	Prediction of low-pressure phase equilibria using the NRTL-PR model . . . . .	66
2.2.2.1	Generalized NRTL model . . . . .	66
2.2.2.2	Generalized reference state at constant volume GRS-CV . . . . .	68
2.2.2.3	Association of the generalized NRTL model with the Peng-Robinson EoS . . . . .	72
2.3	Results and discussion . . . . .	77
2.3.1	VLE of all binary mixtures . . . . .	77
2.3.2	VLE of the quaternary mixtures . . . . .	82
2.4	Chapter conclusion . . . . .	83
<b>3</b>	<b>Pervaporation as an alternative process for solvent dehydration in dry cleaning machines</b> . . . . .	<b>85</b>
3.1	Literature review . . . . .	86
3.1.1	Pervaporation overview . . . . .	86
3.1.2	Materials of pervaporation membranes . . . . .	87
3.1.2.1	The organic membranes . . . . .	88
3.1.2.2	The inorganic membranes . . . . .	89
3.1.2.3	The hybrid membranes . . . . .	90
3.1.3	Dehydration of organic solvents by pervaporation . . . . .	91
3.2	Experimental study of solvent dehydration by pervaporation . . . . .	92
3.2.1	Materials . . . . .	93

## CONTENTS

---

3.2.2	Experimental unit description . . . . .	93
3.2.3	Analysis by gas chromatography . . . . .	95
3.2.3.1	GC device . . . . .	95
3.2.3.2	GC operating parameters and setup . . . . .	95
3.2.3.3	GC Calibration . . . . .	96
3.2.4	Results and discussion . . . . .	98
3.2.4.1	Membrane Sultzer PERVAP 4102-3184 . . . . .	99
3.2.4.2	Membrane Sultzer PERVAP 4510-2898 . . . . .	100
3.2.4.3	Membrane Sultzer PERVAP 4100-3239 . . . . .	103
3.3	Modelling of solvent dehydration by the solution-diffusion model . . . . .	104
3.3.1	General approach to mass transfer modelling in polymeric membranes . . . . .	105
3.3.2	The solution-diffusion model . . . . .	106
3.3.2.1	Brief mathematical description . . . . .	106
3.3.2.2	Reporting the pervaporation data . . . . .	110
3.3.3	Determining the activity coefficients for solution-diffusion model . . . . .	112
3.4	Results and discussion . . . . .	114
3.4.1	Influence of temperature . . . . .	114
3.4.2	Influence of feed concentration . . . . .	116
3.4.3	Prediction of membrane performance in batch dehydration at different temperatures . . . . .	117
3.5	Chapter conclusion . . . . .	118
<b>4</b>	<b>On the design of the pervaporation unit for solvent dehydration and its integration in the dry cleaning machine</b> . . . . .	<b>121</b>
4.1	ARCAFLEX320 distillation system . . . . .	122
4.1.1	Overview and working principle . . . . .	122
4.1.2	Devices that can be reused . . . . .	124
4.1.3	Process constraints . . . . .	125
4.2	Design of the pervaporation unit . . . . .	126
4.2.1	Membrane module . . . . .	126
4.2.2	Vacuum system . . . . .	129
4.2.3	Permeate condenser . . . . .	130
4.2.4	System layout . . . . .	135
4.2.5	Operational costs estimation and comparison with distillation . . . . .	137
4.3	Chapter conclusion . . . . .	138
	<b>Conclusions and directions for future research</b> . . . . .	<b>146</b>

<b>Bibliography</b>	<b>147</b>
<b>Appendix A Literature reference states and expressions for <math>g^E</math></b>	<b>161</b>
A.1 Zero pressure reference state (Michelsen, 1990) . . . . .	161
A.2 Infinite pressure reference state (Huron and Vidal, 1979) . . . . .	161
A.3 Constant packing fraction (Peneloux et al., 1989) . . . . .	162
A.4 Generalized reference state at constant volume (Neau et al., 2011) . . . . .	162
<b>Appendix B Pure compounds group contribution parameters for the estimation of critical properties</b>	<b>163</b>
<b>Appendix C Measured experimental vapor pressures and VLE data for pure compounds, binary and quaternary mixtures</b>	<b>165</b>
C.1 Pure compounds . . . . .	166
C.2 Aqueous binary mixtures . . . . .	166
C.3 Organic binary mixtures . . . . .	168
C.4 Quaternary mixtures . . . . .	171
<b>Appendix D GC setup and operating conditions used in Chapter 2</b>	<b>173</b>
<b>Appendix E Membrane cell used in experiments for the laboratory scale pervaporation</b>	<b>177</b>

# NOMENCLATURE

## Subscripts

<i>(m)</i>	Membrane interface
$\infty$	Infinite pressure (reference state)
<i>calc</i>	Calculated value
<i>ch</i>	Channel
<i>comb</i>	Combinatorial
<i>cond</i>	Condensation
<i>eos</i>	Equation of state
<i>exp</i>	Experimental value
<i>fin</i>	Final
<i>init</i>	Initial
<i>ls</i>	Limescale
<i>MKS</i>	Value related to MKS sensor
<i>obj</i>	Objective (function)
<i>RA</i>	Rackett (parameter)
<i>res</i>	Residual
<i>vap</i>	Vaporisation
<i>b</i>	Boiling
<i>c</i>	Critical (value)

## NOMENCLATURE

---

$F$	Feed side
$K$	$K$ -th main group
$k$	$k$ -th component
$L$	$L$ -th main group
$P$	Permeate side
$p$	Plate
$r$	Reduced
0	Zero pressure (reference state)

### Greek Symbols

$\alpha$	Heat transfer coefficient
$\alpha$	Separation factor
$\alpha$	Temperature function (EoS)
$\beta$	Selectivity
$\delta$	Thickness
$\eta$	Packing fraction
$\Gamma$	Configurational energy
$\gamma$	Activity coefficient
$\gamma$	Soave function parameter
$\lambda$	Thermal conductivity
$\mu$	Chemical potential
$\mu$	Dynamic viscosity
$\nu$	Cinematic viscosity
$\nu$	Number of functional groups
$\omega$	Pitzer acentric factor

## NOMENCLATURE

---

$\omega$	Velocity
$\phi$	Fugacity coefficient
$\phi$	Volume of a molecule
$\rho$	Density
$\tau$	Time
$\theta$	Surface fraction of a molecule

### Other Symbols

$\mathcal{P}$	Permeability (barrer)
---------------	-----------------------

### Superscripts

$EV$	excess at constant volume
$in$	Inlet
$MV$	Mixing at constant volume
$out$	Outlet
$sat$	Saturated vapor
$E$	Excess
$G$	ideal gas
$L$	Liquid
$M$	Mixing
$V$	Vapor

### Roman Symbols

$A$	Helmholtz energy
$a$	Adjustable parameter
$a$	PR EoS attractive term
$b$	Adjustable parameter



## NOMENCLATURE

---

<i>b</i>	PR EoS covolume
<i>C</i>	Integration constant
<i>c</i>	Concentration
<i>D</i>	Diffusion coefficient
<i>D</i>	Permeate vapor flow
<i>d</i>	Diameter
<i>e</i>	Cubic EoS terms
<i>F</i>	Function
<i>F</i>	Heat exchange area
<i>f</i>	Fugacity
<i>G</i>	Molecular repartition coefficient
<i>G</i>	Total Gibbs energy
<i>G</i>	Transfer medium mass flow
<i>g</i>	Partial molar Gibbs energy
<i>H</i>	Enthalpy
<i>h</i>	Enthalpy
<i>J</i>	Mass permeate flux
<i>j</i>	Molar flux
<i>K</i>	Mass sorption coefficient
<i>L</i>	Coefficient of proportionality
<i>l</i>	Membrane thickness
<i>M</i>	Molar mass
<i>m</i>	Mass
<i>m</i>	Soave function parameter

## NOMENCLATURE

---

$N$	Number of points
$n$	Number of moles
$P$	Permeability
$P$	Pressure
$p$	Pressure
$Q$	Total heat
$Q$	UNIFAC subgroup parameter
$q$	Heat flow density
$q$	Specific heat
$q$	Surface area factor
$R$	Gas constant
$R$	Thermal resistance
$R$	UNIFAC subgroup parameter
$r$	Volume factor
$S$	Entropy
$S$	Surface area
$T$	Temperature
$U$	Internal energy
$V$	Total volume
$v$	Volume
$x$	Liquid fraction (mass or molar)
$y$	Vapor fraction (mass or molar)
$Z$	Compressibility factor
$\hat{K}$	Molar sorption coefficient

# LIST OF FIGURES

1.1	Dry cleaning machine ARCAFLEX320 . . . . .	27
1.2	Flowsheet diagram of solvent regeneration in ARCAFLEX320 . . . . .	28
1.3	IPURA 440/S dry cleaning machine . . . . .	31
1.4	NEBULA dry cleaning machine . . . . .	32
1.5	UNISEC dry cleaning machine . . . . .	33
2.1	Sketch of the used static apparatus . . . . .	42
2.2	Measured raw points and Clapeyron regression for DPM ( $\square$ ) with $R^2 = 0.9998$ ; DPnB ( $*$ ) with $R^2 = 0.9963$ ; PnB ( $\triangle$ ) with $R^2 = 0.9987$ . . . . .	45
2.3	Chromatogram of DPM+DPnB mixture with $x_{DPM} = 0.33$ molar (FID detector) .	47
2.4	Chromatogram of H <sub>2</sub> O+DPM mixture with $x_{H_2O} = 0.5$ molar (TCD detector) . .	47
2.5	GC calibration lines for the mixtures: a) H <sub>2</sub> O+DPM; b) H <sub>2</sub> O+DPnB; c) H <sub>2</sub> O+PnB; d) PnB+DPM; e) DPM+DPnB . . . . .	49
2.6	Measured vapor pressures for pure compounds and their correlation with the Antoine equation: DPM ( $\diamond$ ); DPnB ( $\triangle$ ); PnB ( $\circ$ ); DPM Technical Leaflet from (BASF, 2017) ( $\square$ ) - for comparison; Antoine equation (—) . . . . .	51
2.7	Vapor pressures calculated using the PR EoS and estimated $T_c$ , $P_c$ and $\omega$ from Table 2.2: a) DPM: <i>error</i> = 12.3%; b) DPnB: <i>error</i> = 36.3%; c) PnB: <i>error</i> = 24.15% .	61
2.8	Vapor pressures calculated using the PR EoS and $T_c$ , $P_c$ and $\omega$ from Table 2.4 and final $\gamma$ , $m$ parameters: a) DPM: <i>error</i> = 6.88%; b) DPnB: <i>error</i> = 20.36%; c) PnB: <i>error</i> = 9.85% . . . . .	65
2.9	Examples of VLE used in data set and calculated by NRTL-PR model: a) Diiso- propyl ether (DIPE)+2,2,4-Trimethylpentane; b) H <sub>2</sub> O+Propylene glycol methyl ether, ( $\square$ ) - 353.15 K and ( $\triangle$ ) - 363.15 K . . . . .	75
2.10	Measured (squares) and calculated (solid lines) VLE and VLLE at 283.15÷363.15 K: a) water+DPM; b) water+DPnB . . . . .	79
2.11	Measured (squares) and calculated (solid lines) VLE and VLLE at 283.15÷363.15 K: a) water+PnB; b) PnB+DPM . . . . .	80

LIST OF FIGURES

---

2.12 Measured (squares) and calculated (solid lines) VLE at 283.15÷363.15 K: a) DPM+DPnB; b) PnB+DPnB . . . . .	81
2.13 Measured (squares) and calculated (solid lines) VLE of the quaternary mixture H <sub>2</sub> O+ARCACLEAN (DPM 60%wt, DPnB 30%wt, PnB 10%wt) at 283.15÷363.15 K	82
3.1 Diagram of the pervaporation process (Drioli et al., 2011) . . . . .	86
3.2 Diagram of the pervaporation unit used in this work . . . . .	94
3.3 The GC device Shimatzu GC-2010 (left) and the column Agilent CP-Select 624 CB (right) . . . . .	95
3.4 The programmed mode setup . . . . .	96
3.5 GC calibration line used for sample analysis in pervaporation experiments . . . . .	98
3.6 Permeate composition obtained using the membrane PERVAP 4102-3184 . . . . .	99
3.7 Experimental permeate fluxes for the membrane PERVAP 4102-3184 . . . . .	100
3.8 Permeate composition obtained using the membrane PERVAP 4510-2898 . . . . .	100
3.9 Experimental permeate fluxes for the membrane PERVAP 4510-2898 . . . . .	101
3.10 Permeate flux as a function of (a) feed water concentration and (b) process du- ration at 50°C. Membrane PERVAP 4510-2898 (membrane surface $S_f = 0.00132$ $m^2$ ) . . . . .	103
3.11 Membrane transport through the porous (left) and dense (right) membranes (Baker, 2012) . . . . .	105
3.12 Three steps of mass transfer in solution-diffusion model (George and Thomas, 2001) . . . . .	106
3.13 Driving force gradient in one-component solution permeating a solution-diffusion membrane (Wijmans and Baker, 1995) . . . . .	107
3.14 Hypothetical VLE considered at the feed . . . . .	110
3.15 Water activity coefficients in the liquid ARCACLEAN mixture as a function of molar fraction for 303.15 K, 323.15 K and 343.15 K . . . . .	113
3.16 Experimental data from Figure 3.9 replotted as molar flux over $\Delta p$ with a fitted value of permeance of 1600 gpu (slope) . . . . .	115
3.17 Calculated permeances for the membrane PERVAP 4510-2898 as a function of temperature. Quasi-stationary regime, water content in feed 10%wt . . . . .	116
3.18 Molar flux as a function of $\Delta p$ at 50°C . . . . .	116
3.19 Evolution of water permeance as a function of initial feed concentration at 50°C	117
3.20 Prediction of permeate flux in batch dehydration for 303.15 K ad 343.15 K . . . . .	118
4.1 Distillation system of the ARCAFLEX320 device . . . . .	123
4.2 Initial sketch of the pervaporation dehydration stage . . . . .	124

## LIST OF FIGURES

---

4.3	ARCAFLEX320 gabarit dimensions with solvent tank: W = 1735 mm; D = 1600 mm; H = 2113 mm . . . . .	126
4.4	Prediction of permeate flux in batch dehydration for 303.15 K ad 343.15 K . . . . .	128
4.5	Membrane effective area as a function of: a) final water mass fraction ( $\tau = 65$ min); b) process duration . . . . .	128
4.6	Plot of functions $q_{F2} = f(LMTD)$ (—) and $q_{F1} = f(\theta_0)$ (—) . . . . .	134
4.7	KAORI K050 brazed plate heat exchanger . . . . .	134
4.8	Proposed pervaporation system layout: a) drawing with dimensions; b) 3D model	136
4.9	Comparison of dehydration by distillation and pervaporation in terms of annual costs for 20 liters of solvent mixture with 10%wt of water per cycle (1500 cycles/year) . . . . .	138

# LIST OF TABLES

1.1	CAS No and chemical structure of the compounds forming the ARCACLEAN solvent . . . . .	26
1.2	Formula of the ARCACLEAN solvent . . . . .	27
2.1	Antoine coefficients for DPM, DPnB et PnB (T[K], P[Pa]) and the absolute mean pressure deviation . . . . .	52
2.2	Critical properties and Pitzer acentric factor of DPM, DPnB and PnB estimated using the Wilson and Jasperson (1996) method (1st and 2nd Order estimation) . . . . .	59
2.3	Comparison of the critical properties of PnB estimated using different group contribution methods . . . . .	62
2.4	Final estimated critical properties of DPM, DPnB and PnB providing the minimal error in vapor pressures . . . . .	63
2.5	Literature critical properties of the ethers and glycol ethers used in Section 2.2.2.3 for "-O-" group interaction energies calculation in the NRTL-PR model . . . . .	64
2.6	Groups decomposition of DPM, DPnB and PnB and the corresponding UNIFAC subgroups parameters . . . . .	73
2.7	Data set of different VLE systems containing ethers, glycol ethers, alcohols and water used for fitting of group contribution parameters for the "-O-" group . . . . .	74
2.8	Values (in J/mol) of the NRTL-PR group interaction parameters $\Gamma_{LK}^{(0)}$ used for compounds in this work . . . . .	75
2.9	Values (in J/mol) of the NRTL-PR group interaction parameters $\Gamma_{LK}^{(1)}$ used for compounds in this work . . . . .	76
2.10	Values (in J/mol) of the NRTL-PR group interaction parameters $\Gamma_{LK}^{(2)}$ used for compounds in this work . . . . .	76
4.1	Initial data for membrane effective area calculation . . . . .	127
4.2	Initial data for condenser design . . . . .	131
4.3	Thermophysical properties of streams . . . . .	131

LIST OF TABLES

---

B.1	Constantinou and Gani (1994) group contributions used in Equations (2.16) and (2.17) for DPnB and PnB . . . . .	163
B.2	Wilson and Jasperson (1996) group contributions used in Equations (2.18) to (2.20) for DPM, DPnB and PnB . . . . .	163
B.3	Joback (1984) group contributions used in Equations (2.14) and (2.15) for PnB .	164
C.1	Experimental vapor pressure data and pressures calculated with Equation (2.4) for DPM, DPnB and PnB . . . . .	166
C.2	Measured isothermal VLE and VLLE data of the H <sub>2</sub> O+DPM, H <sub>2</sub> O+DPnB and H <sub>2</sub> O+PnB at 283.15÷363.15 K . . . . .	166
C.2	Measured isothermal VLE and VLLE data of the H <sub>2</sub> O+DPM, H <sub>2</sub> O+DPnB and H <sub>2</sub> O+PnB at 283.15÷363.15 K (Continued) . . . . .	167
C.2	Measured isothermal VLE and VLLE data of the H <sub>2</sub> O+DPM, H <sub>2</sub> O+DPnB and H <sub>2</sub> O+PnB at 283.15÷363.15 K (Continued) . . . . .	168
C.3	Measured isothermal VLE data of the PnB+DPM, DPM+DPnB and PnB+DPnB at 283.15÷363.15 K . . . . .	169
C.3	Measured isothermal VLE data of the PnB+DPM, DPM+DPnB and PnB+DPnB at 283.15÷363.15 K (Continued) . . . . .	170
C.3	Measured isothermal VLE data of the PnB+DPM, DPM+DPnB and PnB+DPnB at 283.15÷363.15 K (Continued) . . . . .	171
C.4	Measured isothermal VLE data of the quaternary system Water + ARCACLEAN at 283.15÷363.15 K . . . . .	171
C.4	Measured isothermal VLE data of the quaternary system Water + ARCACLEAN at 283.15÷363.15 K (Continued) . . . . .	172

# Chapter 1

## Context and problem statement

**N**OWADAYS, the dry cleaning is predominantly a small business industry. The dry cleaner market represents about 575 Million Euros of turnover and employs about 15000 persons. Available and reliable, dry cleaning became an important part of the modern life, which offers us a fast and delicate removal of even the most difficult spots. This technology has a long history and its methods are being changed significantly during many years since its discovery.

Dry cleaning means a cleaning process for textiles, which is done in non-polar solvents instead of water. If water is used, such cleaning process is called "washing" or "laundering". Among the advantages of solvents is their ability to dissolve grease and oils in a way that water cannot. Natural fibers such as wools and silks dry clean beautifully, but can shrink, distort and lose color when washed in water.

Actually, the vast majority of dry cleaners in Europe still use a toxic and carcinogenic perchloroethylene as a solvent. In France it will be completely forbidden by 2020, however, this has already happened in Denmark and USA. The need of replacing the perchloroethylene caused a very fast growing of the amount of "green" laundries in EU during last 3 years. In most of cases, they propose three methods of textile cleaning: water cleaning (which remains the most popular way of cloth cleaning in France), solvents based on hydrocarbons (mostly used in Germany) and silicone derivatives (used in the USA).

To correspond the new standards of dry cleaning, the French company *Arcane Industries* has developed a new "green" solvent for new generations of dry cleaning machines. Offering a high level of environmental security and efficiency, this solution has been already integrated in many dry cleaners all over France and has proven its relevance. Meanwhile,



the *ILSA* company (Italy), in collaboration with *Arcane Industries*, have adapted their AR-CAFLEX320 dry cleaning machine to the new solvent.

Nevertheless, the operation experience has shown that the efficiency of the solvent regeneration process in dry cleaning device is not at its maximum. Also, the energy consumption and costs do not remain negligible and should be improved.

## 1.1 A brief history of the dry cleaning

The dry cleaning concept is not innovative. The first mentions of dry cleaning date back to the ancient period more than 2000 years ago. It was the ancient Romans who first realized that their garments, namely their white woolen togas, were better cleaned by substances other than water (for example, clay). They have noticed that water shrinks the wool and is not as successful at stain removal as other chemicals.

Meanwhile, ancient Greeks have also done some experimenting with non-water cleaning. It was actually them who developed the phrase "dry cleaning" as a way to describe cleaning that was done without water. The Romans have perfected their methods of dry cleaning which remarkably remained as the best known practices until the 1800s. The Romans found that one type of clay, known as *fuller's earth*, was extremely successful in removing oil, dirt and grease. It could be kneaded into textiles to draw out impurities. Then, the fuller's earth combined with ammonia was used once those textiles became dirty from wearing.

The beginning of modern history of dry cleaning is not clear. It is sometimes considered that using of dry cleaning began with an anecdotic story about a happy accident caused by a maidservant. At some point in the 1840s, a french textile maker Jean-Baptiste JOLLY's maid accidentally knocked over JOLLY's kerosene lamp onto a linen tablecloth. JOLLY was surprised to find that the linen in that spot became much cleaner. This revelation was quickly turned into an extension of his business, so the company of Jolly-Belin in Paris, opened in 1840s, is historically credited as the first dry cleaning business, using kerosene as its primary cleaning solvent. This dry cleaning method was at the top secret for a long time and was named by Englishmen as "French cleaning".

Later on, the experiments with kerosene and gasoline-based cleaning was continued all over the Europe through the reminder of the 19th century. The inventors and industrial-

ists have then realized that the form of cleaning predicated on dousing clothes in highly flammable liquids was not a good idea. A history of fires and explosions in dry cleaning plants made that pretty clear.

Industrialists set about finding a better alternative. An American dry cleaner William Joseph Stoddard is credited as the first to develop a successful non-gasoline-based solvent in the 1920th. Cleaners soon settled on chlorine-based solvents, and found their best success with *tetrachloroethylene*. Tetrachloroethylene was first discovered by Michael Faraday, one of the most prominent chemists in science history. Also known as *perchloroethylene*, or "perc", it remained for a long time the primary solvent used by the vast majority of dry cleaners worldwide.

By the end of the World War II, a progressive development of the dry cleaning machines led to the appearance of the public dry cleaners. The time of order processing was reduced from one week to four hours and even less, depending on the type of cloth. But unfortunately, such a fast development led to a decreasing of the cleaning quality. In most of the cases, it was happened because of the lack of knowledge and professional skills of the industrial dry cleaners staff.

As the dry cleaning methods were progressing, a lot of investigation and research work was made in that field. Nowadays, the industrial dry cleaners are equipped with modern machinery which allows to perform a more efficient and delicate cleaning. However, perchloroethylene was classified as carcinogenic to humans by the United States Environmental Protection Agency (EPA, 2011) and must be handled as a hazardous waste. To prevent it from getting into drinking water, dry cleaners that use perchloroethylene must take special precautions. When released into the air, perchloroethylene can contribute to smog when it reacts with other volatile organic carbon substances (EPA, 1994). California firstly declared perchloroethylene a toxic chemical in 1991, and its use will become illegal in that state by 2023. In European Union, according to the INRS report in 2013 (INRS, 2013), perchloroethylene is now forbidden to use in dry cleaners and should be imperatively replaced by a safe "green" solvent by 2020.

As a response to the above problem, in France, *Arcane Industries* company has developed a solvent called ARCACLEAN which is as highly performant in dry cleaning as perchloroethylene, but, contrary to it, is non toxic, non carcinogenic and biodegradable. ARCACLEAN is useful for even higher range of spots due to its compatibility with water. As a result, Ar-

*cane Industries*, in collaboration with *ILSA* (Italy), has developed a new line of dry cleaning machines ARCAFLEX which are fully compatible with the ARCACLEAN solvent.

## 1.2 The ARCACLEAN solvent

During its development, the ARCACLEAN solvent has undergone changes in its formula, becoming more and more efficient and balanced. The last composition of the ARCACLEAN solvent by the time of writing the present Thesis comprises the following compounds:

- **Dipropylene Glycol Methyl Ether (DPM):**

DPM is a mid-to-slow evaporating solvent. This hydrophilic solvent has 100% water solubility and is ideally suited as a coupling agent in a wide range of solvent systems. More broadly, its hydrophilic nature makes it an ideal coupling aid in water reducible coatings and cleaning operations (BASF, 2017);

- **Dipropylene Glycol n-Butyl Ether (DPnB):**

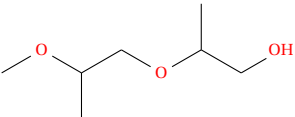
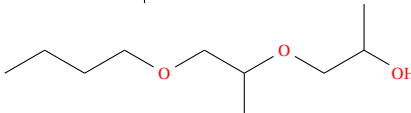
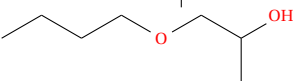
DPnB is a relatively slow-evaporating solvent which is one of the most efficient coalescents in water-borne latex systems. Provides excellent surface tension lowering ability, and is useful in cleaning products by itself or when blended with other products such as DPM. DPnB is a good solvent for removing oils and greases (BASF, 2014a);

- **Propylene Glycol n-Butyl Ether (PnB):**

PnB is extensively used in heavy-duty cleaning formulations. It does an excellent job of solvating and coupling hydrophobic greases and oils in household as well as industrial formulations. It is partly water soluble and miscible with most organic solvents. In coatings, PnB offers good coalescing ability in systems requiring fast evaporation (BASF, 2014b).

Table 1.1 contains structural formulas as well as CAS numbers of the above compounds.

**Table 1.1:** CAS No and chemical structure of the compounds forming the ARCACLEAN solvent

Compound	CAS No	Structure
Dipropylene Glycol Methyl Ether (DPM)	34590-94-8	
Dipropylene Glycol n-Butyl Ether (DPnB)	29911-28-2	
Propylene Glycol n-Butyl Ether (PnB)	5131-66-8	

All the compounds are fully biodegradable and do not present any hazard for the environment. The last formula of the ARCACLEAN solvent is given in Table 1.2. In some cases, a very low content of water in solvent is acceptable.

**Table 1.2:** Formula of the ARCACLEAN solvent

Compound	DPM	DPnB	PnB
Mass percentage	60%	30%	10%

### 1.3 Motivations and problem statement

In the frame of replacing the perchloroethylene by an alternative "green" solvent, *Arcane Industries* and *Innovaclean* companies started an R&D investigation in adaptation of their new ARCACLEAN solvent for efficient using in dry cleaning machines of a current generation ARCAFLEX320 (Figure 1.1), produced by *ILSA*.



**Figure 1.1:** Dry cleaning machine ARCAFLEX320

During multiple dry cleaning cycles, the solvent accumulated dust and water and, thus, needs to be regenerated. Solvent regeneration comprises two main actions: removal of the dirt (mainly consisted of fibers, colorants, grease *etc.*) and solvent dehydration. In fact, after the dry cleaning, the solvent becomes charged in water that contains in garments due to human sweating and environmental humidity. Solvent regeneration is a key task in the whole dry cleaning cycle, as the solvent is too expensive for single use.

### 1.3.1 Current regeneration process in ARCAFLEX320 machines

Process technology in dry cleaning has the target to clean garments as good as possible without damaging them, at lowest possible costs and with highest possible efficiency and safety. In ARCAFLEX320 dry cleaning devices, the solvent regeneration is performed using *distillation*. This classic technique is suitable for removing of both water and dirt from solvent. Due to its principle and operation simplicity, the distillation became extremely popular and widely used process in separation of liquid mixtures. The flowsheet diagram of solvent regeneration process implemented in ARCAFLEX320 is presented in Figure 1.2.

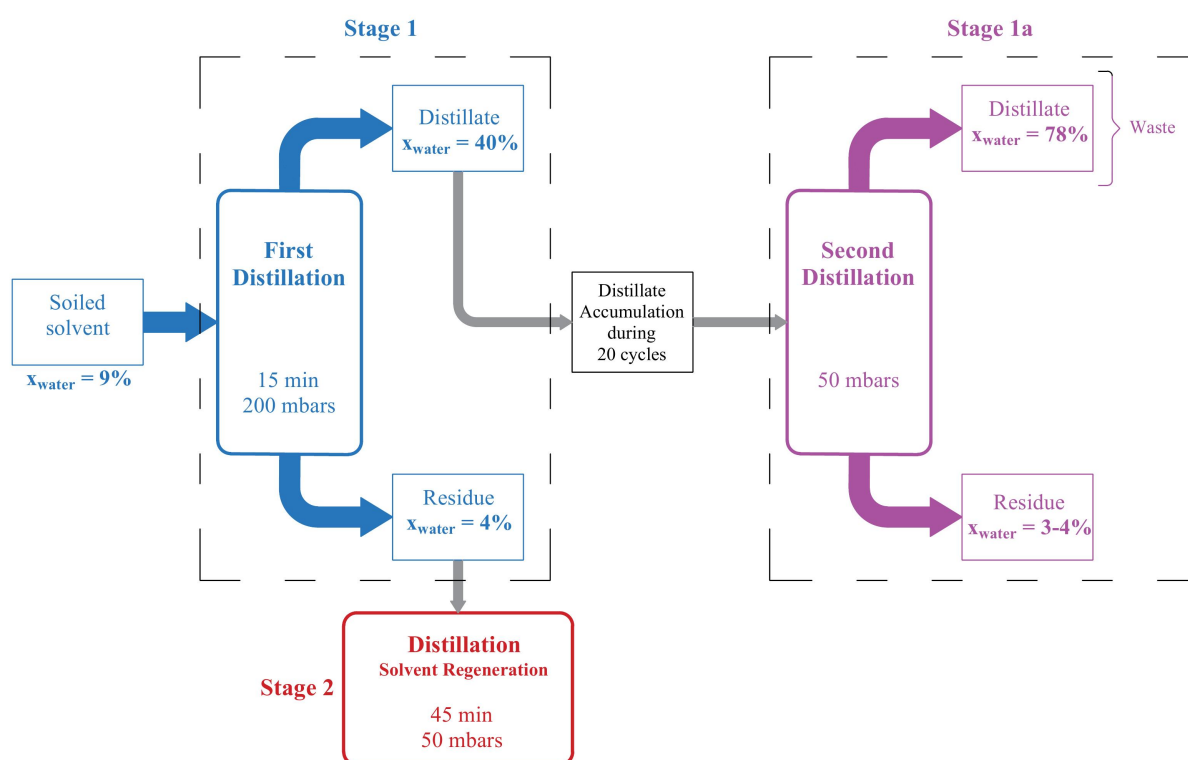


**Figure 1.2:** Flowsheet diagram of solvent regeneration in ARCAFLEX320

The whole regeneration procedure in ARCAFLEX320 is made of two steps:

- *Stage 1:* elimination of water from the solvent (about 20 liters) during 15 minutes under a pressure of 200 mbar. The initial water concentration of about 9 ÷ 10% wt decreases to about 4% wt. The solvent in the distillate is not negligible because the generated distillate (between 1 and 2 liters) contains 60% wt of solvent and 40% wt of water in total mass. After 20 cycles of cleaning, all the produced distillate is mixed and distilled again (stage 1a) in order to recycle a part of solvent. The finally obtained distillate (about 12 liters containing about 78% of water) represents a waste. Both residues from *stage 1* and *1a* are collected together and sent to *stage 2*.

- *Stage 2*: Solvent regeneration during 45 minutes under the pressure of 50 mbar in order to eliminate fibers, dust and colorants dissolved in it.

After regeneration, the majority of dirt particles are eliminated, however, the solvent still contains about 3 to 4% wt of water.

### 1.3.2 Issues and limitations of distillation

Despite numerous advantages of distillation as a separation process, it has some issues and limitations as well. These issues become even more visible when applied to solvent dehydration in dry cleaning devices.

First of all, these issues are represented by a high energy consumption by distiller and auxiliary equipment related to it. In ARCAFLEX320, the distiller is not equipped by electrical resistance heater. Instead, it is heated by the means of water steam produced in steam generator. Such a solution is used due to the risk related to the presence of sludge in solvent-to-regenerate. This sludge can provoke the resistance fouling, in case if the latter would have been used.

Currently, the distillation system consumes about 20 kW of heat per distillation cycle, which yields in huge number in annual perspective. Moreover, our previous study ([Guichardon and Dimitrov, 2018](#)) showed that the distiller is not heat consumption optimized and is enough to be heated 60% less, meaning 8 kW per distillation cycle.

In addition, the heat exchangers used in distillation, are cooled by the tap water from network, resulting in a high water consumption per dry cleaning cycle.

Second issue of distillation lays in its separation limitations in terms of thermodynamics. Indeed, the separation quality in distillation is completely vapor-liquid equilibrium dependent. Depending on the equilibrium curve of a mixture, it can be either easy or difficult to separate by distillation, especially if the boiling points of components are close or an azeotrope is occurred in that mixture. Moreover, if the boiler is heated too much, the high boiling fraction can mechanically entrain the vapor of the low boiling fraction, resulting in unfavourable decreasing of distillate purity and solvent losses. While on the subject, the solvent losses in a currently implemented distillation are very important. The distillate produced during the *stage 1a* (Figure 1.2) and considered as a waste, contains 22% of solvent. It

is about 2.4 liters per day, which represents a huge solvent loss in a long perspective.

The last issue is represented by the fact, that the solvent regeneration in ARCAFLEX320 is performed in a simple one-stage distillation which is, probably, enough to eliminate the solid dirt particles but does not offer a satisfactory separation of solvent and water.

The dehydration is a crucial step in solvent regeneration. When containing the water, the ARCACLEAN solvent becomes aggressive to textiles, provoking their shrinking and fiber degradation. As mentioned before, after the regeneration cycle, the solvent still contains 3 to 4% of water. Therefore, one of the most important tasks of the present work is to reduce the water amount in solvent as much as possible. Generally, *Innovaclean* recommends the water content to be less than 1%, which is practically unachievable by current distillation. In order to achieve such a separation, one should definitely prefer the fractional distillation over the one-stage distillation. However, the fractional distillation is not very favourable to implement in a dry cleaning machine due to eventual fouling.

Instead, *Innovaclean* was interested in implementing another dehydration technique, which will be able to completely replace the current distillation. The new process should demonstrate higher energy and separation efficiency, being at the same time environmentally friendly. In other words, the new dehydration process should be designed with the respect to the *ecodesign principle*.

### **1.3.3 Dry cleaning devices without distillers**

The problem of replacing the distillation by other processes has been already studied by several companies. Nevertheless, the overall number of distillation-free devices is currently very limited. Solvent regeneration in these devices is mostly based on decantation, filtration, adsorption and even bio-treatment techniques. It is in some point difficult to understand the working principle of these devices as very few information is available on the manufacturer's Internet resources due to confidential information and commercial secret. We will try to give several examples of the devices currently available in the market and to describe them in terms of solvent regeneration, basing on the information that could be retrieved.

### 1.3.3.1 "IPURA" by ILSA

IPURA (Figure 1.3) is the first attempt of ILSA company to set aside the solvent regeneration by distillation. Instead, the decantation and filtration techniques are used. IPURA uses aliphatic hydrocarbons as dry cleaning solvents.



*Figure 1.3: IPURA 440/S dry cleaning machine*

The solvent treatment cycle in IPURA is divided into 4 principal stages. After dry cleaning, the solvent is passed through a centrifugal separator in the bottom of which the heavy dust particles are separated. The lighter particles are then retained by a mechanical filter installed right after the centrifugal separator. The solvent dehydration is performed by decantation using the fact that water is non-miscible with hydrocarbons. The dehydrated solvent is then passed through an adsorber where light particles (most probably colorants) are eliminated.

The overall cost of this device is relatively low. To dry the garments after cleaning, a heat pump is used instead of a supplementary electric heater. However, the dehydration process efficiency and especially the process duration (generally, the decantation is not a quick procedure) remain fairly unclear for us.

### 1.3.3.2 "NEBULA" by Renzacci

NEBULA (Figure 1.4) is an energy efficient dry cleaning machine, in which the distillation has been replaced by a double filtration of solvent (using one mechanical and one chemical filter). The following solvent purification systems are implemented: solvent purification "at a continuous independent flow" using a filter cartridge group ("HFC" and "HFD"); solvent filtration "No Flex Ultra Micron".

NEBULA is a multi-solvent device. It uses the "COMBICLEAN" system, allowing to choose multiple solvents for a better cleaning performance depending on textile type. The DSF<sub>TM</sub>





*Figure 1.4: NEBULA dry cleaning machine*

(Dynamic Saving Flow) allows to reduce at 45% the energy consumption. The manufacturer also declared a reduced cleaning cycle time.

### 1.3.3.3 UNISEC

UNISEC (Figure 1.5) is a dry cleaning machine implementing a biological treatment of solvent using the Effective Microorganisms technology (EM). The EM filters as well as EM Soap solvent contain microorganisms that decompose the dirt. The monomerized pollutants are eliminated by a filter. All the non-monomerized pollutants are trapped at the final stage of regeneration and then monomerized by the bacteria in EM filters.

The odours are also eliminated by the bacteria. The EM forms such an environment, in which harmful bacteria cannot spread and reproduce. In addition, the anti-oxidation effect of the solvent prevents the acidification and protects the interior parts of device, increasing its durability. The solvent is not pollutant and does not contain dangerous substances.

This machine raises respective questions concerning two points: bio-treatment process duration and solvent dehydration. Knowing that the treatment of liquids by a bacterial degradation is usually a long-duration process, the principle of implemented regeneration technology remains unclear for us. Concerning the solvent dehydration, any useful information was found on the company's resources.



**Figure 1.5:** UNISEC dry cleaning machine

### 1.3.4 Other classic dehydration processes

The current progress in chemical engineering technology offers a variety of processes for dehydration of liquid solutions. These processes are based on different mechanisms and are used in a wide range of applications. Some of them can be applied (and even be promising) to dry cleaning solvent dehydration. Here, we present only a short list of processes that can be potentially interesting for the above stated application.

#### 1.3.4.1 The extractive distillation

The *extractive distillation* is an another variation of a classical distillation, but, contrary to it, can be more efficient. In the extractive distillation, a third body is added to the aqueous solution in order to increase the relative volatility of the components-to-separate. This third body usually has a very high boiling temperature and is used to change the activity coefficients of mixture components and, thus, to increase the separation factor. This method is often used in the industry to separate such mixtures, whose components are very close in boiling temperatures or form an azeotrope. The added third body can be a liquid solvent, an ionic liquid, a dissolved salt or a polymer. In case of dry cleaning device, the third body can be used to create an impact on the relative volatility and/or to break the azeotrope (if present) (Huang et al., 2008).

#### 1.3.4.2 The adsorption

The solvent can also be dehydrated by *adsorption*. This process is well studied when applied to dehydration of ethanol. In this case, there exist two types of adsorption: the adsorption of water in vapor phase from the fermentation broth and the adsorption of water in vapor phase from a downstream flow of a distillation column (Beery and Ladisch, 2001).

The most used adsorbents are inorganic materials, as molecular sieve, lithium chloride, silica gel, activated aluminium oxide and different bio-adsorbents (Crawshaw and Hills, 1990). The vapor phase adsorption consumes less energy compared to distillation because only one evaporation is needed (Hu and Xie, 2001). The main drawback of the adsorption is the necessity to regenerate the adsorbent every time, which is an energy dependent procedure. For example, the zeolite molecular sieves are very selective, but the water is strongly adsorbed. Therefore, high temperatures and/or low pressures are necessary to regenerate them (Hu and Xie, 2001). The bio-adsorbents have lower adsorbing capacity, requiring at the same time lower regeneration temperatures.

### 1.3.4.3 Membrane processes

During last decades, the *membrane processes* have become a very prominent dehydration method. The membrane process principle is to use a dense (or porous) semi-permeable interface to separate the aqueous mixture. This interface is capable to retain one mixture component and to let the other one to permeate through it. The most developed industrial membrane processes that are used in dehydration are *the pervaporation, the reverse osmosis, the forward osmosis, the ultra- and nanofiltration*. The driving force of these processes can be produced by either applying a high pressure to the upstream (feed) side of a membrane (ultrafiltration, nanofiltration and reverse osmosis), or creating a vacuum at the downstream (permeate) side of a membrane (pervaporation). The driving force can be also due to concentration gradient (forward osmosis).

#### The reverse osmosis

The *reverse osmosis (RO)* remains currently one of the most dominant processes for separation of liquid mixtures. A great variety of RO membranes were developed since this process was firstly implemented. Until recent times, the application of RO was mainly limited to seawater desalination and purification. However, nowadays the RO application has widened to a vast range of separation technologies. The fractionation of organic and inorganic substances of aqueous and non-aqueous solutions is one example among different possible applications. The advantage of the RO is that the phase change is not needed. Back in the 1980s, Choudhury et al. (1985) were the first who succeeded in separation of ethanol from an aqueous solution using the RO and the acetate cellulose membrane. This membrane was tested with the solutions having from 5 to 20% wt of ethanol. During this study, 93% wt pure ethanol was obtained by applying a transmembrane pressure of 50 ÷ 100 bar.

The transmembrane pressure in RO is mostly dictated by the osmotic pressure of the solution at given feed concentration and should be greater than the latter one. In separation of aqueous and organic solutions, the osmotic pressures are very high, especially at low "solute" concentrations in the feed. Another example of ethanol dehydration was published by [Gravelle et al. \(2016\)](#), where the osmotic pressures reached 200 bar and special carbon nanotubes and graphene oxide membranes were used. Such high pressures represent a main drawback of the RO when applied to dehydration of alcohols and organic compounds. Therefore, implementation of the RO in dry cleaning machines is possible but fairly complicated due to the necessity of creating very high pressures in the system. The high pressure systems are generally related to high energy expenses.

### **The nanofiltration**

The principle of the *nanofiltration (NF)* remains the same as that of the reverse osmosis, having a difference in membranes used. For nanofiltration, the pores of a selective membrane matrix are greater than those of the RO and have a diameter of  $0.5 \div 5$  nm ([Mulder, 2012](#)). The sieve transport mechanism is valid for NF ([Lopes, 2014](#)).

To separate water from solvent due to a steric hindrance effect using the NF membranes represents an advantage to increase the flux across the membrane and, thus, to reduce the required effective membrane area and membrane module cost.

When the NF is performed in the organic media, it is usually referred to as "Solvent resistant nanofiltration" (SRNF) or "Organic solvent nanofiltration" (OSN). This process can be advantageous when it is important to prevent the degradation of sensitive molecular products. SRNF is often used as a part of hybrid separation processes ([Vandezande et al., 2008](#)). As for the membrane materials used in SRNF, the key requirement is their compatibility with a wide range of organic solvents, mechanical strength and thermal resistance. The polymeric membranes are preferred over the inorganic ones due to their cost-effectiveness and processability. The polymers used in NF membranes are cellulose acetate, aromatic or aliphatic polyamide, polyimide or sulfonated polysulfone, polyacrylonitrile, poly(ether ether ketone) and polybenzimidazole. These polymers, containing structural elements like aromatic groups or imide bonds, demonstrate a very good solvent resistance ([Vandezande et al., 2008](#)). All the membranes can be divided into four main types: integrally skinned asymmetric membranes (ISA), mixed matrix membranes (MMM), thin film composite membranes

(TFC) and thin film nanocomposite membranes (TFN) (Lim et al., 2017).

Some of the recent studies on this technology were published by Aburabie and Peinemann (2017); Ben Soltane (2014); Darvishmanesh et al. (2011).

### **The forward osmosis**

The *forward osmosis (FO)* is a process in which the osmotic pressure is used as a driving force instead of an external hydraulic pressure (Zhao et al., 2012). Due to its unique qualities, the forward osmosis has attracted great interest of the scientific community towards different applications, such as seawater desalination (Phuntsho et al., 2012), electricity production (She et al., 2012) and, of course, the separation of aqueous and organic solutions (Nayak and Rastogi, 2010).

It was found that the inorganic salts can be used as solutes in order to generate high osmotic pressures. As an example, the ethanol dehydration using the FO and a cellulose triacetate membrane was recently studied by Zhang et al. (2013). Its principle is to use an ethanol solution tank on one side, draw solution with salt on the other side and a membrane contactor between them. The ethanol solution had an ethanol concentration of 82.5% wt. The draw solution contained about 26% wt of NaCl salt, which corresponded to an osmotic pressure of 500 bar. When these two solutions are placed at the opposite sides of the membrane contactor, the water from ethanol solution is permeated through the membrane towards the salt solution due to the osmosis phenomena, so the ethanol solution is, thus, dehydrated and the ethanol of 90.1% wt purity is obtained during 800 minutes.

The above study proves the feasibility of the aqueous solutions dehydration by FO. The significant disadvantage is, however, a very long process time, making it not rational to use in dry cleaning machines, where the regeneration cycle time plays a key role in the working efficiency of dry cleaners. Moreover, the forward osmosis has an issue known as *reversed salt diffusion*, meaning the small amount of salt ions that diffuse across the membrane from the draw solution to the feed solution (Zhang et al., 2013).

### **The pervaporation**

The *pervaporation (PV)* is a process of choice for dehydration of various solvents (Sommer and Melin, 2005). A separation membrane represents an interface between two adja-

cent phases, acting as a selective barrier that regulates the substance transport between two compartments. The pervaporation is used in gas and liquid separation, separation of ions or biological substances. In pervaporation, a liquid mixture is fed on the upstream side of the membrane and the permeate is evaporated on the downstream of the membrane. The process driving force is the pressure or chemical potential gradient across the membrane. In order to increase the flux, the permeate side is always maintained at a pressure lower than the permeant's saturated vapor pressure (generally at low vacuum). The permeate is a vapor which is then condensed and recovered in a liquid state.

There are two main commercial applications of pervaporation in liquid-liquid separation. The first is, traditionally, the ethanol dehydration, allowing to produce the ethanol of a very high purity (99.9%wt). The advantage of pervaporation is that the separation does not depend on the nature of compounds, so, for instance, the azeotrope occurred in water+ethanol mixture has no influence on separation. The second application of pervaporation is the retention of the volatile organic compounds, which are present in contaminated waters.

In the dehydration of aqueous solutions, the PV membranes can be either hydrophilic or organophilic, which will decide on the permeant nature.

Due to its features, the pervaporation is considered by us as the most promising dehydration process for dry cleaning. It is also important to implement the solvent pre-treatment in order to eliminate sludge and protect the membrane from fouling and damage. However, the latter issue is out of frame of the present Thesis.

## 1.4 Thesis workflow

Following this introductory Chapter (1), the Thesis is arranged in three Chapters, that are dedicated to one particular part of the study.

Chapter 2 focuses on the theoretical and experimental thermodynamic study of ARCA-CLEAN compounds, their organic and aqueous mixtures. Valuable data concerning their vapor pressures, as well as phase equilibria, will be obtained experimentally. A thermodynamic model for phase equilibria representation will be developed as well.

Chapter 3 presents a research on dehydration of ARCACLEAN solvent by pervaporation. For this part of the work, we aim to figure out whether the dehydration of the ARCACLEAN solvent is feasible or not by means of pervaporation. In this context, the process will be studied theoretically and experimentally.

The fourth and the last Chapter is fully devoted to the design and sketching of a solvent dehydration stage based on pervaporation. The main parameters necessary for the design will be estimated.

The main body of the Thesis ends by general conclusions related to the whole study as well as the perspectives and directions for future research.

## Chapter 2

# Thermodynamics of solvents: theoretical and experimental study

**A**FTER each working cycle in a dry cleaning machine, the ARCACLEAN solvent is charged in different kinds of fibers, dirt, colorants and especially in water. The latter represents the main problem of the present Thesis. Indeed, as stated in Chapter 1, when charged in water, the solvent becomes aggressive towards the garment tissues, so it is imperative to reduce the amount of water in solvent before its reusing.

The mixture to dehydrate is a complex system containing 4 compounds: the glycol ethers DPM, DPnB, PnB (forming the ARCACLEAN solvent) and water. The dehydration of this mixture is not as evident as one could think. First of all, we need to know the exact composition of the mixture prior to dehydration and the desired amount of water in solvent after dehydration. The initial amount can vary and depends on many factors but does not usually exceed 10%wt. Concerning the final water amount, it was recommended by the dry cleaning machines operator to be around 1%. Second, one should know the nature of mixture as well as its physical and chemical behavior. In other words, one should study the mixture in terms of *thermodynamics*.

The thermodynamic study allows us to figure out whether the mixture is miscible, partially miscible or non-miscible at different compositions, and whether the glycol ethers are easy to separate from water by distillation and pervaporation.

If the answer for the first statement can be found by making several simple experimental manipulations even before choosing the dehydration process, the last statement requires a deeper investigation. In Chapter 1 we have shown how the solvent dehydration was per-



formed in dry cleaning devices by distillation, together with the advantages and the limits of this process. The aim of this Thesis is to replace the distillation by a membrane dehydration process, namely, pervaporation. Both distillation and pervaporation involve the vapor-liquid equilibria (VLE), so two reasonable questions come out. Do we have enough experimental data to perform the preliminary calculations for the process design? Then, which thermodynamic model to use for these calculations? The present Chapter is dedicated to these questions.

The DPM, DPnB and PnB are very rarely mentioned in the literature. Some main physical properties of these compounds, such as the normal boiling temperature, the molar mass, the density *etc*, were available in the respective technical datasheets of different manufacturers, for example, in BASF (2017, 2014a,b). However, in separation processes, we always need experimental data of phase equilibria for mixtures involving desired compounds. For instance, in pervaporation, one needs to know the activity coefficients of the mixture in the feed to calculate the process driving force and the membrane permeability (or permeance). In addition, the pure compound vapor pressure data are also necessary. Unfortunately, any of these data concerning DPM, DPnB and PnB were published in literature. Moreover, it was unable to find their experimental critical properties as well.

In this context, we have investigated the required phase equilibria experimentally and then proposed a suitable thermodynamic model to represent our systems. The experimental procedure and results are reported in Section 2.1. The vapor pressures were measured for all the compounds at different temperatures. Then, the vapor-liquid equilibria of 6 binary mixtures (water+DPM, water+DPnB, water+PnB, PnB+DPM, DPM+DPnB, PnB+DPnB) and 1 quaternary mixture (water+DPM+DPnB+PnB) were measured as well. The vapor-liquid equilibrium data of binary mixtures are necessary because the thermodynamic model should firstly be validated for binary mixtures and then for quaternary one.

In Section 2.2 the thermodynamic model (NRTL-PR), used to represent all the systems in this work, is presented and detailed. The unavailable critical properties, acentric factor and molecule interaction parameters are computed and reported.

Section 2.3 is devoted to all modelling results concerning the phase equilibria occurring in binary and quaternary mixtures. The calculated equilibria curves will be compared to the experimental points. This comparison will be accompanied by the discussion, also evoking different issues encountered during this study.

## 2.1 Experimental measurements of solvents properties

The low-pressure vapor-liquid equilibria measurements are generally carried out using two main methods. In the literature ([Sandler, 2017](#)), these methods are reported as the *dynamic method* and the *static method*. In the dynamic method, the mixture is placed inside an ebulliometer and heated until its boiling point. The samples of liquid and vapor phases are then taken and analysed, for example, by a gas chromatography. As the pressure and temperature are measured as well, one can obtain an experimental point  $P - T - x - y$ .

In this work, the static method of measuring the vapor pressure was applied. The principle of this method is such that the gravimetrically prepared liquid sample is placed into a static cell, held under the deep vacuum and a constant temperature. The pressure of saturated vapors formed inside the cell are measured and the experimental point  $P - T - x$  is then obtained. Therefore, the vapor phase is not sampled and its composition remains unknown experimentally.

The present experimental work was carried out at the Laboratoire des Multimatériaux et Interfaces (LMI), University of Lyon 1, under the supervision of the Prof. Jacques JOSE and Dr. Ilham MOKBEL. The working principle of a static apparatus used in this work, is thoroughly detailed, first of all, in ([Mokbel, 1993](#)), as well as in many other works, published by the above cited scientists and their students. Among them [Belabbaci et al. \(2010\)](#); [Sarraute et al. \(2008\)](#); [Mahi et al. \(2019\)](#); [Bouzina et al. \(2016\)](#) and others. In Section 2.1.1.2 we describe the most important points related to the operation of static apparatus.

### 2.1.1 Experimental materials and methods

#### 2.1.1.1 Materials

The dipropylene glycol methyl ether (DPM), the dipropylene glycol n-butyl ether (DPnB) and the propylene glycol n-butyl ether (PnB) were provided by Arcane Industries, France. No particular impurities of the compounds were reported by the supplier. For the aqueous samples preparation, the water purified in the ion exchange unit was used. All the compounds were used without further purification but were degassed under the vacuum prior to experiment.

The high purity acetone and methanol ( $\geq 99.9\%$ ) were used as solvents to prepare the samples for the gas chromatography.

### 2.1.1.2 Working principle of a static apparatus

The sketch of the used static apparatus is presented in Figure 2.1. Its working principle, as well as the algorithm of the experiment, are following.

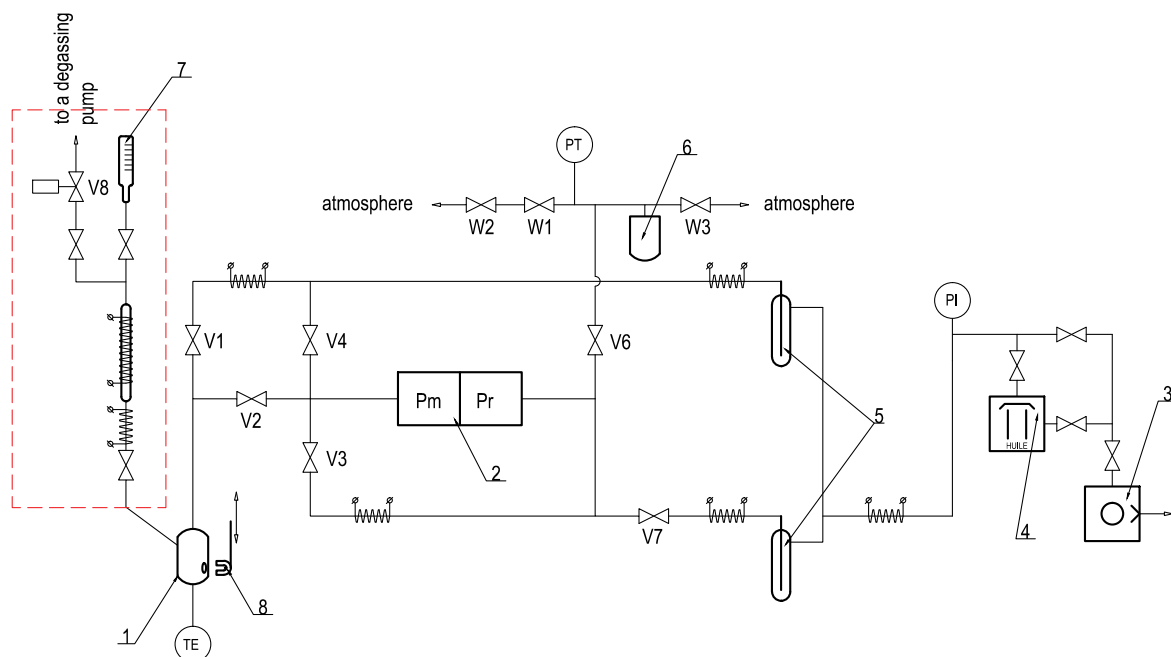


**Figure 2.1:** Sketch of the used static apparatus

The liquid sample is placed in the graduated funnel (7) installed on top of the degassing system (surrounded by a red dashed line). The degassing system is sealed and held under the vacuum. The sample liquid is then transferred to a degassing system by opening the valve on the bottom of the funnel. Once the valve is closed, the liquid is boiled and the degassing procedure is started; the duration can be varied from 1 to 2 hours. Its aim is to remove all possible volatile compounds as well as the air which can be dissolved in a sample and thus perturb the vapor pressure measurements. The volatile compounds are evacuated from the degassing system by an electric valve (V8) programmed to a certain number of triggering cycles. After the degassing, the sample is then transferred to the static cell (1). The cell itself as well as the whole apparatus is maintained under the vacuum. During the transfer, the valves (V1) and (V2) are kept closed. Then, the valve between the degassing system and the cell is closed. The cell is immersed into a thermostatic bath (not presented at the diagram) and the

magnetic mixer (8) is turned on.

The vapor is then formed in the static cell above the liquid. The measurements start by closing the valves (V1), (V3) and (V4) and by opening the valve (V2). The valves (V6) and (V7) are kept opened. The vapor is passed to measurements part of the differential manometer MKS, type 670, model 616A (2). The reference part of the manometer is maintained under the continuous pumping, the residual pressure was  $10^{-4}$  Pa. Once the stability of the pressure and temperature is reached, one can obtain one  $P, T$  experimental point. Then, the valve (V2) is closed and the valves (V4) and (V3) are opened in order to evacuate the vapor from the measurements part of manometer. Next, the valve (V4) is closed and the purge of the vapor from the static cell is made by opening the valve (V1) during 15 to 30 seconds. The measurement is then repeated several times to check the reproducibility of results.

The primary vacuum in the system is provided by a rotary vane-cell pump EDWARDS ES35 (3) with a vacuum limit up to  $10^{-3}$  kPa. The gas diffusion pump EDWARDS E02 (4) with a vacuum limit up to  $< 10^{-6}$  kPa is used in order to create a deeper vacuum. The cell temperature is controlled by a Chromel/Alumel thermocouple (TE). The total condensation of vapors in the system is ensured by two cold traps immersed in the liquid nitrogen (5). These traps protect the pumping group against the accidental suction of a liquid able to damage the pumps mechanisms.

The MKS manometer capacity is limited to about 1300 Pa. In case if the measured vapor pressure is higher than this limit, the valves (W1) and (W2) are opened and the reference part of the manometer is filled with the air in order to compensate the excess pressure. The reference part pressure is measured by a pressure sensor type Keller (PT). During this operation, the secondary pump (4) is shut down.

The experiment is finished by a complete cleaning of the apparatus. The degassing part and the cell are thoroughly rinsed with acetone and dried. Then, the system is again pumped to the vacuum. One should emphasise the importance of the vacuum to be very deep. If it is not the case, the system should be verified and every non-sealing should be eliminated.

The calibration of the system was previously checked by measuring the water vapor pressure and compared to the values from different literature sources, resumed also in [\(Mokbel, 1993\)](#).

### 2.1.1.3 Treatment of experimental points

As described before, the vapor pressure measurements for one liquid sample of one determined composition, at the temperatures ranging from 283.15 K to 363.15 K, represent one experimental cycle. At each temperature, the measurements are performed several times, depending on sample stability. By the sample stability we understand the ability of each particular sample to show a constant value for vapor pressure on the MKS sensor during the active phase of measurement. In fact, the pressure values were not taken instantaneously as one should firstly wait for the thermodynamic equilibrium in the cell to be established. This waiting time can vary depending on the experiment conditions, but as a general rule, it does not exceed 20 minutes. In this work, this time was equal to 16 minutes. During this time, the pressure value was constantly recorded from the MKS sensor. After 16 minutes, an average pressure value was estimated by a digital acquisition software, depending on the pressure changing ratio and according to the following expression:

$$P = aP_{MKS} + bP_{MKS}^2 \quad (2.1)$$

where  $a$  and  $b$  are the MKS parameters determined empirically during the MKS calibration and  $P_{MKS}$  is a pressure value registered by the MKS sensor. As a result, for each temperature, many raw points having slightly different pressure values were obtained. Then, these points were processed following the procedure described below:

1. All raw points obtained for all temperatures were firstly plotted as  $\ln P_{vap} = f(1/T)$ ;
2. Then, these points were correlated with the Clapeyron equation:

$$\ln P_{vap} = -\frac{\Delta H_{vap}}{R} \left( \frac{1}{T} \right) + C \quad (2.2)$$

with  $P_{vap}$ , the vapor pressure in Pa;  $\Delta H_{vap}$ , the enthalpy of vaporization in J/g;  $T$ , the temperature in K and  $R$ , a gas constant in J/(mol·K). The Clapeyron correlation results to a straight line with a slope  $\frac{\Delta H_{vap}}{R}$ . The reason of using it is that it allows to estimate the vapor pressures for a wider range of temperatures, but also to observe the stability of compounds during the measurement. In certain cases, the most unstable points were omitted in order to improve the correlation;

3. If the error between the correlation and experimental results is small enough, the final vapor pressure points for each temperature are determined from the Clapeyron equation. This procedure allows to avoid the problems related to instability which can occur due to different causes.

An example for DPM, DPnB and PnB is illustrated in Figure 2.2. One can see from these plots that the obtained measurements are perfectly coherent with the Clapeyron correlation.

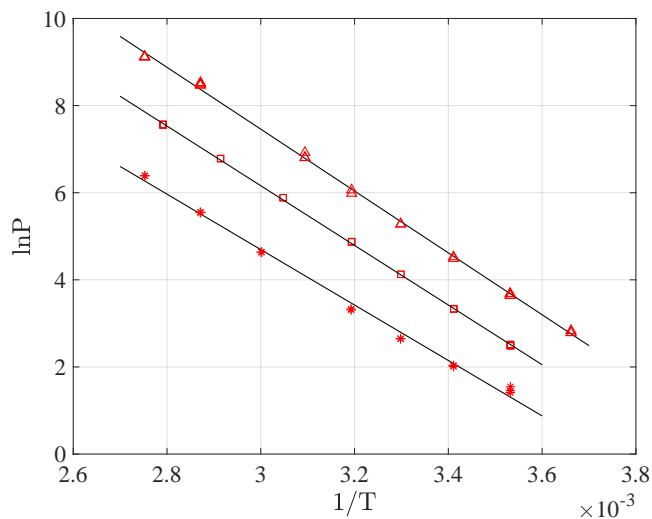


**Figure 2.2:** Measured raw points and Clapeyron regression for DPM ( $\square$ ) with  $R^2 = 0.9998$ ; DPnB ( $*$ ) with  $R^2 = 0.9963$ ; PnB ( $\triangle$ ) with  $R^2 = 0.9987$

## 2.1.2 Sample analysis by the gas chromatography

Once the phase equilibria measurements were finished, all the samples were analysed by the gas chromatography (hereinafter, GC) in order to check their composition.

The GC analysis was carried out in two steps in order to distinguish organic and aqueous mixtures. A FID<sup>1</sup> type detector and a column Agilent HP-5 were used for the organic mixtures. The analysis of the aqueous mixtures were performed using a Restek RT-Q-BOND column and a TCD<sup>2</sup> type detector.

### 2.1.2.1 Importance of the quantitative sample analysis

During vapor pressure measurements in a static apparatus, multiple purges are performed in order to evacuate the vapor accumulated in the differential pressure sensor MKS. These purges, lasting usually from 15 to 30 seconds, can perturb the initial composition of the sample in the static cell. The difference between the initial and final sample composition can

<sup>1</sup>FID - Flame Ionization Detector

<sup>2</sup>TCD - Thermal Conductivity Detector

become significant especially for high temperatures (even if the purge duration is short).

For this reason, every final sample recuperated from the cell at the end of experiment was analysed by the GC in order to determine its exact composition.

### **2.1.2.2 Analysis performing**

A GC device Hewlett Packard 6890 Series equipped with an automatic injector Agilent 7683B was used. The device was connected to a hydrogen generator in order to provide a necessary flow rate of a carrier gas, and an air line necessary to connect the FID detector.

Prior to the injection, every liquid sample was diluted in a solvent according to a sample/solvent volume ratio of 1/20 approximately. Every analysis was performed 3 times in order to confirm the reproducibility.

The analysis was carried out in two phases, separately for aqueous and organic solutions. The reason is that two different GC columns were used to analyse the respective solution. The used GC setup and operating conditions are detailed in Appendix [D](#).

### **2.1.2.3 Peaks identification and calibration**

Before starting any GC results treatment, it is necessary to firstly identify all the compounds in a chromatogram. For that, each compound is injected separately in the GC device and the characteristic retention time is determined. The examples of chromatograms illustrating the mixture DPM+DPnB and water+DPM are presented in Figures [2.3](#) and [2.4](#) respectively.

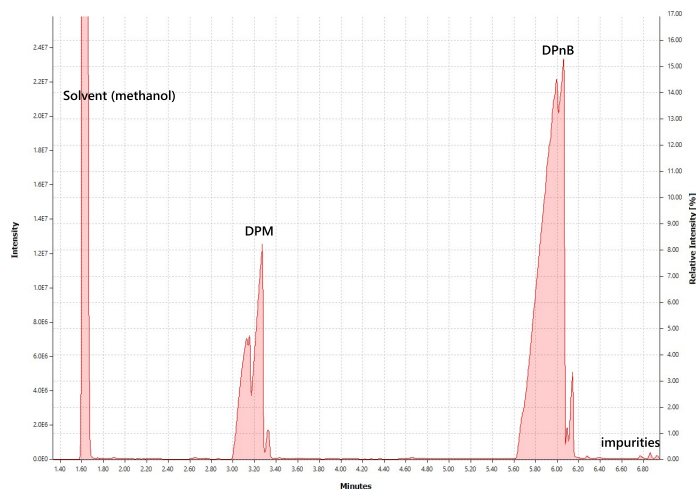


**Figure 2.3:** Chromatogram of DPM+DPnB mixture with  $x_{DPM} = 0.33$  molar (FID detector)

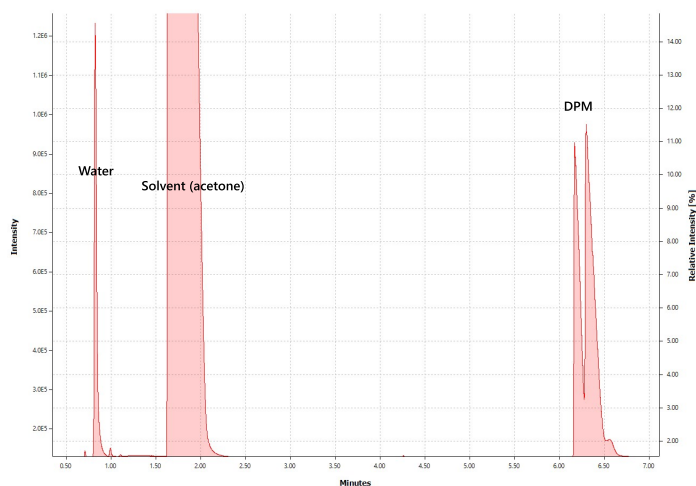


**Figure 2.4:** Chromatogram of  $H_2O$ +DPM mixture with  $x_{H_2O} = 0.5$  molar (TCD detector)

The next step is a GC calibration. The calibration was done using a direct response method as it was assumed that a mixture to analyse is a binary mixture. The mixture samples initially prepared for the vapor pressure measurements and diluted in solvents (methanol or acetone, depending on the sample nature) were used as standard samples for calibration. Each analysis was performed three times and a mean surface ratio  $S_1/S_2$  was then obtained. Next, these ratios were plotted as a function of mole fractions ratios  $x_1/x_2$ . The resulting plot, being a straight line, means that the calibration was done correctly. The calibration lines for 5 mixtures ( $H_2O$ +DPM,  $H_2O$ +DPnB,  $H_2O$ +PnB, PnB+DPM, DPM+DPnB) are illustrated in Figure 2.5. In case of the PnB+DPnB mixture, it was assumed that its composition after vapor pressure measurements has not been perturbed as the purge cycles were con-



siderably shorter than for other mixtures (due to very low vapor pressures of this particular system). Therefore, no GC calibration and analysis was needed for this mixture.

One very important comment concerning the calibration should be added. As said before, the samples are diluted in solvent prior to the GC analysis. In our work, acetone and methanol were used as solvents. The important point is that these solvents should be GC suitable, that means they should have a very high purity. However, as it was observed during the calibration, both of solvents used by us still contained a small amount of water. This should be taken into account and a solvent peak area should be corrected for aqueous samples. That was done by firstly determining the peak area relative to water containing in solvent, then this area was subtracted from the peak area relative to water containing in sample.

It was noticed as well that, in case of the Figures 2.5(b) and 2.5(d), there were two standard calibration points situating far relatively to other points (but were still collinear with them). For visual simplicity, these points were omitted.

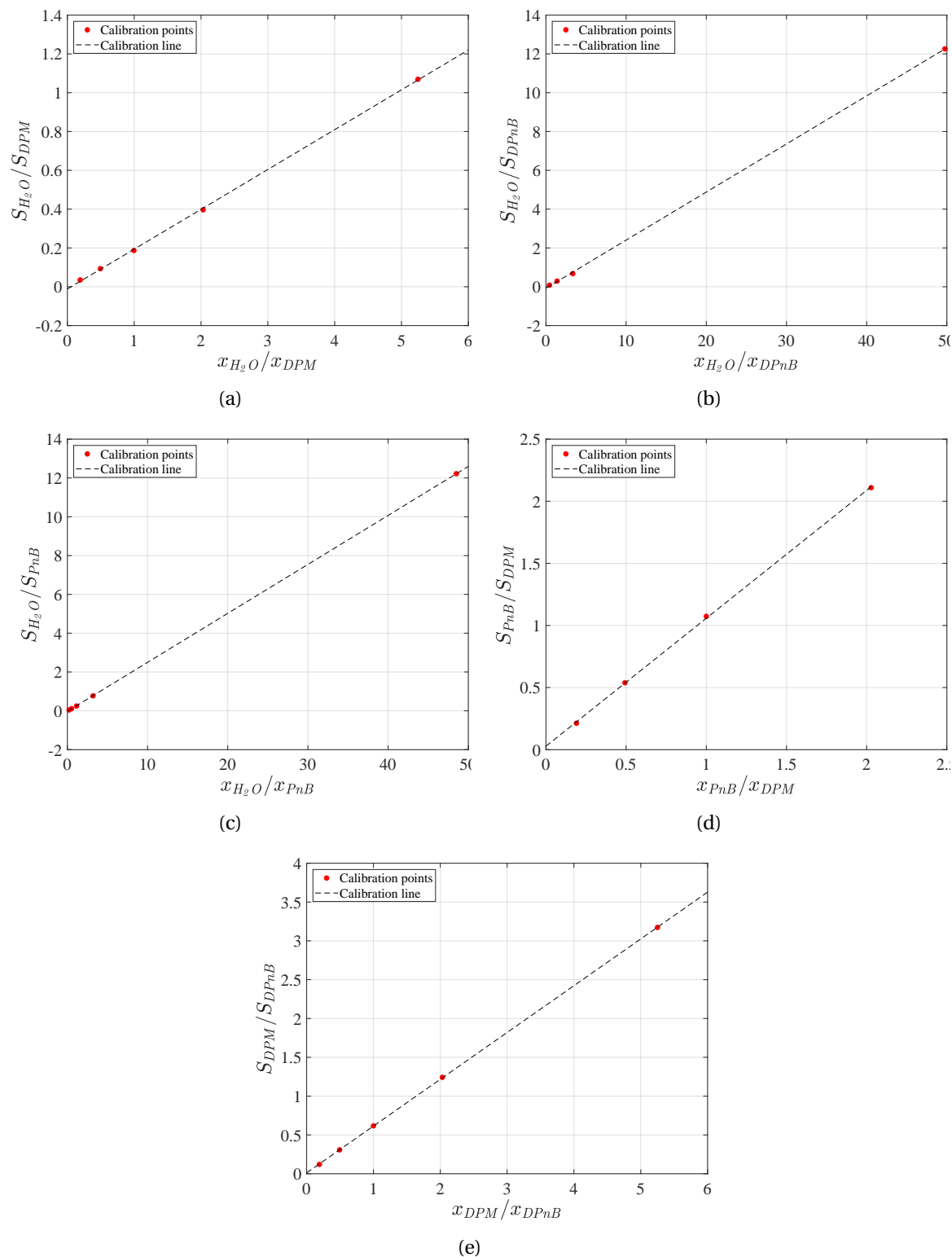


**Figure 2.5:** GC calibration lines for the mixtures: a)  $H_2O+DPM$ ; b)  $H_2O+DPnB$ ; c)  $H_2O+PnB$ ; d)  $PnB+DPM$ ; e)  $DPM+DPnB$

Once the calibration done, it becomes possible to determine the unknown molar fractions  $x_1$  and  $x_2$  of mixture components by solving the following system of equations (2.3):

$$\begin{cases} A \frac{x_1}{x_2} = \frac{S_1}{S_2} \\ x_1 = 1 - x_2 \end{cases} \Rightarrow \begin{cases} x_2 = \frac{1}{1 + A \frac{S_1}{S_2}} \\ x_1 = 1 - x_2 \end{cases} \quad (2.3)$$

with  $\frac{S_1}{S_2}$ , the peak surface ratio (value obtained using the GC) and  $A$ , the slope of the calibration line.

### 2.1.3 Experimental measurements workflow

One of the biggest problems that we have encountered in our study was a lack of experimental data in the literature for our compounds and their mixtures. For instance, in their technical leaflet, [BASF \(2017\)](#) provides some vapor pressure data for DPM, however, as stated in this document, these data were measured or estimated by the company to give their customers a rough idea of the DPM properties, so they provide no guarantee of properties in the legal sense. As for DPnB and PnB, there is not any data available in the literature related to vapor pressure or VLE of mixtures containing these compounds. Therefore, these data were measured for the first time.

As pure compounds, the VLE of mixtures were measured using the same experimental setup and procedure. The only one difference is that for mixtures, for each temperature, one should obtain multiple points having different composition in order to construct the phase diagram. We have measured the VLE for 6 binary mixtures in total, 3 of them were aqueous solutions of DPM, DPnB and PnB, another 3 mixtures were combinations of glycol ethers (PnB+DPM, DPM+DPnB and PnB+DPnB). Finally, a VLE of quaternary mixture H<sub>2</sub>O+ARCACLEAN was measured as well. For this particular system, the composition of glycol ethers was maintained constant according to the ARCACLEAN formula (Table 1.2) and only the water composition was altered. This allowed us to obtain the VLE data for a real mixture that was formed in the dry cleaning machine.

#### 2.1.3.1 Pure compounds vapor pressure

The measurements for DPM, DPnB and PnB are presented in Table C.1, Appendix C. While reporting pure compounds vapor pressure data, it is always very useful to provide some correlation with parameters, for instance, the widely used Antoine equation which is written in the next form:

$$\log_{10} P_{vap} = A - \frac{B}{T + C} \quad (2.4)$$

with  $A, B$  and  $C$ , the Antoine parameters. For the components of our interest, these parameters were obtained by the fitting to the experimental data in the temperature range 283.15 K–363.15 K according to the objective function 2.5, and can be found in Table 2.1 below.

$$F_{obj} = \sum_n \left( \frac{P_{exp} - P_{calc}}{P_{exp}} \right)^2 \quad (2.5)$$

The overall mean deviation in pressure is written as:

$$\delta P/P[\%] = \frac{1}{N} \sum \left( \frac{P_{exp} - P_{calc}}{P_{exp}} \right) \quad (2.6)$$

where  $N$  is the number of experimental points.

Figure 2.6 demonstrates a very good agreement between experimental results and the Antoine equation for all three pure compounds.

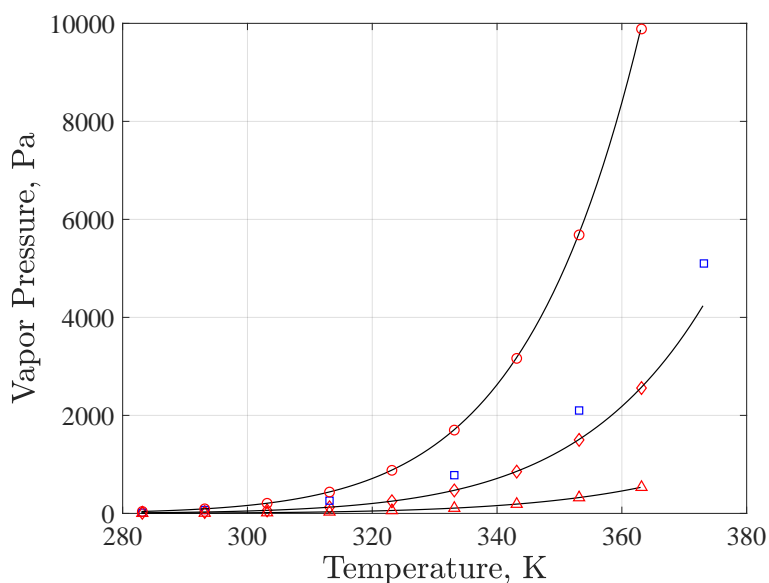


**Figure 2.6:** Measured vapor pressures for pure compounds and their correlation with the Antoine equation: DPM ( $\diamond$ ); DPnB ( $\triangle$ ); PnB ( $\circ$ ); DPM Technical Leaflet from (BASF, 2017) ( $\square$ ) - for comparison; Antoine equation (—)

**Table 2.1:** Antoine coefficients for DPM, DPnB et PnB ( $T[K]$ ,  $P[Pa]$ ) and the absolute mean pressure deviation

Component	Temperature [K]	A	B	C	$\delta P/P$ , %
DPM	283,15÷363,15	11,6	2974	0,01141	0,697
DPnB	283,15÷363,15	10,45	2805	0,09988	0,084
PnB	283,15÷363,15	12,49	3084	0,002486	0,583

### 2.1.3.2 VLE and VLLE of aqueous binary mixtures

First of all, the VLE was measured for H<sub>2</sub>O+DPM system in the temperature ranging from 283.15 K to 363.15 K. As expected, this mixture was completely miscible in the whole range of compositions. Generally, this system was quite stable during measurements (the pressure value change ratio was close to zero).

The mixtures H<sub>2</sub>O+DPnB and H<sub>2</sub>O+PnB are partially miscible by nature. Therefore, in this case we talk about a vapor-liquid-liquid equilibrium (VLLE). The miscibility gap can easily be recognized in the phase diagram by the points which have the different composition but the same vapor pressure. In this work, the composition of aqueous and organic phases in the non miscible region were not measured, so the result is reported in terms of total system pressure as a function of overall water mole fraction. These mixtures were stable as well, but a more deep primary degassing<sup>3</sup> was needed for PnB.

The results for all the aqueous mixtures are collected together and presented in Table C.2, Appendix C, and will be discussed in Section 2.3.

### 2.1.3.3 VLE of organic binary mixtures

Next, the VLE for organic mixtures containing DPM, DPnB and PnB were measured at the same temperature range. All the mixtures (PnB+DPM, DPM+DPnB and PnB+DPnB) were completely miscible. The distinctive feature of these systems is their extremely low vapor pressure (up to 10<sup>-4</sup> bar at low temperatures). This fact requires a particular attention and thoroughness while performing measurements. The degassing time has a key role in the quality of the result as the slightest amount of non-condensable gases or impurities in the sample can easily perturb the measurements.

<sup>3</sup>By the primary degassing we consider a degassing of the pure compound prior to sample preparation

For example, let us consider the system PnB+DPM. This system has demonstrated a very unstable character (especially when PnB was a majority component) during the experiment so the measurements were complicated. The measurements at low temperatures were relatively stable, but starting from 313,15 K the pressure value of the MKS sensor was changing quickly and was never stabilizing. As a result, the obtained experimental points were incorrectly placed on the phase diagram. This issue was fixed by increasing considerably the sample degassing time and we were able to correct certain points. As this system has a very low vapor pressure, there was no risk that the sample composition will be modified.

The same problem was encountered for PnB+DPnB system, but with much less effect.

As for DPM+DPnB, this system was the most stable among all tested systems. The pressure value was almost constant during 16 minutes of measurement.

Table C.3, Appendix C presents the results of the VLE measurements for PnB+DPM, DPM+DPnB and PnB+DPnB systems. These results will be discussed in Section 2.3.

#### 2.1.3.4 VLE of the quaternary mixture ARCACLEAN + water

The final point of the present experimental study was to obtain data for mixtures having compositions close to those occurring in the dry cleaning device. Having these data is essential and mandatory for performing any calculations and design of the pervaporation unit.

For these measurements, the samples of the ARCACLEAN solvent mixed with different water compositions were prepared, resulting to quaternary mixtures of Water+DPM+DPnB+PnB. The original ARCACLEAN formula was, of course, preserved (60%wt DPM, 30%wt DPnB and 10%wt of PnB). The samples were prepared with a small excess of water (about 2%wt) in order to take into account the losses during the degassing and thus to obtain the desired compositions for measurements. The water amount in samples was checked by the GC after the experiment<sup>4</sup>. All the measurements were stable and did not show any particular issue.

The results for the quaternary mixture are presented in Table C.4, Appendix C and will be discussed and detailed in Section 2.3.

---

<sup>4</sup>As water has a much higher vapor pressure than all glycol ethers, the original formula of the ARCACLEAN solvent was not perturbed

## 2.2 Thermodynamic modelling of phase equilibria occurring in H<sub>2</sub>O+ARCACLEAN mixtures

### 2.2.1 Pure compounds parameters estimation

#### 2.2.1.1 Definition of the equation of state parameters

The physical properties of pure components were estimated using the Peng-Robinson equation of state (Peng and Robinson, 1976):

$$P = \frac{RT}{v - b} - \frac{a}{v^2 + 2bv - b^2} \quad (2.7)$$

for which, in case of pure components, the attractive term  $a$  and the covolume  $b$  are obtained from the critical temperature and pressure of the compound of interest,  $T_c$  and  $P_c$ , as:

$$a = 0.45724 \frac{R^2 T_c^2}{P_c^2} \alpha(T_r) \quad \text{and} \quad b = 0.0778 \frac{RT_c}{P_c} \quad (2.8)$$

with  $T_r = T/T_c$ , a reduced temperature and  $\alpha(T_r)$ , a function depending on temperature. It is extremely important to choose the appropriate  $\alpha(T_r)$  function for representing the properties of pure compounds in vapor and liquid phases. In the articles (Neau et al., 2009a,b) an exhaustive theoretical analysis of different alpha functions was done in a wide range of temperatures and pressures. It was proven in the above mentioned study, that the generalized Soave function (Equation (2.9)) (Robinson and Peng, 1978) provides the most satisfactory vapor pressure representation together with Peng-Robinson EoS in the range of temperatures and pressures generally used in chemical engineering applications. That was the first reason of considering namely this function in the present thesis:

$$\alpha(T_r) = [1 + m(1 - T_r^\gamma)]^2 \quad (2.9)$$

In the above Equation, it is necessary to know the critical temperature  $T_c$  as well as the parameters  $\gamma$  and  $m$ . When calculating the  $\alpha(T)$  function for any compound, a value of  $\gamma = 0.5$  (Soave, 1972) can be considered as a classical estimation. For the  $m$  parameter, a piecewise expression was proposed by Robinson and Peng (1978). The  $m$  parameter is expressed by the 2<sup>nd</sup> or 3<sup>rd</sup> order polynomial correlation to the acentric factor  $\omega$ . One should choose the appropriate correlation for substances whose acentric factor is lower than or greater than

that of n-decane:

$$\begin{aligned} m &= 0.37464 + 1.54226\omega - 0.26992\omega^2 & \text{if } \omega < 0.49 \\ m &= 0.379642 + 1.48503\omega - 0.164423\omega^2 + 0.16666\omega^3 & \text{if } \omega \geq 0.49 \end{aligned} \quad (2.10)$$

Nevertheless, in case of bad estimations, the  $\gamma$  and  $m$  parameters can be modified in a reasonable range ( $0 < \gamma < 1$ ) (Neau et al., 2009b) in order to improve the vapor pressure representation.

To summarize, at this point, in order to calculate the Peng-Robinson EoS pure compound parameters  $a$  (attractive term) and  $b$  (covolume), one needs to know the critical temperature and pressure of a compound,  $T_c$ ,  $P_c$ , the parameters of the Soave function,  $\gamma$ ,  $m$ , and the acentric factor  $\omega$ .

In order to improve the volume estimations by the Peng-Robinson EoS, a volumetric correction  $c$  of Peneloux et al. (1982) was applied. The procedure of this correction is the same for different models from literature. Firstly, the equation of state is solved and the obtained volume  $v_{eos}$  is considered to be  $v_{eos} = v$ . Then, the final volume is found as  $v_{final} = v_{eos} - c$ .

There are several correction expressions reported by Peneloux et al. (1982). The first one:

$$c = 0.40768(RT_c/P_c)(0.29441 - Z_{RA}) \quad (2.11)$$

uses the Rackett compressibility factor  $Z_{RA}$  (Spencer and Danner, 1972, 1973) obtained from the saturated density data:

$$\ln Z_{RA} = \frac{\ln(1/\rho_s) + \ln(P_c/RT_c)}{1 + (1 - T_r)^{2/7}} \quad (2.12)$$

A second correction is obtained in case if  $Z_{RA}$  is not known, so it can be substituted by the critical compressibility factor  $Z_c$  (Yamada and Gunn, 1973) (calculated from the experimental critical volumes) giving fairly reasonable results:

$$Z_c = 0.2920 - 0.0967\omega \quad (2.13)$$

### 2.2.1.2 Application of the Peng-Robinson EoS to glycol ethers

From the equations described above, one can notice that the pure components critical parameters  $T_c$ ,  $P_c$  and the acentric factor  $\omega$  are required in order to calculate the component



thermodynamic and transport properties using a cubic equation of state.

### Critical properties

The experimental critical properties of DPM, DPnB and PnB are not available in the literature. Therefore, they should be estimated using one of the predictive methods proposed during last several decades. The first successful *group contribution* method for critical properties estimation was proposed by Lydersen (1955). Since that time, more experimental values were reported and efficient statistical techniques have been developed that allow determination of alternative group contributions and optimized parameters. Among them, the methods of Joback (1984), Constantinou and Gani (1994), Wilson and Jaspersion (1996) and Marrero-Morejón and Pardillo-Fontdevila (1999). The most accurate comparison of these methods was done by Poling et al. (2001). Here, we briefly describe the most important of them.

**Method of Joback (J).** This method was developed by the reevaluation and the addition of some new functional groups to the Lydersen group contribution method. The proposed relation for critical parameters is:

$$T_c[K] = T_b \left[ 0.584 + 0.965 \left\{ \sum_k N_k(tck) \right\} - \left\{ \sum_k N_k(tck) \right\}^2 \right]^{-1} \quad (2.14)$$

$$P_c[bar] = \left[ 0.113 + 0.0032 N_{atoms} - \sum_k N_k(pck) \right]^{-2} \quad (2.15)$$

where  $tck$ ,  $pck$  are the contributions. The normal boiling temperature  $T_b$  can be taken from experiment or estimated, however, if one uses the estimated value, the error can increase significantly. The method is quite reliable for estimating the  $T_c$ . For  $P_c$ , the error is larger for larger molecules and the estimates can be either too high or too low. The Joback method has no obvious improvements.

**Method of Constantinou and Gani (C&G).** This is an advanced group contribution method based on UNIFAC groups. It allows using more sophisticated expressions for critical properties and also the estimations of Second Order level. At the First Order level, the proposed functions cannot distinguish special configurations such as isomers, multiple groups located close together, resonance structures etc. These limits are overcome in the Second Order estimations. For the critical properties, the Constantinou & Gani expressions are

$$T_c[K] = 181.128 \ln \left[ \sum_k N_k(tc1k) + W \sum_j M_j(tc2j) \right] \quad (2.16)$$

$$P_c[bar] = \left[ \sum_k N_k(pc1k) + W \sum_j M_j(pc2j) + 0.10022 \right]^{-2} + 1.3705 \quad (2.17)$$

where  $N_k$  is the number of First Order groups of type  $k$  in the molecule.  $tc1k$  and  $pc1k$  are the First Order group contributions. Equally,  $M_j$  is the number of Second Order groups of type  $j$  in the molecule and  $tc2j, pc2j$  are the Second Order group contributions. The parameter  $W$  is set to be zero for First Order contribution calculations and unity for Second Order calculations. It is important to say that this method does not require a value for  $T_b$ .

Unlike the Joback method, the Constantinou & Gani method is reliable for estimation of all critical parameters and for molecules of all sizes, though some significant errors for  $T_c$  and  $P_c$  could occur in case of smaller substances. As reported in the original paper (Constantinou and Gani, 1994), the largest errors occur for the very smallest and the very largest molecules. Second Order estimations can improve the accuracy 1 to 3 times as often as it can degrade them.

**Method of Wilson and Jasperson (W&J).** This method uses, in its First Order, the atomic contributions along with boiling point and number of rings, while the Second Order also includes the group contributions. Comparing to Joback and Constantinou & Gani methods, there was no large difference in errors reported between small and large molecules. According to the comparison tables published by Poling et al. (2001), the Wilson & Jasperson method is very reliable for all the critical properties estimation. Even if this method is the simplest of those considered in this work, it stays remarkable in its accuracy. The First and Second Order methods use the following equations:

$$T_c = T_b / \left[ 0.048271 - 0.019846N_r + \sum_k N_k(\Delta tck) + \sum_j M_j(\Delta tcj) \right]^{0.2} \quad (2.18)$$

$$P_c = 0.0186233 T_c / [-0.96601 + e^Y] \quad (2.19)$$

$$Y = -0.00922295 - 0.0290403N_r + 0.041 \left[ \sum_k N_k(\Delta pck) + \sum_j M_j(\Delta pcj) \right] \quad (2.20)$$

where  $N_r$  is the number of rings in the compound,  $N_k$  is the number of atoms fo type  $k$  ith First Order atomic contributions  $\Delta tck$  and  $\Delta pck$  while  $M_j$  is the number of groups of type  $j$

with Second Order group contributions  $\Delta tcj$  and  $\Delta pcj$ .  $T_b$  is the normal boiling point temperature of the compound (at 760 mmHg).

Basing on the comparison stated above, the Wilson & Jasperson method was firstly used in order to estimate the critical properties of DPM, DPnB and PnB. Values of the contributions are listed in Table B.2, Appendix B according to following facts:

1. DPM has 7 atoms of -C, 16 atoms of -H, 3 atoms of -O and there are no rings. For groups, there is 1 -OH for "C5 or more";
2. DPnB has 10 atoms of -C, 22 atoms of -H, 3 atoms of -O and there are no rings. For groups, there is 1 -OH for "C5 or more";
3. PnB has 7 atoms of -C, 16 atoms of -H, 2 atoms of -O and there are no rings. For groups, there is 1 -OH for "C5 or more".

### Pitzer acentric factor

Along with the critical parameters, a commonly used constant for properties estimation is the Pitzer acentric factor, originally defined by Pitzer (1955) as

$$\omega = -\log_{10} \left[ \lim_{T_r=0.7} (P_{vap}/P_c) \right] - 1.0 \quad (2.21)$$

To obtain values for  $\omega$  from its initial definition, one must know the critical parameters  $T_c$ ,  $P_c$  and the vapor pressure  $P_{vap}$  at the reduced temperature,  $T/T_c = 0.7$ . Usually, a value of the acentric factor is obtained by using an accurate equation for  $P_{vap}(T)$  along with the required critical properties.

As for DPM, DPnB and PnB, along with the critical parameters  $T_c$ ,  $P_c$ , the experimental value for the acentric factor is not available and should also be estimated. One of the most reliable methods to estimate an unknown acentric factor is called Ambrose-Walton corresponding states method (Ambrose and Walton, 1989). It uses the Pitzer expansion:

$$\omega = -\frac{\ln(P_c/1.01325) + f^{(0)}(T_{br})}{f^{(1)}(T_{br})} \quad (2.22)$$

where  $T_{br} = T_b/T_c$  and  $f^{(0)}$  and  $f^{(1)}$  are the analytical expressions proposed by Ambrose and Walton:

**Table 2.2:** Critical properties and Pitzer acentric factor of DPM, DPnB and PnB estimated using the *Wilson and Jasperson (1996)* method (1st and 2nd Order estimation)

Compound	$T_b$ [K]	$T_c$ (1st) [K]	$T_c$ (2nd) [K]	$P_c$ (1st) [bar]	$\omega$
DPM	461,15	627,8832	622,1666	26,9307	0,7022
DPnB	503,15	655,5000	655,6945	25,0000	0,7996
PnB	444,15	616,9559	610,7654	28,0563	0,5167

$$f^{(0)} = \frac{-5.97616\tau + 1.29874\tau^{1.5} - 0.60394\tau^{2.5} - 1.06841\tau^5}{T_{br}} \quad (2.23)$$

$$f^{(1)} = \frac{-5.03365\tau + 1.11505\tau^{1.5} - 5.41217\tau^{2.5} - 7.46628\tau^5}{T_{br}} \quad (2.24)$$

with  $\tau = 1 - T_{br}$ . Here,  $P_c$  is in bars while  $T_b$  and  $T_c$  are both absolute temperatures.

The results of the critical properties and the acentric factor estimation are presented in Table 2.2. Both the estimations of the First and Second Orders were obtained. However, as there were no literature data containing the experimentally obtained values, it was impossible for us to conclude which estimation, First or Second Order, to use and if, in general, the obtained results were acceptable. Nevertheless, according to the original papers recommendations, the Second Order estimations were used for all calculations in the Peng-Robinson EoS.

### 2.2.1.3 Fitting of estimated pure compound properties

The pure compound properties determined further with the Peng-Robinson EoS and compared to experimental values from Table C.1 brought us to the following conclusions. First of all, it was noticed that the First Order critical properties estimations provided better results for all the compounds than the Second Order estimations. The contribution due to the molecule size (in terms of the "-OH" groups) slightly underestimates the critical temperature. Thus, all the further calculations were done using the First Order estimations as a starting point. The results are presented in Figure 2.7.

The error between experimental and calculated data was found as:

$$error, \% = \frac{P_{exp} - P_{calc}}{P_{exp}} \cdot 100 \quad (2.25)$$

where  $P_{exp}$  and  $P_{calc}$  are the experimental and calculated vapor pressures, respectively.

For DPM, using presented in Table 2.2 critical parameters yields to satisfactory results for vapor pressure in the whole temperature range. The vapor pressures of DPM and PnB are roughly of the same order of magnitude. As for DPnB, its high errors for lower temperatures are explained by the extremely low vapor pressures, where a slight difference of several Pa between the experiment and estimation yields to a huge error.

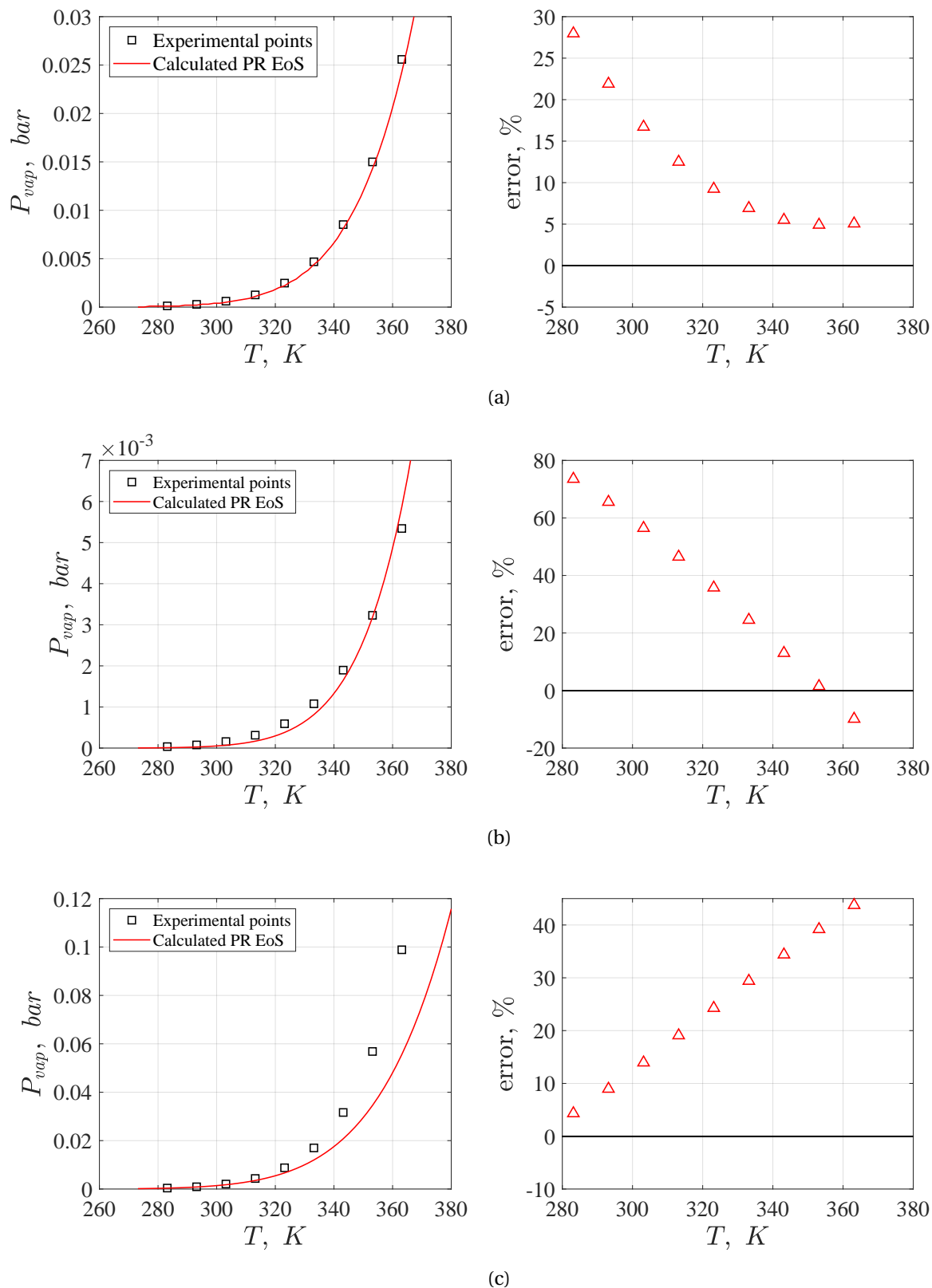


**Figure 2.7:** Vapor pressures calculated using the PR EoS and estimated  $T_c$ ,  $P_c$  and  $\omega$  from Table 2.2: a) DPM: error = 12.3%; b) DPnB: error = 36.3%; c) PnB: error = 24.15%

The results were less encouraging for the other compounds and especially for PnB. It can be seen from Figure 2.7, that the errors become significant for higher temperatures. For that reason, it was decided to verify if other estimation methods will provide similar results. We have used the Joback and Constantinou & Gani methods and have compared them with the estimations made previously with Wilson & Jasperson method. The group contribution parameters used for both methods can be found in Tables B.1 and B.3, Appendix B. Table 2.3 compares the obtained results between these methods.

**Table 2.3:** Comparison of the critical properties of PnB estimated using different group contribution methods

Method	$T_c$ (1st)	$T_c$ (2nd)	$P_c$ (1st)	$P_c$ (2nd)
W&J method	616,9559	610,7654	28,0563	-
C&G method	654,8136	640,6051	25,4186	26,4884
J method	637,45	-	30,6255	-

It is remarkable from the above Table that these methods provide the results with a significant difference. One should emphasize once more that there were no critical properties published for PnB, so the only one solution was to integrate all the estimations into the EoS and perform the vapor pressure calculation. The results were, however, far from being evident. On one hand, some of the methods apparently overestimate the critical temperature and underestimate the critical pressure. On the other hand, the vapor pressures were overestimated for high temperatures and underestimated for low temperatures and vice versa. A possible conclusion here could be that none of the above described group contribution methods are sufficient for a correct estimation.

Finally, we have adjusted the values of  $\omega$  and  $P_c$  in order to minimize the error in vapor pressures. Different combinations of the results from Table 2.3 were used as initial points for minimization. If needed, the values of  $T_c$  were adjusted as well. All the properties were, of course, adjusted in a reasonable range of values (for example, it is clear that the  $P_c$  cannot be 80 bar, or, the PnB acentric factor cannot be higher than those of DPnB and DPM due to the respective molecule size). The results obtained by this approach have considerably improved the representation of vapor pressures of all the three ethers and not only of PnB. Only for DPM the adjusted values were almost identical to those estimated using the W&J method. These new and last obtained values are presented in Table 2.4. These values will be further used for the VLE predictions in the NRTL-PR model and the results will be presented in the following sections.

**Table 2.4:** Final estimated critical properties of DPM, DPnB and PnB providing the minimal error in vapor pressures

Compound	$T_b$ [K]	$T_c$ [K]	$P_c$ [bar]	$\omega$
DPM	461,1500	626,8800	27,8000	0,7022
DPnB	503,1500	655,9000	24,5000	0,7996
PnB	444,1500	619,5000	38,3000	0,5800

Now, if the vapor pressures of DPM, DPnB and PnB will be estimated using the parameters from Table 2.4, one will notice that the errors of the Figure 2.7 will be reduced. At the same time, some of the  $P_{vap}$  representation problems still persist in case of DPnB and PnB, and namely the simultaneous representation of their vapor pressures in both low and high temperature ranges. In fact, if we try to correctly represent the vapor pressures in the low temperature range, the high temperature range will have higher error and vice versa. This phenomena can occur for some compounds (for example, the monoethylene glycol). The reason for that is actually hidden in the  $\alpha(T)$  function of the equation of state as this function represents the temperature influence.

In their work, [Neau et al. \(2009b\)](#) have illustrated, using multiple examples, the influence of different  $\alpha(T)$  functions on the vapor pressure representation. It was also proven there, that, for the PR EoS, the original Soave (Equation (2.9)) function with  $\gamma = 0.5$  yields to the best results. When it is not possible to satisfactorily represent the vapor pressures in both low and high temperature ranges simultaneously, the  $\gamma$  parameter becomes adjustable and its value can be estimated by fitting to the experimental data. In this case, we talk about the *generalized* Soave function. Moreover, in some cases, not only  $\gamma$  parameter can be fitted, but also the  $m$  parameter (Equation (2.10)).

These parameters were fitted for DPnB and PnB respecting the condition  $0 < \gamma < 1$ . Using this method, the errors for these compounds were reduced more and the vapor pressure representation became more homogeneous in the whole temperature range. Thus, the errors obtained at this point are mostly due to very low vapor pressures. It is well known that the cubic equations of state were initially designed for high vapor pressure systems, such hydrocarbons, and it is sometimes very hard to obtain a perfect representation of systems having very low pressures. Having taken all the previous hypotheses into account, our main intention was to obtain such  $\gamma$  and  $m$  values that yield to the lowest errors for the temperatures that will be further used in pervaporation process as the operating conditions, namely 323.15 and 343.15 K. The final results are presented in Figure 2.8. The final values of the Soave  $\gamma$  and  $m$  parameters, that will be used for further calculations, are as follows:



- DPM:  $\gamma = 0.5$ ,  $m = 1.3471$ ;
- DPnB:  $\gamma = 0.9$ ,  $m = 0.8886$ ;
- PnB:  $\gamma = 0.18$ ,  $m = 2.9958$ ;

Furthermore, in Section 2.2.2.3 the principle of the NRTL-PR model will be explained. It will be also shown that this model requires the interaction parameters estimated for group contribution. The parameters for one of the functional groups, namely the group "-O-" (ethers) were not yet included into the NRTL-PR group contribution parameters matrix. Therefore, they were calculated using a compilation of different VLE data containing the ethers and glycol ethers.

At the current point, we do not intend to give the details of this calculation but only to present the critical properties of the compounds used thereafter. Table 2.5 presents these critical properties together with the literature sources they were taken from.

**Table 2.5:** Literature critical properties of the ethers and glycol ethers used in Section 2.2.2.3 for "-O-" group interaction energies calculation in the NRTL-PR model

Compound	$T_b$ [K]	$T_c$ [K]	$P_c$ [bar]	$\omega$	Source
Diisopropyl ether	341,4	500,32	28,32	0,3286	NIST
Diethyl ether	307,7	466,7	36,4	0,281	(Yaws, 2008)
Di-n-propyl ether	363	530,6	30,28	0,369	(Yaws, 2008)
Butyl ethyl ether	364,7	526,03	28,25	0,543	(Yaws, 2008)
Methyl tert-butyl ether	328,2	496,4	33,97	0,2756	NIST
Dimethyl ether	248,31	400,1	54	0,2	(Poling et al., 2001)
Propylene glycol methyl ether	391,7	579,8	43,13	0,475	NIST + (Yaws, 2008)
Ethylene glycol methyl ether	397,6	597,6	51,5	0,444	(Hatami et al., 2011)
Ethylene glycol ethyl ether	408,3	604,52	36,2	0,454	(Hatami et al., 2011)

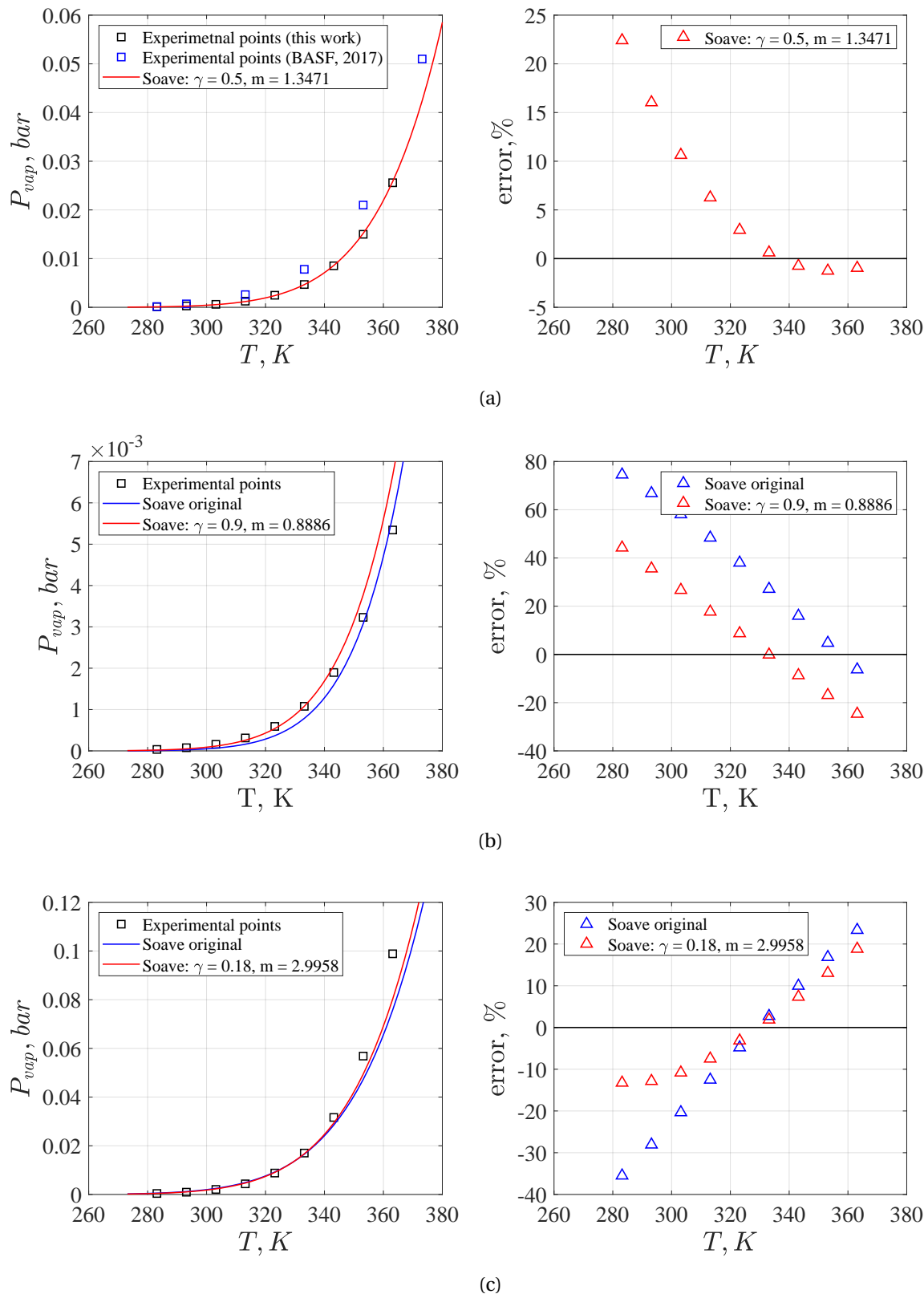


**Figure 2.8:** Vapor pressures calculated using the PR EoS and  $T_c$ ,  $P_c$  and  $\omega$  from Table 2.4 and final  $\gamma$ ,  $m$  parameters: a) DPM: error = 6.88%; b) DPnB: error = 20.36%; c) PnB: error = 9.85%

## 2.2.2 Prediction of low-pressure phase equilibria using the NRTL-PR model

The NRTL-PR model (Neau et al., 2010b) was specially developed to predict both vapor-liquid and liquid-liquid equilibria of highly non-ideal systems containing very asymmetric compounds, for example, water, glycols and hydrocarbons. It is based on the coupling of the Peng-Robinson equation of state (Equation (2.7)) and the generalized NRTL model (Equation (2.36)) using the  $EoS/G^E$  approach. The main advantages of this model are listed below:

- NRTL-PR is a predictive model, so it does not depend on the experimental points;
- It is based on the Peng-Robinson equation of state, which allow both vapor-liquid and liquid-liquid equilibria to be calculated;
- It is capable to study the stability of each calculated point;
- Designed to represent strongly non-ideal systems made of big size molecules.

### 2.2.2.1 Generalized NRTL model

The generalized NRTL model, for its part, was derived from the lattice-two fluid theory and serves to represent the VLE and LLE of non-ideal mixtures mainly at low pressures (Neau et al., 2010a). The main difference between the original and generalized NRTL models is that the latter model takes into consideration the differences in size and shape between compounds. These two effects are suggested to be the deviations from system ideality.

As a starting point, one should consider the Helmholtz energy of mixing at constant volume, which is expressed as:

$$A^{MV} = -TS^{MV} + U^{MV} \quad (2.26)$$

This expression leads to the excess Helmholtz energy at constant volume:

$$A^{EV} = -TS^{EV} + U^{EV} \quad \text{with} \quad S^{EV} = S^{MV} + R \sum_i n_i \ln x_i \quad (2.27)$$

with  $S^{EV}$  and  $U^{EV}$  are the excess entropy and energy, respectively, and  $U^{EV} = U^{MV}$ .

The *combinatorial* part, or, in other words, a non-ideal entropy of mixing, is represented by a general Staverman-Guggenheim equation for athermal mixtures of molecules of arbitrary size and shape (Neau et al., 2010a):

$$S^{EV} = -R \left( \sum_i n_i \ln \frac{\phi_i}{x_i} + \frac{z}{2} \sum_i n_i q_i \ln \frac{\theta_i}{\phi_i} \right) \quad (2.28)$$

with  $\phi_i$  and  $\theta_i$ , the volume and surface fractions of a molecule  $i$ , respectively. The coordination number,  $z$ , is usually fixed to be equal to 10 (Poling et al., 2001). Here, we have also:

$$\phi_i = \frac{x_i r_i}{r} \quad \text{and} \quad \theta_i = \frac{x_i q_i}{q} \quad \text{with} \quad r = \sum_l x_l r_l, \quad q = \sum_l x_l q_l \quad (2.29)$$

with  $r_i$  and  $q_i$ , the volume and surface area factors, respectively. These parameters are calculated using the UNIFAC subgroup parameters  $R_k$  and  $Q_k$  (in the present work, taken from (Hansen et al., 1991) and also presented in Table 2.6, Section 2.2.2.3) as:

$$r_i = \sum_k v_{ik} R_k \quad \text{and} \quad q_i = \sum_k v_{ik} Q_k \quad (2.30)$$

where  $v_{ik}$  is the number of subgroups  $k$  in a molecule  $i$ .

As for the *residual* part, the excess energy of mixing at constant volume,  $U^{EV}$ , is represented by the next equation:

$$U^{EV} = n \sum_i x_i q_i \frac{\sum_j x_j q_j G_{ji} \Gamma_{ji}}{\sum_l x_l q_l G_{li}} \quad \text{with} \quad \Gamma_{ji} = \frac{z}{2} (U_{ji} - U_{ii}) \quad (2.31)$$

In the Equation (2.31), the term  $\Gamma_{ji}$  is the configurational energy which is needed to replace  $z/2$  pair interactions  $i-i$  by  $z/2$  pair interactions  $j-i$ . The term  $G_{ji}$  is called a molecular repartition coefficient, which is expressed as:

$$G_{ji} = \exp \left[ -(z/2) \alpha_0 (U_{ji} - U_{ii}) / RT \right] = \exp (-\alpha_0 \Gamma_{ji} / RT) \quad (2.32)$$

with  $\alpha_0$ , a non-randomness factor, assumed to be constant. It was proposed by the authors of the original NRTL model to fix this parameter as  $\alpha_0 = 0.2$  (Renon and Prausnitz, 1968), or, in case of a strong demixing solutions, as  $\alpha_0 = -1$  (Marina and Tassios, 1973)<sup>5</sup>. These values can be used in generalized NRTL model as well. The terms  $U_{ji}$  and  $U_{ii}$  are the configurational energies of one pair interaction.

According to the excess Gibbs energy principle, one can reformulate the Equation (2.27) to the next form:

---

<sup>5</sup>Namely this value was used in the present thesis

$$g^E = g_{combinatorial}^E + g_{residual}^E \quad (2.33)$$

with the combinatorial and residual parts equivalent to

$$g_{combinatorial}^E = -TS^{EV}/n \quad \text{and} \quad g_{residual}^E = U^{EV}/n \quad (2.34)$$

The Equation (2.27) can now be rewritten to the formulation of the generalized NRTL model:

$$g^E = RT \left[ \sum_i x_i \ln \frac{r_i}{r} + \frac{z}{2} \sum_i x_i q_i \ln \frac{q_i r}{q r_i} \right] + \sum_i x_i q_i \frac{\sum_j x_j q_j G_{ji} \Gamma_{ji}}{\sum_l x_l q_l G_{li}} \quad (2.35)$$

As it was stated in (Neau et al., 2010a), the combinatorial term can be simplified, as the ratio  $q_i/r_i$  become constant and small for long alkane chains, so the final expression of the generalized NRTL model is written as:

$$g^E = RT \sum_i x_i \ln \frac{r_i}{r} + \sum_i x_i q_i \frac{\sum_j x_j q_j G_{ji} \Gamma_{ji}}{\sum_l x_l q_l G_{li}} \quad (2.36)$$

The presented generalized NRTL model is able to satisfactorily represent highly non-ideal systems, allowing physically meaningful estimations of the binary interaction parameters. Due to the fact, that this model is derived from the two-liquid lattice fluid theory and takes into account the combinatorial impact, it is suitable for predicting the low-pressure vapor-liquid equilibria of mixtures containing asymmetric due to the size and polar compounds (which is exactly the case of aqueous mixture of ARCACLEAN solvent, studied in this work).

### 2.2.2.2 Generalized reference state at constant volume GRS-CV

The  $EoS/G^E$  formalism is originated from the works of Vidal (1978) and was mainly developed for cubic equations of state. It signifies an important and major development for chemical engineering thermodynamics. This approach assumes that, in a given reference state, excess properties obtained from an EoS and from a low-pressure  $G^E$  model are equal. In principle, this should allow to define more physically meaningful mixing rules for the EoS parameters. Subsequently, the present approach was completed due to the following works:

1. Huron and Vidal (1979): with the infinite pressure reference state  $P_\infty$ ;

2. Mollerup (1986), Heidemann and Kokal (1990) and Michelsen (1990): with the zero pressure reference state  $P_0$  and the MHV1 (Modified Huron-Vidal 1<sup>st</sup> order) mixing rule;
3. Peneloux et al. (1989): with the constant packing fraction reference state.

Among all these reference states, the infinite pressure,  $P_\infty$ , and the zero pressure MHV1 mixing rules have been widely used in the literature either to develop completely predictive models or to allow the prediction of high-pressure phase equilibria from low-pressure parameters which have been obtained without using an EoS. It was demonstrated, however, in the work of Kontogeorgis and Vlamos (2000) that, contrary to the theory, the  $\alpha^M$  function, defined as a difference between the alpha function (Equation (2.47)) and the sum  $\sum_i x_i \alpha_i$  of the pure components, depend not only on the residual term  $g_{res}^E$  (Equation (2.31)) of the excess Gibbs energy model, but also on combinatorial contributions. Practically, predictive equation of state which are based on the zero pressure reference state (VTPR (Ahlers and Gmehling, 2002), UMR-PRU (Voutsas et al., 2006)), on the constant packing fraction (PPR78 (Jaubert and Mutelet, 2004)) or on the generalized reference state at constant volume (NRTL-PR (Neau et al., 2010b)) avoid this inconsistency as they assume that the Flory-Huggins term of the  $g^E$  model is equal to that of the EoS. However, if one would use low-pressure models with parameters determined without an EoS, the problem will still remain.

As a solution to the above problem, a generalized reference state at constant volume (GRS-CV) was proposed (Escandell et al., 2011). The authors proposed a mixing rule associated with the Peng-Robinson EoS. This mixing rule was then applied to the modelling of vapor-liquid equilibria for mixtures of hydrocarbons and polar or associating compounds, such as water and alcohols.

In the cubic equations of state, the compressibility factor is expressed as:

$$Z = \frac{Pv}{RT} = \frac{1}{1-\eta} - \frac{\alpha\eta}{(1+e_1\eta)(1+e_2\eta)} \quad \text{with} \quad \alpha = \frac{a}{bRT}, \quad \eta = \frac{b}{v} \quad (2.37)$$

where  $a$  and  $b$  are the attractive term and the covolume respectively,  $\eta$  and  $v$  are the packing fraction and a molar volume at a given temperature  $T$ . The terms  $e_1$  and  $e_2$  characterize the cubic equation of state (for a Peng-Robinson EoS,  $e_1 = 1 + \sqrt{2}$  and  $e_2 = 1 - \sqrt{2}$ ).

The attractive term  $a$  is obtained by assuming that, in a given reference state  $V_0$ , the excess Helmholtz energies at constant volume  $A^{EV}$ , derived from an EoS and from a low-pressure model, are equal. That gives:

$$\frac{A^{EV}(T, V^0, n)_{eos}}{nRT} = \frac{A^{EV}(T, x)}{nRT} \approx \frac{g^E(T, x)}{RT} \quad (2.38)$$

where  $g^E$  is the molar excess Gibbs energy at constant pressure.

As estimated from the equation of state, the excess Helmholtz energy at constant volume equals to:

$$A^{EV}(T, V^0, n)_{eos} = A^{res}(T, V^0, n) - \sum_i A_i^{res}(T, V_i^0, n_i) + RT \sum_i n_i \ln \frac{V_i^0}{V^0} \quad (2.39)$$

where  $V_i^0$  is the total volume of component  $i$  and  $n_i$  is its mole number.  $V^0 = \sum_i V_i^0$ .

If formulated with the respect to the cubic EoS (Equation (2.37)), the above equation becomes:

$$\frac{A^{EV}(T, V^0, n)_{eos}}{nRT} = - \sum_i x_i \ln \left( \frac{1 - \eta^0}{1 - \eta_i^0} \right) - \alpha C(\eta^0) + \sum_i x_i \alpha_i C(\eta_i^0) + \sum_i x_i \ln \frac{V_i^0}{V^0} \quad (2.40)$$

with:

$$C(\eta^0) = \frac{1}{(e_1 - e_2)} \ln \left( \frac{1 + e_1 \eta^0}{1 + e_2 \eta^0} \right) \quad \text{and} \quad C(\eta_i^0) = \frac{1}{(e_1 - e_2)} \ln \left( \frac{1 + e_1 \eta_i^0}{1 + e_2 \eta_i^0} \right) \quad (2.41)$$

so, as  $g^E \approx A^{EV}$ , it can now be assumed that:

$$\frac{g^E}{RT} = - \sum_i x_i \ln \left( \frac{1 - \eta^0}{1 - \eta_i^0} \right) - \alpha C(\eta^0) + \sum_i x_i \alpha_i C(\eta_i^0) + \sum_i x_i \ln \frac{V_i^0}{V^0} \quad (2.42)$$

The Equation (2.42) can be used to deduce all the literature reference states mentioned above in this paragraph. Hereinafter, the only basic principles of this deduction will be presented. The equations for  $g^E$  and  $\alpha^M$  for the literature models are summarized in the Chapter A.

1. Zero pressure reference state (Michelsen, 1990) can be obtained from the Equation (2.42) if one eliminates the volumes in the right hand side by assuming that the packing fractions  $\eta^0 = nb/V^0$  and  $\eta_i^0 = nb_i/V_i^0$  are equal. The functions  $C(\eta^0) = C(\eta_i^0)$  are fixed as a constant value  $C = 0.53$ .
2. At the infinite pressure reference state (Huron and Vidal, 1979), the packing fractions

$\eta^0$  and  $\eta_i^0$  tend to 1, so that:

$$\left(\frac{V_i^0}{V^0}\right)\left(\frac{1-\eta_i^0}{1-\eta^0}\right) \rightarrow 1 \quad \text{since at } P_\infty: \begin{cases} P_\infty V_i^0 \left(\frac{1-\eta_i^0}{nRT}\right) = Z_{i,P_\infty}^0 (1-\eta_i^0) \rightarrow 1 \\ P_\infty V^0 \left(\frac{1-\eta^0}{nRT}\right) = Z_{P_\infty}^0 (1-\eta^0) \rightarrow 1 \end{cases}$$

The same reference constants value  $C(\eta^0) = C(\eta_i^0) = C = 0.623$  is used.

3. Constant packing fraction approach (Peneloux et al., 1989) is based on the same principle as the zero pressure reference state, but using for the excess Gibbs energy the expression from the Equation (2.33). The combinatorial part is expressed by Flory-Huggins term in which the volume factors are calculated from the EoS covolumes.

It is considered in the GRS-CV approach that:

- The reference volumes  $V_i^0$  and  $V^0$  in the Equation (2.42) are directly expressed from the volume factors  $r_i$  and  $r$  from the  $g^E$  model and not from the covolumes  $b_i$  and  $b$  of the equation of state;
- To eliminate the volumes in the Equation (2.42), it is assumed that the packing fractions in the reference state satisfy the condition  $1 - \eta^0 = \prod (1 - \eta_i^0)^{x_i}$  and no more the classical equality  $\eta^0 = \eta_i^0$ ;
- As in the reference states previously described, the functions  $C(\eta^0) = C(\eta_i^0)$  are fixed at the same constant value  $C$ , giving the following expression for  $g^E$ :

$$\frac{g^E(T, x)}{RT} = C \left[ -\alpha + \sum_i x_i \alpha_i \right] + \sum_i x_i \ln \frac{r_i}{r} \quad (2.43)$$

and finally, to the following  $\alpha^M$  function:

$$\alpha^M = \alpha - \sum_i x_i \alpha_i = -\frac{1}{C} \left[ \frac{g^E}{RT} - \sum_i x_i \ln \frac{r_i}{r} \right] \quad (2.44)$$

This mixing rule is referred to as a "generalized" reference state mainly due to the  $C$  constant, which, in principle, can have any value (for example,  $C = 0.53$  or  $C = 0.623$  as in Michelsen (1990) and Huron and Vidal (1979) reference states). As for Peng-Robinson EoS, its value was chosen as  $C = 0.56$  (Neau et al., 2011).

The principle of application of the GRS-CV mixing rule to a generalized NRTL model and the NRTL-PR model is further discussed in Paragraph 2.2.2.3 of this Chapter.



### 2.2.2.3 Association of the generalized NRTL model with the Peng-Robinson EoS

The vapor-liquid equilibrium of the non-ideal systems can be predicted by coupling of the generalized NRTL model (Equation (2.36)) described before, and the cubic Peng-Robinson EoS (Equation (2.7)) basing on the generalized reference state at constant volume (GRS-CV) (Neau et al., 2011). The resulting predictive NRTL-PR model is reliable and simple. Its main advantage is that it depends on very few interaction parameters. The model allows a satisfactory prediction of excess enthalpies, vapor-liquid and liquid-liquid equilibria for mixtures of asymmetric compounds, such as hydrocarbons, water and glycols (Neau et al., 2010b).

In terms of the compressibility factor  $Z$ , the Peng-Robinson EoS is expressed as:

$$Z = \frac{Pv}{RT} = \alpha Q(\eta) \quad \text{with} \quad Q(\eta) = \frac{\eta}{1 + 2\eta - \eta^2}, \quad \eta = \frac{b}{v} \quad (2.45)$$

The attractive term  $a$  of the Equation (2.7) is obtained according to Section 2.2.2.2 and Equations (2.33) and (2.44):

$$\alpha = \frac{a}{bRT} = \sum_i \alpha_i x_i - \frac{1}{C} \left[ \frac{g^E}{RT} - \sum_i x_i \ln \frac{r_i}{r} \right] \quad (2.46)$$

The covolume  $b^6$  is found as  $b = \sum_i x_i b_i$ , and  $b_i$ , the covolume of a pure compound, is obtained using the Equation (2.8). The volume area factors  $r$  and  $r_i$  are defined using the Equations (2.29) and (2.30) respectively. The excess Gibbs energy,  $g^E$ , is represented by the generalized NRTL model, according to the Equation (2.36). The reference state constant,  $C$ , is equal to  $C = 0.56$  (Neau et al., 2011).

If we now substitute the  $g^E$  term in the Equation (2.46) by the expression from the Equation (2.36), we obtain:

$$\alpha = \sum_i \alpha_i x_i - \frac{1}{C} \left[ \frac{g_{eos}^E}{RT} \right] \quad (2.47)$$

knowing that  $g^E = g_{comb}^E + g_{eos}^E$ . Then, according to Equations (2.33) and (2.36), we have:

$$g_{comb}^E = RT \sum_i x_i \ln \frac{r_i}{r} \quad (2.48)$$

$$g_{eos}^E = \sum_i x_i q_i \frac{\sum_j x_j q_j G_{ji} \Gamma_{ji}}{\sum_l x_l q_l G_{li}} \quad (2.49)$$

<sup>6</sup>The covolume  $b$  is a linear function of a mixture molar fraction  $x$

For computing the  $\Gamma_{ji}$  binary interaction parameter of Equation (2.36) a group contribution method was developed (Neau et al., 2010b). That makes the NRTL-PR a completely predictive model:

$$\Gamma_{ji} = \sum_K \theta_{iK} \sum_L (\theta_{jL} - \theta_{iL}) \Gamma_{LK}, \quad \theta_{iK} = \sum_k v_{ik(K)} \frac{Q_k}{q_i} \quad (2.50)$$

with  $\Gamma_{KK} = 0$ ,  $\Gamma_{KL} \neq \Gamma_{LK}$ .  $\theta_{iK}$  is a probability that a contact from a molecule  $i$  involves a main group  $K$  and  $v_{ik(K)}$  is the number of subgroup  $k$  that belongs to the main group  $K$  in the molecule  $i$ . For the group interaction parameter  $\Gamma_{LK}$  the following expression was considered with respect to temperature (Neau et al., 2018):

$$\Gamma_{LK} = \Gamma_{LK}^{(0)} + \Gamma_{LK}^{(1)} \left( \frac{T_0}{T} - 1 \right) + \Gamma_{LK}^{(2)} \left( \frac{T}{T_0} - 1 \right) \quad \text{with} \quad T_0 = 298.15 \text{ K} \quad (2.51)$$

It is important to take into account that the parameters  $\Gamma_{LK}$  and  $\Gamma_{KL}$  should be different for highly non-ideal mixtures according to the two-fluid theory. However, one of the main objectives of the NRTL-PR model is to reduce as much as possible the number of interaction parameters. Therefore, it is considered no interaction parameters between subgroups  $k$  and  $l$  which belong to the same group  $K$ , so that the interaction energies are not required, as  $\Gamma_{ji} = 0$  (a case of a paraffin mixture).

In order to perform VLE calculations, the molecules of DPM, DPnB and PnB were decomposed into functional groups, listed in Table 2.6 together with the respective  $v_{ik}$  values. The UNIFAC subgroup parameters  $R_k$  and  $Q_k$  are presented as well for each group. The molecule of H<sub>2</sub>O represents a single functional group by itself and thus does not need a decomposition.

**Table 2.6:** Groups decomposition of DPM, DPnB and PnB and the corresponding UNIFAC subgroups parameters

Group	$v_{ik}$ (DPM)	$v_{ik}$ (DPnB)	$v_{ik}$ (PnB)	$v_{ik}$ (H <sub>2</sub> O)	$R_k$	$Q_k$
CH <sub>3</sub>	3	3	2	—	0,9011	0,848
CH <sub>2</sub>	2	5	4	—	0,6744	0,540
CH	2	2	1	—	0,4469	0,228
H <sub>2</sub> O	—	—	—	1	0,9200	1,400
OH <sub>(1)</sub>	1	—	—	—	1,2700	1,152
OH <sub>(2)</sub>	—	1	1	—	1,2700	1,152
-O-	2	2	1	—	0,2439	0,240

When we were making the calculations, the NRTL-PR parameter matrix already had the parameters for all needed groups, except the group "-O-" (ethers) which has been added by us.

The parameters  $\Gamma_{LK}^{(0)}$ ,  $\Gamma_{LK}^{(1)}$  and  $\Gamma_{LK}^{(2)}$  for the "-O-" group were estimated by a fitting to a data set made up of different ether, glycol ether, alcohol and water systems. Usually, a group contribution method requires a large database for parameters fitting made up of hundreds of systems. However, as previously stated, one of the main problems of our research was a very limited amount (or even a complete absence) of experimental VLE data for such systems. Assuming that fact, our main target was to collect as much data as possible to be able to satisfactorily represent our binary systems of interest and not to develop a real group contribution method. For that reason, we have chosen the systems containing paraffin (CH<sub>3</sub>, CH<sub>2</sub>, CH), alcohol (OH<sub>(1)</sub>, OH<sub>(2)</sub>), water (H<sub>2</sub>O) and, of course, "-O-" group. Our data set used for fitting contains 16 VLE systems listed in Table 2.7 below.

**Table 2.7:** Data set of different VLE systems containing ethers, glycol ethers, alcohols and water used for fitting of group contribution parameters for the "-O-" group

System	Source
Diisopropyl Ether (DIPE) + n-Heptane	Vijayaraghavan et al. (1967)
Diethyl Ether + n-Hexane	Goloborodkina et al. (1981)
Diisopropyl Ether (DIPE) + 2.2.4-Trimethylpentane	Ku and Tu (2006)
Di-n-propyl Ether (DNPE) + n-Heptane	Cripwell et al. (2016)
Butyl Ethyl Ether (BEE) + n-Heptane	Cripwell et al. (2016)
Dimethyl Ether (DME) + 1-Propanol	Park et al. (2007)
Dimethyl Ether (DME) + 1-Butanol	Park et al. (2007)
Diisopropyl Ether (DIPE) + 1-Propanol	Vijayaraghavan et al. (1966)
Diisopropyl Ether (DIPE) + 2-Propanol	Shawaqfeh (2010); Verhoeve (1970)
Methyl tert-butyl Ether (MTBE) + 2-Propanol	Segura et al. (2002)
Dimethyl Ether (DME) + 2-propanol	Elbaccouch and Elliott (2001)
Diethyl Ether + Water	Signer et al. (1969)
Water + Propylene glycol methyl ether (PM)	Chiavone-Filho et al. (1993)
Water + Ethylene glycol methyl ether (EM)	Chiavone-Filho et al. (1993)
Water + Ethylene glycol ethyl ether (EE)	Chiavone-Filho et al. (1993)
Water + Ethylene glycol isopropyl ether (EISOP)	Chiavone-Filho et al. (1993)

All the binary mixtures used for fitting were previously tested in order to confirm their good prediction by the NRTL-PR model. Figure 2.9 demonstrates two of them as an example.

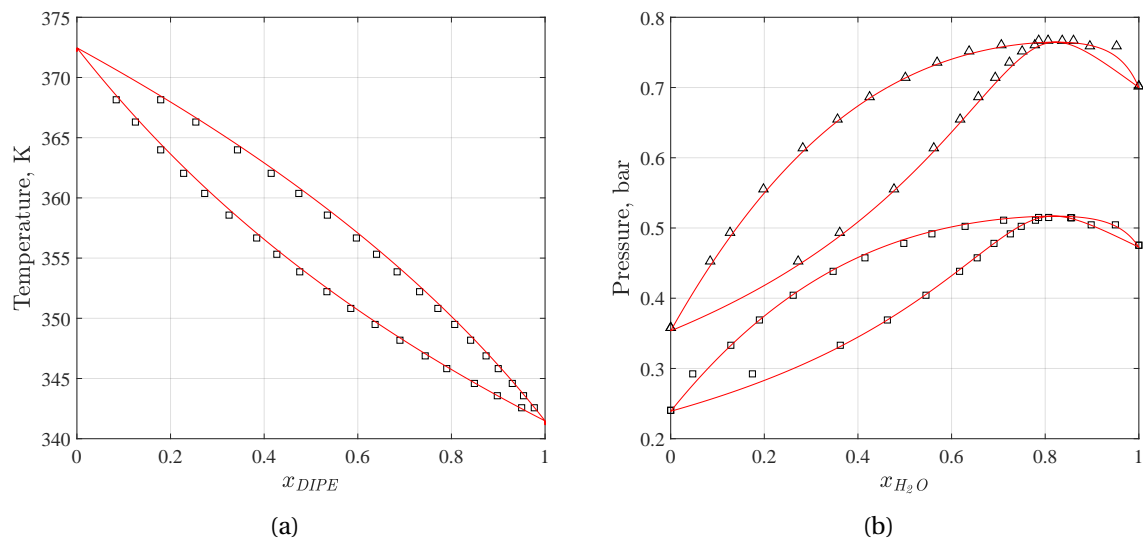


**Figure 2.9:** Examples of VLE used in data set and calculated by NRTL-PR model:

a) Diisopropyl ether (DIPE)+2,2,4-Trimethylpentane;

b)  $H_2O$ +Propylene glycol methyl ether, ( $\square$ ) - 353.15 K and ( $\Delta$ ) - 363.15 K

This data set had one significant drawback. In fact, the VLE of all the systems included in the data set were measured at pressures much higher than the pressures of DPM, DPnB, PnB and water mixtures. This led to a group contribution parameters that yield in overestimated bubble pressures for our systems, especially  $H_2O + DPM$ . In order to fix this issue, we found mandatory to include the  $H_2O + DPM$  system into the data set. Of course, in this case we cannot talk about the full prediction of the VLE and VLLE anymore. Nevertheless, the quaternary systems will be fully predicted using the obtained group contribution parameters.

The corresponding values for  $\Gamma_{LK}^{(0)}$ ,  $\Gamma_{LK}^{(1)}$ ,  $\Gamma_{LK}^{(2)}$  are reported in Tables 2.8 to 2.10 respectively.

**Table 2.8:** Values (in J/mol) of the NRTL-PR group interaction parameters  $\Gamma_{LK}^{(0)}$  used for compounds in this work

L/K	CH <sub>3</sub>	CH <sub>2</sub>	CH	C	H <sub>2</sub> O	OH <sub>(1)</sub>	OH <sub>(2)</sub>	-O-
CH <sub>3</sub>	0,00	0,00	0,00	0,00	2398,94	4413,01	4413,01	-751,36
CH <sub>2</sub>	0,00	0,00	0,00	0,00	2398,94	4413,01	4413,01	-131,61
CH	0,00	0,00	0,00	0,00	2398,94	4413,01	4413,01	-530,42
C	0,00	0,00	0,00	0,00	2398,94	4413,01	4413,01	-530,42
H <sub>2</sub> O	3245,43	3245,43	3245,43	3245,43	0,00	2818,87	2843,36	-8058,60
OH <sub>(1)</sub>	3460,73	3460,73	3460,73	3460,73	-969,98	0,00	0,00	-13414,40
OH <sub>(2)</sub>	3460,73	3460,73	3460,73	3460,73	-1075,32	0,00	0,00	-17451,93
-O-	-209,18	165,93	-1533,82	-1533,82	-9157,88	644,45	735,12	0,00

**Table 2.9:** Values (in J/mol) of the NRTL-PR group interaction parameters  $\Gamma_{LK}^{(1)}$  used for compounds in this work

L/K	CH <sub>3</sub>	CH <sub>2</sub>	CH	C	H <sub>2</sub> O	OH <sub>(1)</sub>	OH <sub>(2)</sub>	-O-
CH <sub>3</sub>	0,00	0,00	0,00	0,00	-3417,62	-6467,13	-6467,13	472,34
CH <sub>2</sub>	0,00	0,00	0,00	0,00	-3417,62	-6467,13	-6467,13	-3505,06
CH	0,00	0,00	0,00	0,00	-3417,62	-6467,13	-6467,13	567,81
C	0,00	0,00	0,00	0,00	-3417,62	-6467,13	-6467,13	567,81
H <sub>2</sub> O	-294,87	-294,87	-294,87	-294,87	0,00	-6350,58	-5370,02	-447,12
OH <sub>(1)</sub>	-470,23	-470,23	-470,23	-470,23	-1115,52	0,00	0,00	5989,73
OH <sub>(2)</sub>	-470,23	-470,23	-470,23	-470,23	-2112,07	0,00	0,00	7812,21
-O-	331,80	407,42	887,82	887,82	1746,05	1812,40	2429,93	0,00

**Table 2.10:** Values (in J/mol) of the NRTL-PR group interaction parameters  $\Gamma_{LK}^{(2)}$  used for compounds in this work

L/K	CH <sub>3</sub>	CH <sub>2</sub>	CH	C	H <sub>2</sub> O	OH <sub>(1)</sub>	OH <sub>(2)</sub>	-O-
CH <sub>3</sub>	0,00	0,00	0,00	0,00	0,00	0,00	0,00	0,00
CH <sub>2</sub>	0,00	0,00	0,00	0,00	0,00	0,00	0,00	0,00
CH	0,00	0,00	0,00	0,00	0,00	0,00	0,00	0,00
C	0,00	0,00	0,00	0,00	0,00	0,00	0,00	0,00
H <sub>2</sub> O	0,00	0,00	0,00	0,00	0,00	-1037,78	-527,76	0,00
OH <sub>(1)</sub>	0,00	0,00	0,00	0,00	-518,21	0,00	0,00	0,00
OH <sub>(2)</sub>	0,00	0,00	0,00	0,00	-326,80	0,00	0,00	0,00
-O-	0,00	0,00	0,00	0,00	0,00	0,00	0,00	0,00

Finally, in order to solve the equilibrium condition, one need to calculate the fugacity coefficients  $\phi_i$  for each phase. For the NRTL-PR model, the fugacity coefficient of a component  $i$  is following:

$$\ln \phi_i = -\ln Z(1-\eta) + (Z-1) \frac{1}{b} \left( \frac{\partial nb}{\partial n_i} \right)_{n_j} - \frac{1}{2\sqrt{2}} \ln \left( \frac{1+(1+\sqrt{2})\eta}{1+(1-\sqrt{2})\eta} \right) \left( \frac{\partial n\alpha}{\partial n_i} \right)_{T,n_j} \quad (2.52)$$

where:

$$\left( \frac{\partial n\alpha}{\partial n_i} \right)_{T,n_j} = \frac{a_i}{b_i RT} - \frac{1}{C} \left( \frac{\partial g_{eos}^E / RT}{\partial n_i} \right)_{T,n_j} \quad (2.53)$$

In a more general way, the procedure of a phase equilibria calculation using the NRTL-PR model is described below:

1. We start from the general formulation of the equation of state (Equation (2.45));

2. For each phase, we express the characteristics of the equation of state as a function of molar fractions  $x_i$ , according to the Equation (2.47);
3. We represent a free excess enthalpy (energy)  $g_{eos}^E$  using an appropriate model depending on the nature of compounds present in each phase. For this work, the used  $g_{eos}^E$  model is given as a residual part of the Equation (2.36);
4. Then, we calculate the EoS properties and solve the equilibrium condition:

$$\text{VLE: } \phi_i^L x_i^L = \phi_i^V x_i^V$$

$$\text{LLE: } \phi_i^{L1} x_i^{L1} = \phi_i^{L2} x_i^{L2}$$

For that, we need to know, for each phase, the expressions of the fugacity coefficients  $\phi_i$  as a function of mole fractions  $x_i$ , according to Equation (2.52), for  $T, P$ . We also need to correctly calculate the partial derivatives  $[\partial(n g_{eos}^E / RT) / (\partial n_i)]_{n_i, T}$  as a function of mole number  $n_i$ . At the end, we calculate the fugacity coefficients  $\ln \phi_i$  of each species for each phase using the Equation (2.52).

## 2.3 Results and discussion

This Section is dedicated to all obtained results corresponding to binary and quaternary mixtures. Our main goal was to obtain a satisfactory representation of these systems, first of all, the quaternary system at 323.15 and 343.15 K (the operating conditions of the pervaporation unit), and, later, to express the correct mixture activity coefficients necessary for the pervaporation design. The latter will be presented in Chapter 3.

### 2.3.1 VLE of all binary mixtures

According to the procedure described in Section 2.2.2, the VLE of 6 binary mixtures were calculated using the NRTL-PR model. The modeling has shown no azeotropes in these mixtures. The water critical properties and acentric factor used in our calculations were taken from Poling et al. (2001) and are:  $T_c = 647.14$  K,  $P_c = 220.64$  bar and  $\omega = 0.344$ .

The predictive ability of the NRTL-PR model was one of the main criteria for the model choice. When the VLE is measured for systems having such a low vapor pressure, the experimental errors can be sometimes significant. These errors occur mainly due to many factors,

for instance, the measurements uncertainty, the precision of pressure and temperature control and acquisition, sample stability. The latter can be perturbed by the presence of different impurities and non-condensable gases in samples, which can be difficult to control. As a result, some experimental points can be obtained with errors. On one hand, one can use the semi-empirical low-pressure VLE models. On the other hand, these models are basically the experimental data correlations with a physical sense and will lead to false bubble and dew curves, as they will try to follow the experimental points. Moreover, some semi-empirical models are known as inconsistent for complex mixtures including liquid-liquid equilibria. The predictive models are independent of the VLE data and, thus, are able to represent the bubble and dew curves regardless of incorrect experimental points.

However, as explained in Section 2.2.2.3, in our case the representation of 6 binary systems was not fully predicted as the H<sub>2</sub>O+DPM mixture data were used to adjust the interaction parameters for the "-O-" group. Nevertheless, the quaternary system water+ARCACLEAN was fully predicted afterwards using the obtained group interaction parameters.

The results for 6 binary mixtures are presented in Figures 2.10 to 2.12 with the respective overall mean deviations in vapor pressure. Some mixtures are better represented at low temperatures (water+DPM, water+DPnB, water+PnB, PnB+DPM). The mixtures having very low vapor pressures (DPM+DPnB and PnB+DPnB) are in turn better represented at high temperatures, as the errors become less significant with the high pressure.

The aqueous mixtures water+DPnB and water+PnB are partially miscible. The two liquids coexistence zone is correctly represented by the NRTL-PR model. Also, it can be seen in Figure 2.11 a) that the dew pressure curve is correctly represented in a whole range of compositions. The same is for the dew pressure curve of water+DPnB mixture (Figure 2.10 b)), however, due to the plot scale it is almost not recognizable.

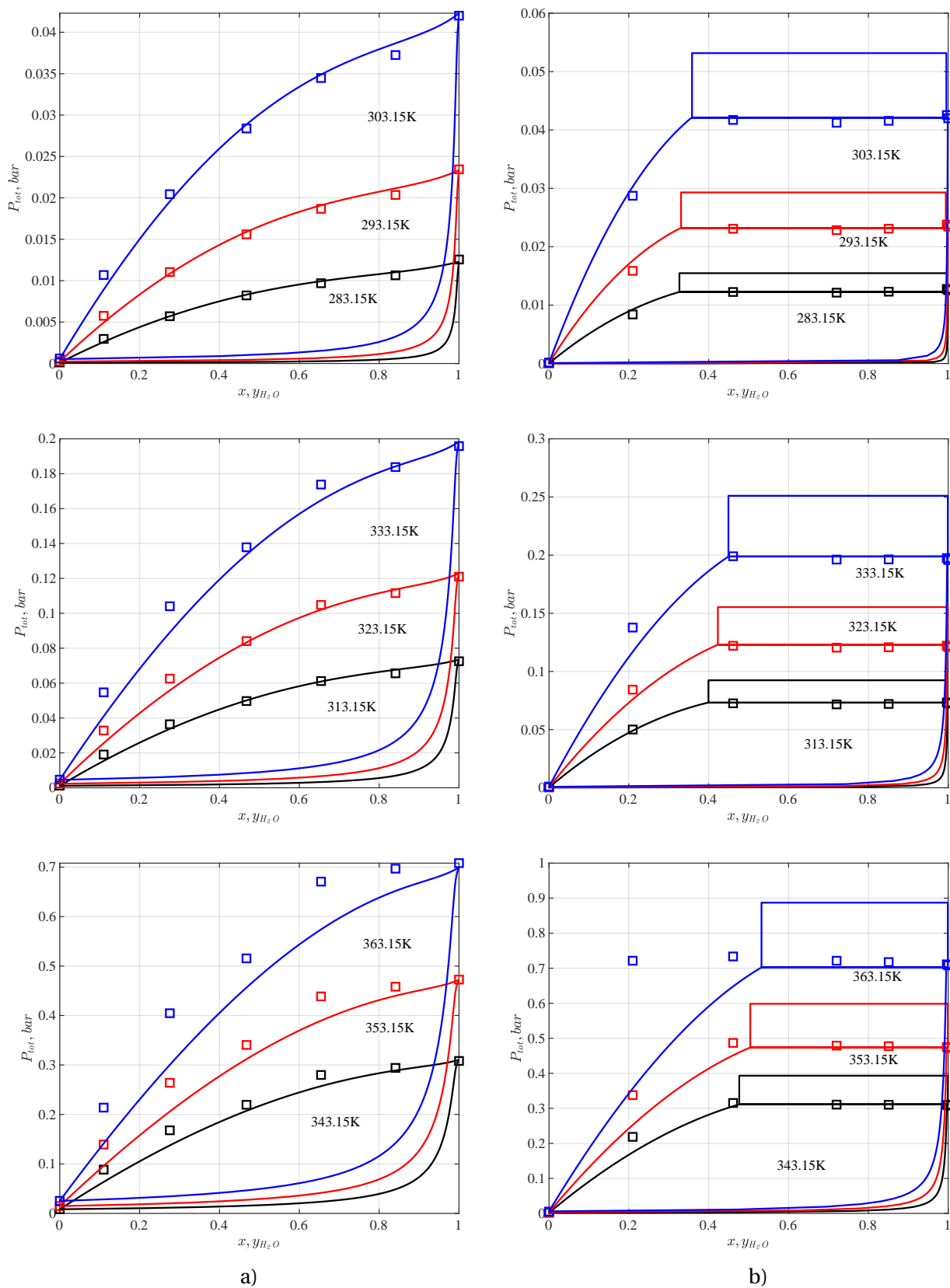


**Figure 2.10:** Measured (squares) and calculated (solid lines) VLE and VLLE at 283.15-363.15 K: a) water+DPM; b) water+DPnB



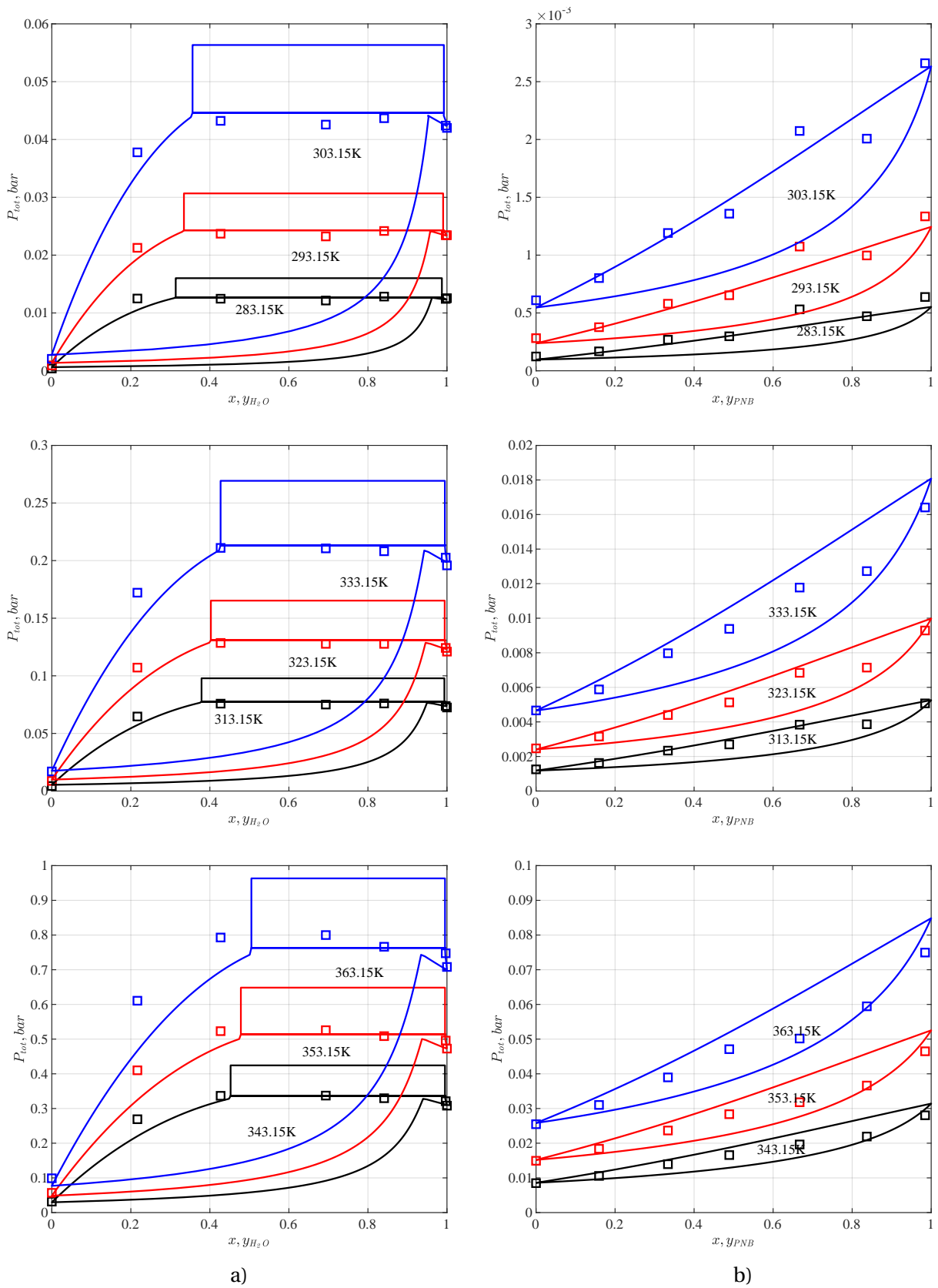


**Figure 2.11:** Measured (squares) and calculated (solid lines) VLE and VLLE at 283.15÷363.15 K: a) water+PnB; b) PnB+DPM

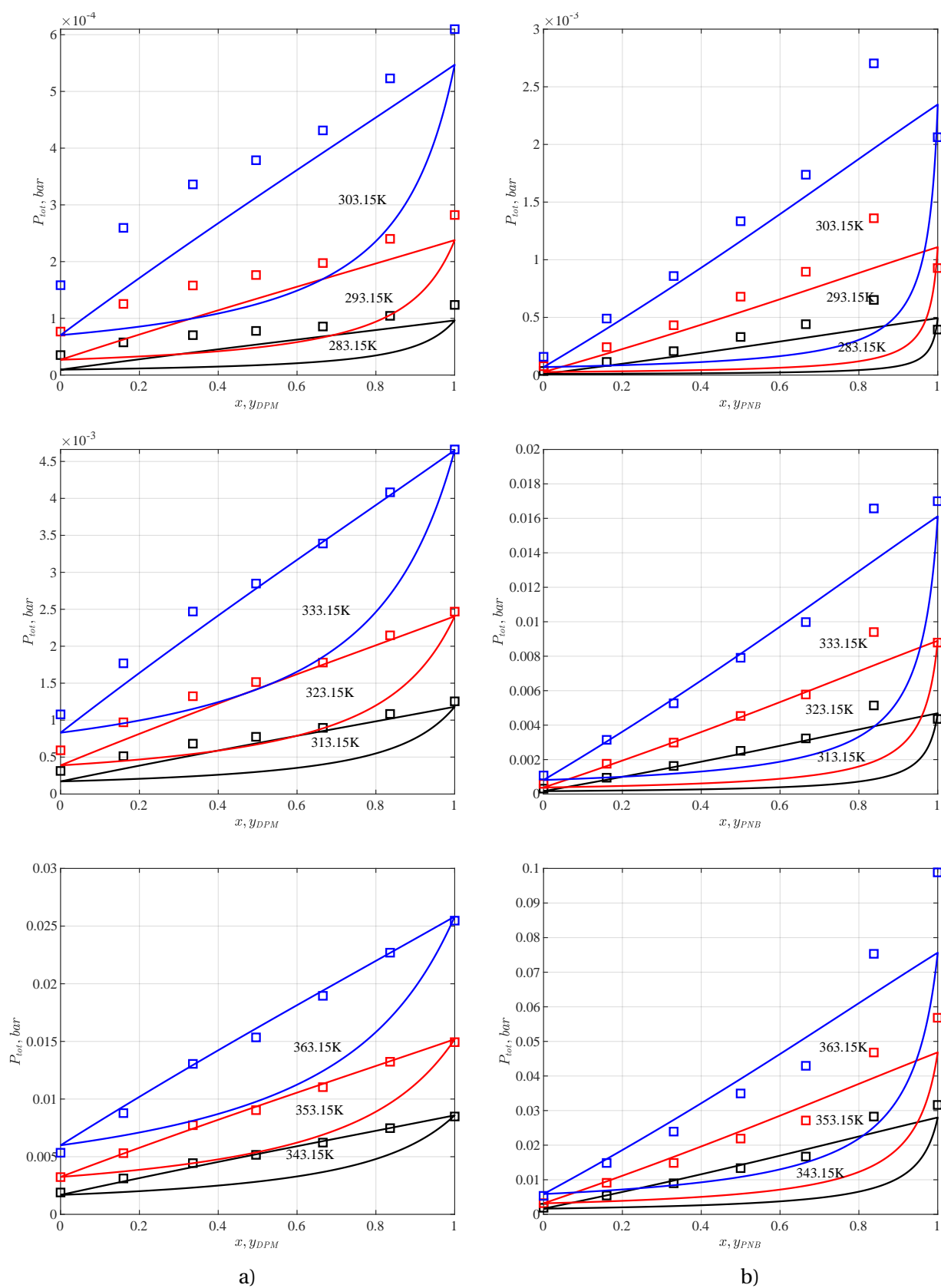


**Figure 2.12:** Measured (squares) and calculated (solid lines) VLE at 283.15÷363.15 K:  
a) DPM+DPnB; b) PnB+DPnB

### 2.3.2 VLE of the quaternary mixtures

The results for the quaternary mixture are presented in Figure 2.13. We find, that the VLE representations become worse when the temperature raises. Moreover, one can observe an abnormal behavior of the dew pressure curve at the zone where  $x_{water}$  is almost 1. This is mostly due to the fact that we did not have any data related to this zone where the water is infinitely diluted, so it was not taken into account during modelling. In spite of these facts, we consider these fully predicted results satisfactory enough, especially at 343.15 K, as namely this temperature will be used in pervaporation as feed temperature.

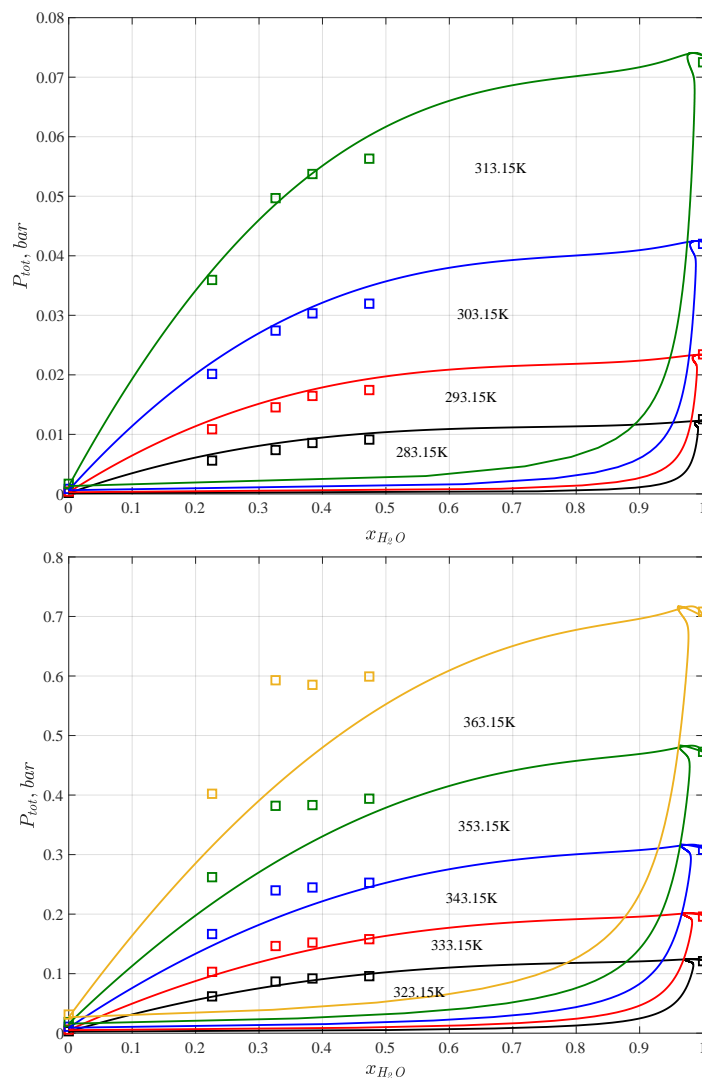


**Figure 2.13:** Measured (squares) and calculated (solid lines) VLE of the quaternary mixture  $H_2O$ +ARCACLEAN (DPM 60%wt, DPnB 30%wt, PnB 10%wt) at 283.15÷363.15 K

## 2.4 Chapter conclusion

In the present Chapter, the ARCALCEAN solvent and its interactions with water were studied from the point of view of thermodynamics. Studying the thermodynamics of solvents is an essential step towards the industrial units design.

The experimental investigation was successfully carried out. The measurements of pure compounds vapor pressures, as well as the phase equilibria of binary and quaternary systems were performed. In total, 27 experimental points for the pure compounds, 279 experimental points for the binary systems and 45 experimental points for the quaternary system were obtained for the temperature ranging from 283.15 K to 363.15 K. It was found that the aqueous mixtures of DPnB and PnB are partially miscible. The two liquids coexistence zone was measured and reported in terms of total system vapor pressure. The liquid-liquid compositions were not determined. The main experimental challenges were the stability of samples during measurements and very low system vapor pressures. Fortunately, the first problem depends mainly on the sample degassing as this allows to evacuate any impurity or non-condensable gas that can strongly influence the measurement results. By performing the degassing more thoroughly, we were able to improve the majority of experimental points. However, in case of PnB, much more effort was made in order to obtain satisfactory experimental points as this particular compound had demonstrated the worst stability compared to the others, regardless of degassing. Its vapor pressure was progressively increasing during measurements and was never stable, showing the pressure fluctuations in a very large range. Again, any experimental uncertainty or instability is even more visible when measuring very low vapor pressures. If, in case of high vapor pressures, the measurements are not very sensible to small instabilities, they can easily be perturbed when the pressures are low. Moreover, the precision of measurements was very high (the MKS sensor is capable to detect a pressure difference of  $10^{-2}$  Pa). This problem was partially solved by paying a particular attention to the experimental unit maintenance and cleaning, sample preparation and degassing, increasing the number of measurements for problematic points. In spite of these facts, we were, however, unable to improve the results for certain points.

We attend to develop a theoretical tool allowing to correctly model and represent the obtained experimental points. The model should correspond to some important requirements, namely, to have a predictive ability, to be universal and flexible, to represent all the systems of interest satisfactorily, to be simple and have low computational costs. As a part of the study, different semi-empirical and predictive models were tested. But, having based on the above requirements, our choice fell on the NRTL-PR model that was adapted to our systems. For

that, a new group "-O-" (ethers) was added to the matrix of interaction parameters. These parameters were obtained by fitting to an experimental VLE data set composed from 16 systems containing "-O-", "H<sub>2</sub>O", "-OH<sub>(1,2)</sub>" and paraffins groups. In order to solve the very low pressure issue, the system H<sub>2</sub>O+DPM was also included in the data set. This led to the fact that the binary systems were not fully predicted, but rather represented. In spite of this, the quaternary system H<sub>2</sub>O+ARCACLEAN was completely predicted.

The modeling has shown a good overall representation of the isothermal VLE and VLLE of all systems. The estimation quality of the pure compounds vapor pressures strongly depends on their critical parameters. The critical parameters, also absent in the literature, were not experimentally determined in this work. was improved by adjusting the  $\gamma$  and  $m$  parameters of the Soave function. For the mixtures, the problem of low vapor pressures still persists and is visible on the phase equilibria curves. The solution presents several difficulties related to the model limits in representation of very low pressures as the model was initially developed for high pressures.

Regardless of the issues stated above, the quaternary mixture was predicted and the results were satisfactory for the desired composition range.

Finally, when designing an industrial scale pervaporation unit, one needs the feeding mixture activity coefficients in order to correctly represent the driving force through the membrane and, thus, to compute the appropriate membrane effective surface. The theoretical and experimental study of the pervaporation process applied to the dehydration of the ARCACLEAN solvent, involving driving force, permeability and separation efficiency, is the theme of the coming Chapter.

## Chapter 3

# Pervaporation as an alternative process for solvent dehydration in dry cleaning machines

It was shown in Chapter 1, that distillation has certain limits in terms of energy and separation efficiency. When applied to the solvent dehydration in a dry cleaning device, it lowers the overall performance of the system. A high energy consumption of distillers actually integrated in dry cleaning device increases the costs of each washing cycle. Moreover, the solvent losses during the regeneration are important and, thus, cannot be neglected.

Alternatively to distillation, the implementation of *pervaporation* process was proposed for solvent dehydration purposes. Offering numerous advantages compared to distillation, the pervaporation represents a rational and efficient solution in terms of energy, separation quality and operational costs. Being more compact and simple to automate, the pervaporation unit can be easily integrated in the existing dry cleaning machines and fully replace the distillation.

The aim of the present Chapter is, on one hand, to study the feasibility of solvent dehydration by pervaporation, using commercially available and cost affordable membranes. On the other hand, we will determine membrane performance with respect to solvent-water mixture. Valuable experimental data, which was not published before, will be obtained to characterize the main parameters of the pervaporation, namely the permeate flux, the selectivity and the permeance.

The Chapter ends by a modelling part based on the well-known solution-diffusion model.

## 3.1 Literature review

### 3.1.1 Pervaporation overview

The pervaporation membrane separation process represents an energy efficient combination of membrane permeation and evaporation. It is schematically presented in Figure 3.1. Pervaporation is considered as an attractive alternative to numerous separation methods for different applications. Nowadays, the pervaporation is used in more than 100 industries for alcohols dehydration (Dong et al., 2006). Compared to classical processes, such as distillation, the pervaporation is more energy efficient and has higher separation performance, especially in case of azeotropic mixtures. Pervaporation is also used for the dehydration of organic solvents or for the removal of the organic compounds from aqueous solutions (Mahesh, 1992).

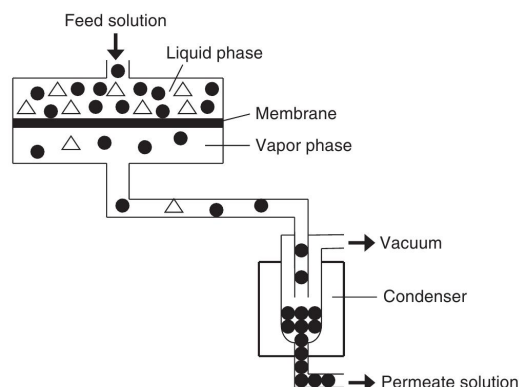


**Figure 3.1:** Diagram of the pervaporation process (Drioli et al., 2011)

In pervaporation, a feed liquid is applied on the upstream side of a dense membrane and the permeate is evaporated from the downstream side due to the applied vacuum. The partial pressures of permeants is maintained close to zero in order to ensure a best removal of permeating compounds from the membrane surface. To increase the mass transfer and, thus, the process performance, the feed solution is usually preheated which increases the partial pressures of its components. The permeate vapor is condensed and then recovered in liquid state. The species separation occurs due to their different diffusivity and sorption rate through the membrane. Thus, the separation efficiency in pervaporation is independent of the mixture's nature.

In order to characterize the pervaporation in terms of overall performance, several pa-

rameters are selected. Firstly, the *permeate flux*,  $J_i$ , which is related to driving force and expressed as the volume, moles or mass of a permeant divided by the permeating time and membrane surface area. Second, the *permeability*,  $P_i$ , to characterize the rate of diffusivity and sorption of the permeant through dense layer of the membrane.

Other parameters for the pervaporation description are the *enrichment factor* of component  $i$ ,  $\beta_i$ , the membrane *selectivity* of a component  $i$  with respect to the component  $j$ ,  $\alpha_{ij}$ , and the *separation factor* of a component  $i$  with respect to a component  $j$ . These parameters illustrate how preferably the component  $i$  is permeated through the membrane compared to the component  $j$ . The relations for these parameters are given below:

$$\beta_i = \frac{c_{P,i}}{c_{F,i}} \quad (3.1)$$

$$\alpha_{ij} = \frac{P_i}{P_j} \quad (3.2)$$

$$\text{Separation factor} = \frac{c_{P,i}/c_{P,j}}{c_{F,i}/c_{F,j}} = \frac{J_i/J_j}{c_{F,i}/c_{F,j}} \quad (3.3)$$

where the subscripts  $F$  and  $P$  mean the property at the feed-side or permeate-side, respectively. When comparing different pervaporation results, permeabilities and selectivities should preferably be used.

### 3.1.2 Materials of pervaporation membranes

As in all membrane processes, the membrane in pervaporation is considered to be the key element. The separation in pervaporation is performed using the *nonporous dense* membranes. The right choice of membrane material is crucial for the quality and success of pervaporation. In more general terms, a good pervaporation membrane should provide a high level of selectivity, productivity and stability.

Due to its chemical and physical properties, as well as the interactions of the permeants with the membrane material, a membrane can be either *selective* or *non-selective* to some species. The *productivity* of a membrane is usually expressed in terms of the permeate flux that depends on the process operating conditions (namely the temperature, pressure and feed concentration), but also on the membrane thickness. The latter becomes a very important parameter for determining the economical viability of the process. The membrane



*stability* depends on the physical and chemical properties of its material and is extremely important for long-term usage and maintenance investment forecasting (Figoli et al., 2015).

As a separation process, the pervaporation was firstly proposed by Kober (1917), who has performed the first experiments on removing water from albumin/toluene solution using collodion (cellulose nitrate) film. Since that time, a huge amount of scientific effort was dedicated to the development of new membrane materials for different applications (Binning and James, 1958; Heisler et al., 1956; Binning et al., 1961). The next historic improvement in membrane separation field was the development of composite membranes having a selective layer of cross-linked polyvinyl alcohol supported on a porous polyacrylonitrile, leading to the construction of the first pervaporation plant for ethanol dehydration in 1982 (Ballweg et al., 1982). Later on, three main branches of pervaporation application were established: solvents dehydration, organic compounds removal from aqueous solutions and organic-organic separation.

Generally, pervaporation is best performed at high temperatures as the diffusion of molecules through the membrane is improved. Therefore, a thermal stability of a membrane is a very important property. There are three main types of membrane material used nowadays that satisfies the above condition. According to these types, the pervaporation membranes are divided in *organic*, *inorganic* and *hybrid* membranes. A brief characterization of each type is provided below.

### 3.1.2.1 The organic membranes

The organic membranes consist of a polymer casted and formed as a dense film. Due to a relatively simple manufacturing and reasonable cost, the polymeric membranes are widely used in modern membrane processes, including pervaporation. Their main drawback is a relatively low chemical and thermal resistance, a moderate permeability and separation efficiency, compared to other types of membranes. However, their advantages are much more important and outweigh the drawbacks in membrane applications. Moreover, the polymeric membranes are easy to scale-up.

For aqueous solution treatment, the choice of a polymeric membrane depends on its hydrophilic or hydrophobic (organophilic) properties. The performance of a polymeric membrane is generally defined by the diffusivity and solubility of permeating species. The water coefficient of diffusion is always higher than that of organic compounds due to its smaller

size. In case of a hydrophilic membrane, both water diffusivity and solubility are high, whereas a hydrophobic membrane has a high solubility of organic compounds (Koops and Smolders, 1991).

Certain hydrophobic membranes, such as polyethylene and polypropylene, are widely used in organic/organic, and particularly in polar/non-polar separations. Generally, these polymers have a low selectivity due to the leak of functional groups that are able to interact with compounds in the feed mixture (Yoshikawa et al., 1986). Another examples of hydrophobic polymers are nitrile, urethane, styrene butadiene rubber, polydimethylsiloxane (PDMS), poly(1-(trimethylsilyl)-1-propyne) (PTMSP) *etc* (Watson et al., 1992; Sikdar et al., 2013; Lietz et al., 2007).

Among the hydrophilic membranes, one can distinguish the polyvinyl alcohol (PVA), being a very popular material in dehydration of organic solutions. It is strongly hydrophilic due to the presence of "-OH" groups and the low contact angle and high degree of swelling when being in contact with water. The swelling acts unfavourably towards the membrane stability as it increases the free volume of PVA network and decreases the interaction with permeants. For that reason, the PVA membranes are usually cross-linked, which prevents the swelling and improves the stability and separation quality (Xie et al., 2011).

Wan et al. (2006) studied the chitosan (CS) membranes, produced from the chitin, a compound containing in the cuticle of various marine crustaceans. The advantages of this polymer are its biodegradability and strong hydrophilicity, making it a new promising material for water treatment.

A high hydrophilicity and water selectivity are also the properties of sodium alginate membranes (NaAlg). Extracted from the cell walls of brown algae, it showed very good film-formation characteristics. The hydrophilicity of this material is explained by the presence of carboxyl and hydroxyl groups in its structure. The dehydration of organic solutions involving NaAlg membranes were studied by Moulik et al. (2016); Kuila and Ray (2014); Nigiz et al. (2012); Kalyani et al. (2008) *etc*.

### 3.1.2.2 The inorganic membranes

The key advantage of inorganic membranes is their very high permeability, selectivity, thermal/chemical resistance and very low swelling degree. They are, however, difficult and

expensive to produce, compared to organic membranes. The inorganic membranes are mostly represented by ceramic membranes (based on metal oxides and nanostructures such as zeolites) and metal organic frameworks and carbon based materials (Goh and Ismail, 2018).

Zeolites are a porous crystalline structure made of  $TO_4$  frameworks, able to accommodate different cations such as  $Na^+$ ,  $K^+$ ,  $Mg^{2+}$  etc. When deposited on a porous support, zeolites form zeolite membranes. The first zeolite membrane was produced in 1987 by Suzuki (Suzuki, 1987) and quickly became promising solutions for membrane separation applications.

Zeolites contain molecular-size pores, made up of rings in the framework. Each pore is designated by the number of oxygen atoms that constitute the ring. There exist small-pore (8-member ring), medium-pore (10-member ring) and large-pore (12-member ring) (Wee et al., 2008; Van Hoof et al., 2006).

The separation in zeolite membranes occurs due to the difference in transport rate of different molecules. A kind of molecular sieving can also take place, as the pores are usually well-defined in size. For example, the dehydration of solvents involving the type A zeolite membranes having a pore size of about 0.4 nm (for reference, a kinetic diameter of water is 0.296 nm). Zeolites can be made either hydrophilic or hydrophobic, depending on the chemical composition of the network.

### 3.1.2.3 The hybrid membranes

Hybrid, or mixed matrix membranes (MMMs) represent a polymeric matrix in which an inorganic filler is dispersed. This kind of membranes offers the manufacturing simplicity of polymeric membranes together with excellent mass transport properties of inorganic membranes. The MMMs are usually used in gas separation processes. One of the first publications highlighting the MMMs is Paul and Kemp (1973).

The complexity in MMMs preparation is hidden in the homogeneous dispersion of the filler, as well as the compatibility and adhesion of filler-to-polymer. Moreover, the addition of a solid phase changes the structure of polymer, influencing the process into a membrane in a negative way. Therefore, the membrane should be prepared in such a manner to provide good transport properties. A variety of publications propose solutions for the above issues

Li et al. (2006); Qiu and Peinemann (2006); Husain and Koros (2007); Chung et al. (2007).

### 3.1.3 Dehydration of organic solvents by pervaporation

Our choice of the dehydration process can be reinforced even more by the fact that the pervaporation is widely used in solvents dehydration. Nowadays, the pervaporation is mostly popular in dehydration of various alcohols, as well as heat-sensitive compounds. We would like to demonstrate this using some examples from the literature.

A study of the dehydration of isopropanol using the silica and PVA membranes was reported by Gallego-Lizon et al. (2002) for the water content in feed of  $\leq 20\%$ wt. The used membranes were purchased from *Sultzer*, Switzerland. The obtained water flux through the PERVAP2510 PVA membrane at  $70^{\circ}\text{C}$  and  $10\%$ wt of water in feed was about  $0.9$  to  $1 \text{ kg}/(\text{m}^2\cdot\text{h})$  and a separation factor of  $200$ . Analogically, the obtained water flux through the silica membrane was much higher and equal to  $4$  to  $4.5 \text{ kg}/(\text{m}^2\cdot\text{h})$ . However, such a high flux was obtained at the expense of lower separation factor, which was equal to  $50$ .

Pervaporation is also used in dehydration of monomers, for example, the  $\epsilon$ -caprolactam (CPL), as studied and reported by Zhang et al. (2007). In such mixtures, the distillation is inappropriate because the CPL is highly heat-sensitive. On the other hand, the pervaporation allows to separate the CPL from water at  $40^{\circ}\text{C}$ . Using the cross-linked PVA composite membranes, the water flux of  $0.5 \text{ kg}/(\text{m}^2\cdot\text{h})$  and the selectivity of  $55$  were obtained at  $40\%$  water content in feed. The results have shown a high dehydration performance of the PVA membranes. High fluxes are reached due to the hydrophilicity of the PVA.

In order to obtain more flexible materials, blend membranes have been proposed. Their particular interest is explained by the capability of combining different materials and obtaining the desirable performance. For example, one material provides a good permeability, while the other one reinforces the mechanical strength of the membrane (Aminabhavi et al., 2005; Naidu et al., 2005). One of the examples was studied by Rao et al. (2006). It was proposed by the authors to use blended chitosan-PVA membranes to dehydrate the isopropanol and the tetrahydrofuran (THF). The most interesting conclusions are as follows. In water+isopropanol mixtures at  $30^{\circ}\text{C}$  and  $10\%$ wt of water in feed, the authors obtained the water flux of  $0.095 \text{ kg}/(\text{m}^2\cdot\text{h})$  and the selectivity of  $77$  within the PVA membrane; the flux of  $0.087 \text{ kg}/(\text{m}^2\cdot\text{h})$  and the selectivity of  $5134$  within the CS membranes. For the same conditions but using a blend CS(40%)-PVA(60%) membrane, both the flux and the selectivity

were increased up to 0.214 kg/(m<sup>2</sup>·h) and 6419, respectively. Concerning the mixture water+THF at the same operating conditions and membrane, the water flux and the selectivity were 0.201 kg/(m<sup>2</sup>·h) and 1170.

Another improvement of membrane properties comprises in placing the active layer in a ceramic support. This increases the membrane's mechanical resistance together with keeping a good performance and selectivity. This was applied by [Xia et al. \(2011\)](#) in dehydration of ethyl acetate, as an alternative process replacing the azeotropic distillation. Again, the hydrophilic PVA has shown a good water permeability. The flux was of  $4 \cdot 10^{-4}$  kg/(m<sup>2</sup>·s) having a selectivity of 105 at 70°C and 5.1% of water content in feed, demonstrating that the pervaporation is a very promising process in dehydration of the ethyl acetate.

As an industrial application of the pervaporation in organic solvents dehydration, the work of [Rautenbach \(1988\)](#) can be considered. The dehydration of 7 organic compounds was carried out in an industrial-scale pervaporation plant. However, the authors do not disclose the names of those compounds for the sake of confidentiality. Moreover, the membrane performance is not reported. The information that can be extracted from the paper, is the estimated effective area of the membrane module as a function of permeate water concentration. The value of 15 to 20 m<sup>2</sup> is reported in order to dehydrate the solvents up to 1%wt with a permeate flow rate of 4.4 kg/h.

## 3.2 Experimental study of solvent dehydration by pervaporation

The present experimental study was carried out at the Laboratoire Réactions et Génie des Procédés (LRGP), Nancy, France, under the supervision of Prof. Denis ROIZARD. Investigating the feasibility of solvent dehydration by pervaporation and determining the membrane mass transfer parameters were the key targets.

Three polymeric membranes PERVAP<sup>TM</sup> (models 4102-3184, 4510-2898 and 4100-3239) were tested. These membranes, having an active layer made of polyvinyl alcohol (PVA), were specially developed for different application in pervaporation and gas permeation. The active layer is differently cross-linked in each membrane. Any information about the nature of porous support layer was communicated by the supplier.

### 3.2.1 Materials

The ARCACLEAN solvent was supplied by Arcane Industries, France, in a quantity of 20 liters. Each component of the solvent (DPM, DPnB and PnB) were supplied a part as well (200 ml each). All the liquids were used for experiments without any additional purification. The ARCACLEAN solvent composition was verified and confirmed by the gas chromatography. The gas chromatography analysis has indicated a presence of certain impurities in the solvent that could not be identified. It is important to point out that their amount was very small and was then considered to be negligible for every sample preparation.

The commercially available polymeric membranes were supplied by DeltaMem (Sultzer) situated in Switzerland. The membranes were purchased as flat sheets having the A4 format.

### 3.2.2 Experimental unit description

The diagram of the experimental pervaporation unit used in this work is presented in Figure 3.2. This laboratory-scale unit is composed of the membrane cell (1) (see Appendix E), the thermostatic bath (2), the two permeate cold traps (3), the vacuum pump (4), the liquid separator (5) and the moisture filter (6).

The unit's working principle is as follows. 100 grams of feed mixture containing 10% wt of water is charged into the reservoir of the membrane cell (1) having a volume of 150 ml. The membrane cell was developed for a membrane with an area of 13 cm<sup>2</sup>. The composition of the feed mixture was verified using the GC. The temperature of the feed is maintained constant using the thermostatic bath (2) which performs a circulation of water having constant temperature between the cell walls. The piston vacuum pump (4) creates the vacuum of about 0.4 ÷ 0.5 mbar in the permeate side of the unit and, thus, the transfer driving force. In order to protect the vacuum pump from the possible liquid penetration (in case of the cell leakage), the liquid separator (5) is placed before the vacuum pump's suction. It is immersed in the liquid nitrogen and provides the full condensation of any humid vapor passing through it. Due to the driving force, the vapor is permeated through the membrane and is condensed in cold traps (3) which are immersed in the liquid nitrogen as well. The unit is equipped by two cold traps connected in parallel. This scheme allows the switching between the cold traps without interrupting the pervaporation experiment. One can remove the first cold trap for sampling while the second one is working. The moisture filter (6) protects the unit from the humidity that penetrates into the system during cold traps removing.

The experiments were carried out according to two working regimes:

- *Quasi-stationary regime* (short time between samplings,  $\approx 2$  hours). At this regime, when the first cold trap was removed, the time since the beginning of the experiment was noted and the permeate was weighed. The feed liquid was analyzed by the GC and the water was added to the feed in order to keep the initial concentration at 10% wt. Then, the production of permeate was continued into the second cold trap. The permeate from the first cold trap was then analyzed by the GC and the trap was cleaned, dried and returned to the unit. Using the measured time of experiment and the obtained permeate mass, the permeate flux was calculated.
- *Transitional regime with water elimination over time* (very long time between samplings, 40 to 60 hours). The experiments at transitional regime were started by filling the membrane cell (1) with a feed liquid having water concentration of about 10% wt. The solvent was then continuously dehydrated and the permeate was withdrawn by removing the cold traps. For each cold trap removal, the time was noted, the permeate was weighed and analyzed by the GC, allowing to obtain one experimental point. The feed liquid composition was analyzed as well.

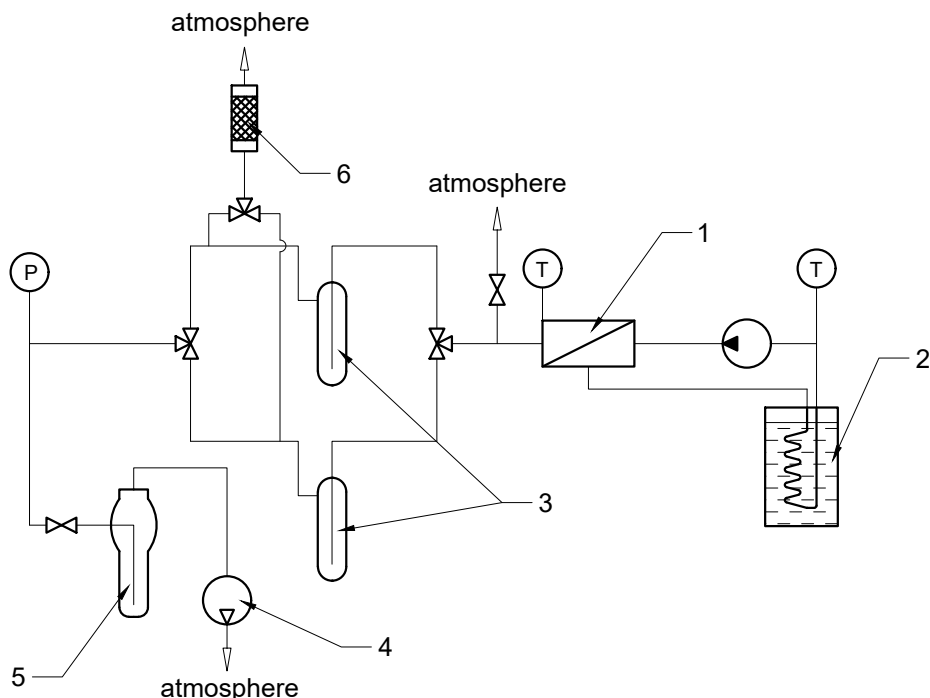


**Figure 3.2:** Diagram of the pervaporation unit used in this work

### 3.2.3 Analysis by gas chromatography

#### 3.2.3.1 GC device

The gas chromatography analysis of all samples was performed using the GC device Shimadzu GC-2010 depicted in Figure 3.3. The chosen GC column was the Agilent CP-Select 624 CB, having a medium polarity and an internal diameter of 0.32 mm, a length of 30 m, a film thickness of 1.8  $\mu\text{m}$  and a maximum working temperature of 265/280°C, which was ideal for analysing the glycol ethers having high normal boiling temperatures.



**Figure 3.3:** The GC device Shimadzu GC-2010 (left) and the column Agilent CP-Select 624 CB (right)

#### 3.2.3.2 GC operating parameters and setup

The injection of liquid samples was made by using an automatic injector. The injector was set at *Split* mode with a split ratio of 100 allowing us to work with a sample volume higher than the column capacity. The injector settings were following: the injection temperature 250°C, the injection pressure 60.2 kPa, the total volumetric flow 113.2 mL/min, the purge flow 3.0 mL/min, the linear velocity 24.9 cm/sec.

The oven can be set either at *isothermal* or *programmed* modes. The isothermal mode is the simplest was of the oven setup. The oven remain at the same temperature until the end of the analysis. The main advantage of this mode is that the oven is always ready for the next analysis, so there is no extra time needed for the oven preparation. The drawback of this method is that the analysis of multi-component mixtures could take considerable time and the last peaks are difficult to detect or measure as they widen with time. Thus, in order to reduce the analysis duration and to obtain well defined peaks, the oven programmed mode was chosen by us. The programmed mode settings are presented in Figure 3.4 below. The temperature gradient was established from 150 to 220°C during 3.5 minutes.



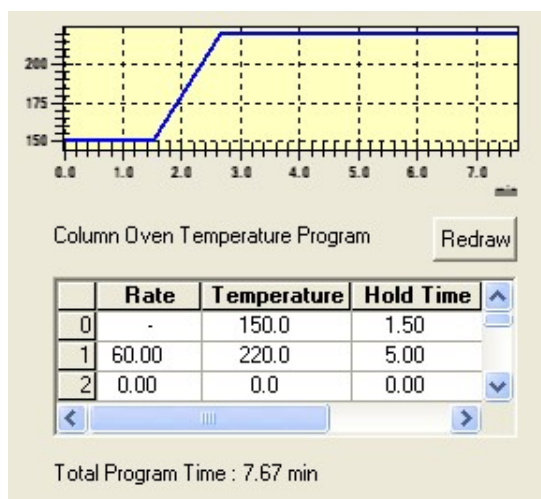


**Figure 3.4:** The programmed mode setup

In this device, the TCD (Thermal Conductivity Detector) was used. Its working principle is following. As it is well known, all the gases have a certain thermal conductivity which can be measured. When some other component is mixed with a carrier gas (in this work, helium was used for this purpose), the detected thermal conductivity is different from that of pure carrier gas. This difference will be measured and used to trace a chromatogram. The detector temperature was set at 250°C and the current was 50 mA.

### 3.2.3.3 GC Calibration

The detector produces a signal when the carrier gas is passed through it. In case if there are no other compounds mixed with the carrier gas, the signal is a baseline. The signal is changed by the presence of a compound and a peak is produced.

There are two basic measurements that can be made on a peak: the time after injection when the peak is detected and the peak size.

The time of a peak appearing is measured between the injection and the detection. It represents a sum of two parts:

- A time necessary for the carrier gas to pass through the column. It can be measured by the injection of the air or some another non-interactive substance.
- The retention time, or, in other words, the supplementary time occurred due to the interaction of the compound with the column stationary phase.

In most of cases, the first point is neglected, so only the retention time is taken as the time of the peak appearing (Agilent, 2002). The peak size can be measured either in terms of its surface or its height, both of these measurements are made relatively to the baseline. These measurements are also called *Measured Response (MR)*.

The GC analysis can be non-calibrated or calibrated. In the non-calibrated analysis, one simply needs to express each peak as a percentage of the total surface or height measured during the analysis (in this case, the detector is supposed to be able to detect all the compounds) and apply an equation:

$$\text{Quantity of peak N} = \frac{\text{MR of peak N}}{\text{Sum of all the MR in the analysis}} \cdot 100\% \quad (3.4)$$

The advantage of the non-calibrated analysis is its using simplicity. For that reason, we have used this type of analysis when determining the appearing time of the pure components. However, this method requires the identification of all the compounds in the multi-component mixture, as every non-identified component will reduce the total sum of MR.

For the mixtures, we used a *Response Factor (RF)* method. This is a method of calibrated GC analysis. A response factor is calculated as the ratio between a known component quantitative value (in our case, the component mass in sample,  $m$ ) and the the peak size produced due to this value (namely the peak surface  $S$ ). The RF can be determined by analyzing different standard mixtures containing all the needed compounds in different composition. Also, this approach should match two important rules that should be experimentally verified:

1. The obtained function should be a straight line;
2. This line should start from the "zero-point" of coordinates.

To construct a calibration line, we have prepared and analyzed 5 standard samples "water+ARCACLEAN" having the water amount of 40, 30, 20, 10 and 0%wt respectively. The percentages of DPM, DPnB and PnB were preserved according to the ARCACLEAN formula. In order to simplify the calibration and the data treatment, the "peak" produced by the ARCACLEAN solvent was assumed to be the sum of three peaks produced by DPM, DPnB and PnB, so the whole mixture (including water) was considered as "binary". The obtained calibration line is presented in Figure 3.5.

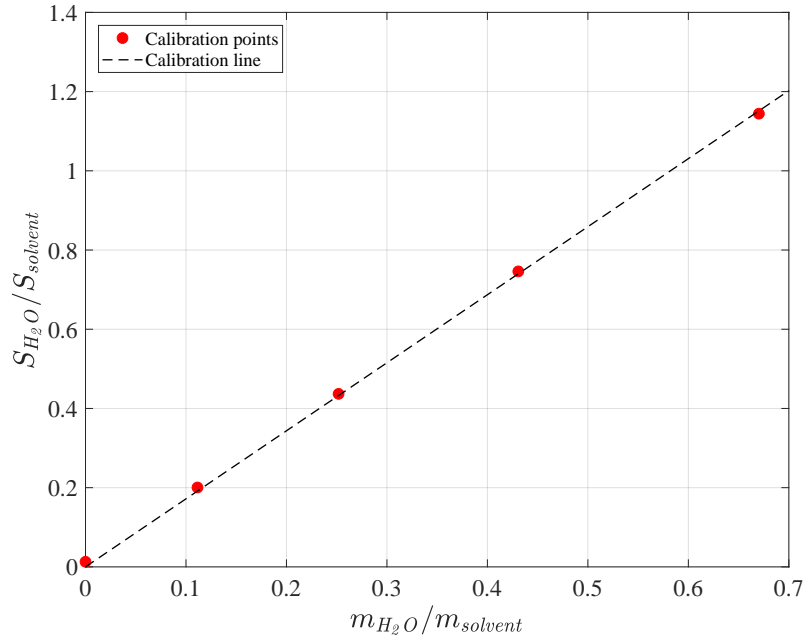


**Figure 3.5:** GC calibration line used for sample analysis in pervaporation experiments

Then, to calculate the mass fraction of water in each desired sample from the pervaporation experiment, the following relation was used:

$$x_{H_2O} = \frac{1}{1 + \frac{1.7178}{\delta}} \quad \text{with} \quad \delta = \frac{S_{H_2O}}{S_{solvent}} \quad (3.5)$$

As we have used a completely new GC column, its conditioning and bleed-test were required prior to the analysis.

### 3.2.4 Results and discussion

During these experiments, permeate fluxes were measured for three membranes having the following characteristics:

1. **Sultz PERVAP 4102-3184.** A highly cross-linked membrane with a polyvinyl alcohol (PVA) active layer. Developed for the organic solutions dehydration. As reported by the supplier, it is *compatible* with the glycol ethers. According to the technical sheet, the maximum water amount in feed solution should not exceed 30%wt.
2. **Sultz PERVAP 4510-2898.** A high flux membrane with a polyvinyl alcohol (PVA) active layer. Developed for the alcohols dehydration. As reported by the supplier, it is *not compatible* with the glycol ethers. According to the technical sheet, the maximum water amount in feed solution should not exceed 30%wt.

- Sultzter PERVAP 4100-3239.** A standard pervaporation membrane with a polyvinyl alcohol (PVA) active layer. Developed for the majority of applications related to the volatile organic compounds (VOC) dehydration. As reported by the supplier, it is *compatible* with the glycol ethers. According to the technical sheet, the maximum water amount in feed solution should be between 30 and 40%wt.

### 3.2.4.1 Membrane Sultzter PERVAP 4102-3184

#### Quasi-stationary regime

During the pervaporation experiment (at constant feed composition, with 10% of water in feed), the membrane 4102 has demonstrated a good stability. Every permeate sample looked clear. Figure 3.6 shows the permeate chromatogram indicating that only water is present in permeate. All the samples obtained during experiments involving the membrane 4102 at 30, 50 and 70°C had the same composition (100% water). It can be, thus, concluded that this membrane was 100% water selective at all operating conditions.



**Figure 3.6:** Permeate composition obtained using the membrane PERVAP 4102-3184

Also, we were able to remark a good reproducibility of the results while measuring the permeate flux. The permeate flux was from 0.04 to 0.06 kg/(m<sup>2</sup>·h) at 30°C, increasing with an order of 2.5 at 50°C (0.12 kg/(m<sup>2</sup>·h)) and with an order of 9 at 70°C, at which the highest obtained value was around 0.45 kg/(m<sup>2</sup>·h). The measured results are plotted over temperature and presented in Figure 3.7.

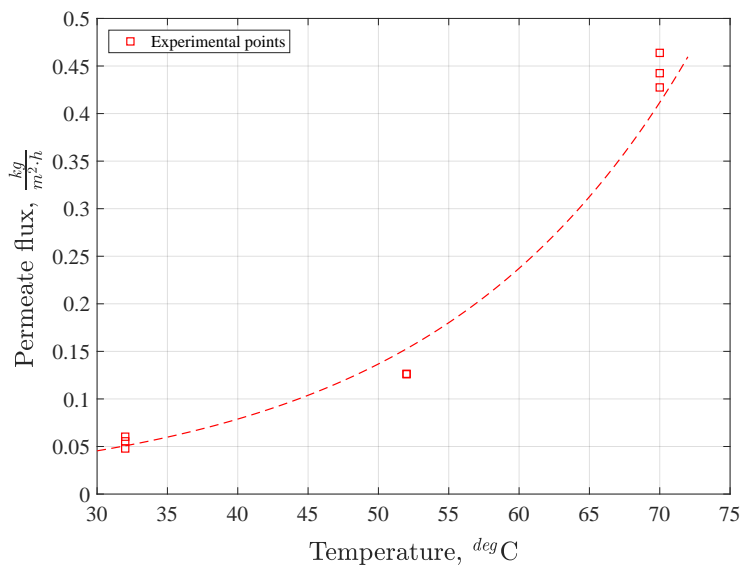


Figure 3.7: Experimental permeate fluxes for the membrane PERVAP 4102-3184

### 3.2.4.2 Membrane Sultzer PERVAP 4510-2898

#### Quasi-stationary regime

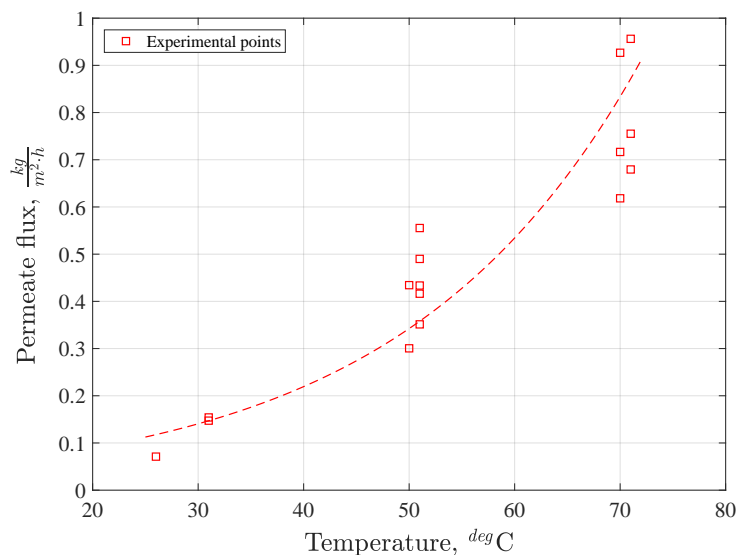
This membrane was presented in its technical sheet as a *non-compatible* with glycol ethers. But, contrary to our expectations, it had no issues during the pervaporation experiment. Moreover, this membrane has demonstrated the highest permeate flux. Its water selectivity was equal to that of PERVAP 4102-3184, so no solvent has passed through it and the obtained permeate contained only pure water (illustrated in Figure 3.8 below).



Figure 3.8: Permeate composition obtained using the membrane PERVAP 4510-2898

The measured permeate fluxes of the membrane 4510-2898 are presented in Figure 3.9. Despite the highest permeate flux among all tested membranes, the reproducibility of the results of this membrane was less good. It can be well seen from the plot. Also, we can see that as the feed temperature increases from 303.15 to 323.15 and 343.15 K, the permeate flux doubles each time. This illustrates the effect of temperature on driving force. This effect is implicitly present namely as the permeant saturated vapor pressure and activity coefficient (which is, in reality, also temperature dependent).

These results attracted our interest. In order to confirm the compatibility of the membrane with the ARCACLEAN solvent, a sample of membrane was immersed into the solvent during 3 weeks, then taken out, dried and tested in the membrane cell at 51°C. The measured permeate fluxes were very close to those obtained using a new membrane. The membrane selectivity was not perturbed. This means that there was no change of the membrane active layer during the period of test that could have some significant influence on the membrane selectivity or on the permeate flux. However, this important change could have happened if the membrane had been exposed to solvent during a more important time.



**Figure 3.9:** Experimental permeate fluxes for the membrane PERVAP 4510-2898

When analyzing the above reported results, one question raises naturally: how can we explain this fairly poor reproducibility of the results, especially at high temperatures? In fact, this could be explained by a couple of hypotheses given below:

1. **The change in feed concentration during the permeate production.** Indeed, the the feed concentration is changed as the permeate is produced. Even if the permeate flux

of the membrane 4510 is considered to be high relatively to other membranes, it still remains less than  $1 \text{ kg}/(\text{m}^2 \cdot \text{h})$ . As the membrane surface used in the cell is very small, one needs a significant time to recuperate even several grams of permeate. According to our measurements, the water concentration was decreasing by 1.5% each 2 hours, causing the decrease in permeate flux by about  $0.2 \text{ kg}/(\text{m}^2 \cdot \text{h})$ . This means that the permeate production was lower close to the end of experiment. Finally, as the experiment time was not identical for each case, the obtained permeate mass was, of course, different.

2. **This effect can be related to a change in polymer structure.** This can be an effect that does not change the order of magnitude of permeate flux, but, at the same time, does not allow to obtain reproducible results. This point is difficult to explain without a proper investigation of the polymer and mixture interaction.

### Transitional regime

For the membrane 4510-2898, the experiments were also carried out including the change in feed concentration. To respond to the industry demand, it is very important to know until which point we can dehydrate the feed solution and how much time we need for that.

The batch experiments were carried out at  $50^\circ\text{C}$  and a permeate pressure of 0.4 mbar. The permeate flux was measured discontinuously during more than 60 hours. The measured water content in feed mixture was 10.1% wt. After each permeate withdrawal the feed sample was taken and its composition was measured by the GC. The same was for the permeate sample. The GC analysis indicated that each permeate sample contained only pure water.

The measured results are presented in Figure 3.10. For each point the permeate was weighed and the permeate flux was calculated. The same as the temperature, the initial feed concentration influences the driving force as well, and, thus, the permeate flux. We can see from the Figure 3.10(a) that the higher the initial water content in feed is, the higher the permeate flux will be. Then, it decreases rapidly with the dehydration of the feed liquid, becoming very low with low water concentration in feed. Figure 3.10(b) indicates that after 63 hours the solvent was dehydrated from 10% to 3.8% of water.

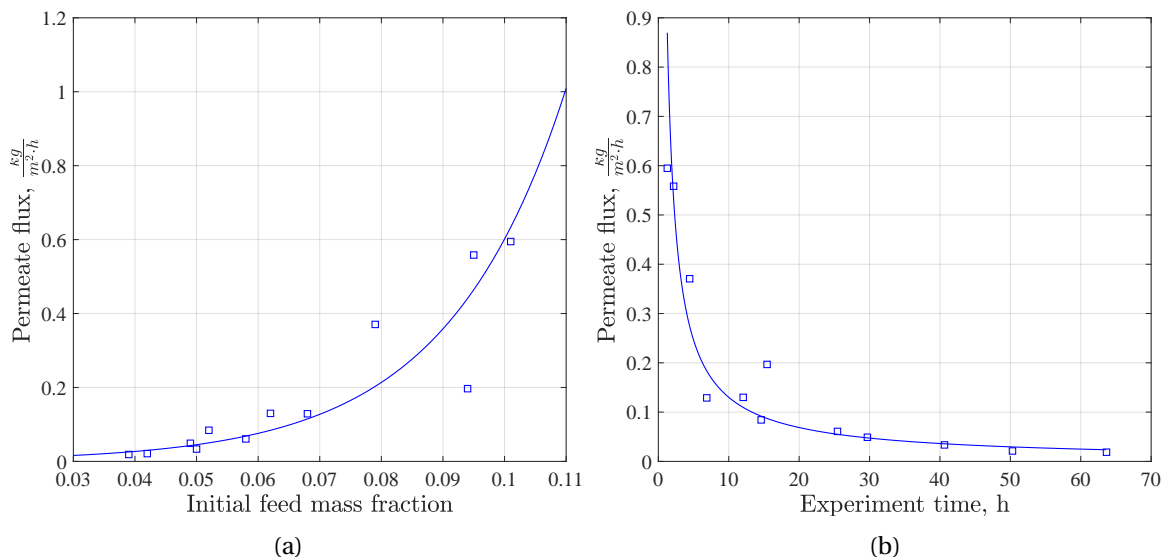


**Figure 3.10:** Permeate flux as a function of (a) feed water concentration and (b) process duration at 50°C. Membrane PERVAP 4510-2898 (membrane surface  $S_f = 0.00132 \text{ m}^2$ )

It is possible to dehydrate the feed mixture even more, but that requires much greater membrane surface and a considerable time in order to reach the desired production level. A necessary membrane surface can be calculated using the obtained experimental data. This part of our work involving the scale-up engineering will be illustrated in Chapter 4.

### 3.2.4.3 Membrane Sultzer PERVAP 4100-3239

#### Quasi-stationary regime

All the permeate samples produced using this membrane were turbid, indicating the presence of ARCACLEAN solvent components. The samples were collected together in a vial. After some time an aqueous and organic phase separation was observed (from the Chapter 2 we know that the DPnB and PnB are not miscible with water at high water compositions). Nevertheless, the obtained total flux was from 0.3 to 0.33  $\text{kg}/(\text{m}^2 \cdot \text{h})$  being in agreement with published values for cross-linked PVA and PVA blended membranes (Zhang et al., 2007, 2017) at the same feed temperature and water composition.

As we wanted all the experimental work carried out at Nancy to be efficient and optimal in terms of time, it was decided to focus on more promising membranes. For that reason, the experiments involving the membrane 4100-3239 were not continued.



### 3.3 Modelling of solvent dehydration by the solution-diffusion model

The pervaporation research is widely carried out all around the world. It comprises generally the study on membrane materials and performance, various applications of pervaporation, coupling with other chemical engineering processes *etc.* In membrane performance study, numerous experiments are carried out in order to measure the main characteristics of membranes, for example permeabilities/permeances and, of course, permeate flux. These experiments are usually carried out at the units of laboratory scale, allowing to obtain necessary data but having a low production due to its small scale. In order to adapt the pervaporation to an industrial scale, one needs to have a mathematical description of the mass transfer occurring in pervaporation.

The main goal of pervaporation models is to describe the mass transfer through the active layer of membrane. In pervaporation, the permeate is in the vapor state whereas the feed mixture is a liquid. It means the presence of a phase change during mixture components transfer. It is very difficult for researchers to indicate the exact place of this phase change. Therefore, some assumptions should be applied to pervaporation modelling because of this system complexity (Luis and Van der Bruggen, 2015).

The most important parameters to be determined via modelling are, on one hand, the mass transfer parameters (permeability/permeance) and separation coefficients (selectivity). On the other hand, one needs to know the permeate flux, as it allows to determine the required effective membrane surface to satisfy the industrial demand. Moreover, the modelling can help to evaluate the pervaporation and to compare it with classical separation processes, such as distillation.

In the present Section, we aimed to model the pervaporation using the solution-diffusion model. The goal of modelling is, first of all, to predict the membrane performance at different feed temperature, to investigate the dependence of mass transfer parameters on operating conditions and membrane material. Second, to determine all necessary values to calculate the effective membrane surface required for the implementation of pervaporation in a dry cleaning machine. The latter task will be, however, raised and explained in Chapter 4.

### 3.3.1 General approach to mass transfer modelling in polymeric membranes

In membrane transport, the two main types of membranes are distinguished. Firstly, the inorganic membranes, which are, mostly made of a *porous* material. Contrary to them, the organic membranes are usually *dense* membranes (Luis and Van der Bruggen, 2015).

Correspondingly, there exist two models to describe the mass transport through these types of membranes. First, the *pore-flow* model, which describes the transport of the permeants through the pores in membrane. The process driving force is an upstream pressure applied to the feed solution. Some permeants are then filtered from pores, through which the other permeants can pass. Second, the *solution-diffusion* model, in which the permeants pass through the dense membrane by a diffusion. The separation occurs due to the different solubilities in membrane and different diffusion rate through the membrane (Baker, 2012). The difference between these two types of membrane transport is graphically shown in Figure 3.11.

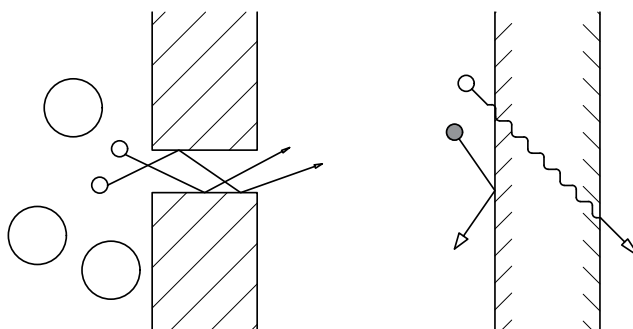


**Figure 3.11:** Membrane transport through the porous (left) and dense (right) membranes (Baker, 2012)

Both models appeared roughly one century ago. Being closer to normal physical experience of that time, the pore-flow model was the most popular until 1940s. Since that time, numerous debates concerning the membrane transport mechanism have taken place (Meares, 1966; Paul, 1976; Yasuda and Peterlin, 1973; Sourirajan et al., 1970). This led to a strong conviction in favour of the solution-diffusion model, so by the 1980s this model has become the leading one for the description of transport phenomena through dense organic membranes (Basile et al., 2015; Baker, 2012).

In pervaporation, the dense polymeric membranes are mostly used nowadays. To de-

scribe the pervaporation, several other models were proposed (Vane and Alvarez, 2005; Bausa and Marquardt, 2001; Ghoreyshi et al., 2002). It can be found from this research that the effect of desorption can be negligible in most cases and can be described by similar sorption models (Basile et al., 2015). This fact adds another positive point in favour of the solution-diffusion model ability to describe the pervaporation.

Namely the solution-diffusion model was chosen to represent the experimental results of pervaporation in this work, due to its good estimation and simplicity. Its description and principle are detailed below.

### 3.3.2 The solution-diffusion model

#### 3.3.2.1 Brief mathematical description

Initially proposed by Lonsdale et al. (1965) and further extended and improved by Wijmans and Baker (1995), the solution-diffusion model divides the flow transport in pervaporation into three main steps: sorption of the permeant in the liquid phase from the feed solution to the membrane, its diffusion through the membrane and then, its desorption from the membrane in the vapor phase as a permeate (see illustration in Figure 3.12). The transport is considered to occur only due to diffusion and not due to convection (as in porous membranes, for example). The transport driving force is a gradient in chemical potential due to the partial pressure.

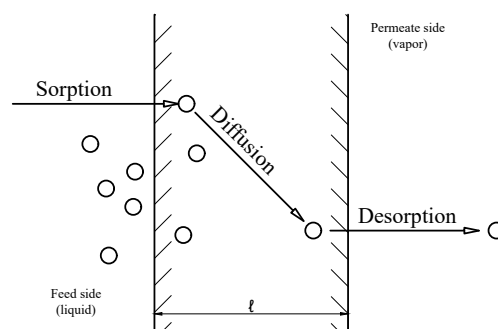


**Figure 3.12:** Three steps of mass transfer in solution-diffusion model (George and Thomas, 2001)

As stated before, the solution-diffusion model is applied with some assumptions. First of all, it is assumed that the fluids on both side of the membrane are in thermodynamic equilibrium with the membrane material at its interface. It means that the chemical potential

gradient is expected to be continuous. This is the case in almost all the membranes except the transport with chemical reactions, where this assumption can fail. Second, the pressure inside the membrane is assumed to be uniform and equal to the high-pressure value, so the chemical potential gradient of a permeant across the membrane is represented only either a concentration gradient or the activity gradient (Baker, 2012). These assumptions are illustrated in Figure 3.13.

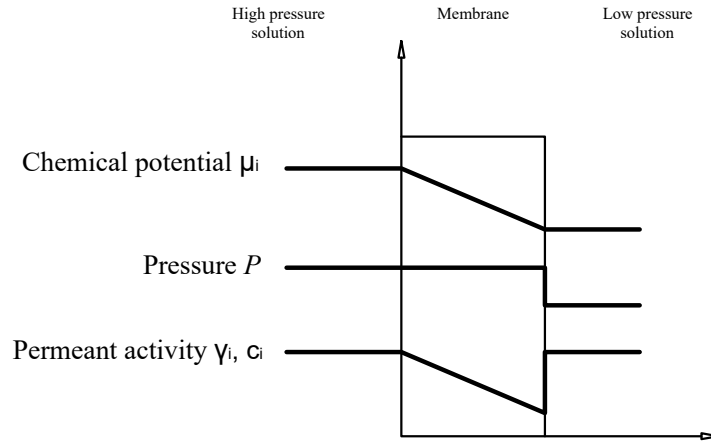


**Figure 3.13:** Driving force gradient in one-component solution permeating a solution-diffusion membrane (Wijmans and Baker, 1995)

A detailed mathematical description of the solution-diffusion model is published in Wijmans and Baker (1995) and Lipnizki and Trägårdh (2001). The starting point of this description is always the fact that, basing on thermodynamics, the overall system driving force required to move a permeant is a gradient in its chemical potential. So, the flux  $J_i$  ( $\text{g}/\text{cm}^2\cdot\text{s}$ ) of a component  $i$  is expressed as:

$$J_i = -L_i \frac{d\mu_i}{dx} \quad (3.6)$$

with  $\frac{d\mu_i}{dx}$ , the chemical potential gradient of a component  $i$ ,  $L_i$  is called a coefficient of proportionality determining the link between this chemical potential and the flux. If the driving force is generated by pressure and concentration gradients, the chemical potential becomes

$$d\mu_i = RT d \ln(\gamma_i x_i) + v_i dp \quad (3.7)$$

where  $x_i$  is the mole fraction of the component  $i$ ,  $\gamma_i$  is its activity coefficient,  $p$  is the pressure and  $v_i$  is the molar volume of the component  $i$ .

Inside dense polymeric membranes, the volume does not change with pressure, so the

integration of the Equation (3.7) gives

$$\mu_i = \mu_i^0 + RT \ln(\gamma_i x_i) + v_i (p - p_i^0) \quad (3.8)$$

where  $\mu_i^0$  is the chemical potential of pure component  $i$  at a reference pressure  $p_i^0$ . The reference pressure  $p_i^0$  is defined as the saturated vapor pressure of the pure component  $i$  at given temperature,  $p_i^{sat}$ . Having this in mind, we obtain:

$$\mu_i = \mu_i^0 + RT \ln(\gamma_i x_i) + v_i (p - p_i^{sat}) \quad (3.9)$$

In pervaporation, the feed pressure is higher than the saturated vapor pressure of permeant,  $p_i^{sat}$ . Then, inside the membrane the pressure remains constant having a value of feed pressure. Along with that, the permeate side pressure is lower than  $p_i^{sat}$ . All these pressures are linked by the expression

$$p_{F,i} \geq p_i^{sat} \geq p_{P,i} \quad (3.10)$$

Let's firstly take a look at the feed/membrane interface system. At this zone, the chemical potential of the feed and the membrane interface are equal at the same pressure, which gives:

$$\mu_i^0 + RT \ln(\gamma_{E,i}^L x_{E,i}) + v_i (p_F - p_i^{sat}) = \mu_i^0 + RT \ln(\gamma_{F(m),i} x_{F(m),i}) + v_i (p_F - p_i^{sat}) \quad (3.11)$$

Meanwhile, at the permeate side/membrane interface, the pressure drops from  $p_F$  to  $p_P$ . The corresponding expression for this system is

$$\mu_i^0 + RT \ln(\gamma_{E,i}^V x_{E,i}) + RT \ln\left(\frac{p_P}{p_i^{sat}}\right) = \mu_i^0 + RT \ln(\gamma_{P(m),i} x_{P(m),i}) + v_i (p_F - p_i^{sat}) \quad (3.12)$$

In the Equations (3.11) and (3.12) the index ( $m$ ) signifies that the value relates to the membrane interface, either at the feed or at the permeate side. The superscripts  $L$  and  $V$  mean the liquid and vapor (or gas) phase.

The Equation (3.12) can be rewritten in terms of molar fraction of the component  $i$  at the membrane interface,  $x_{P(m),i}$ :

$$x_{P(m),i} = \frac{\gamma_{E,i}^V}{\gamma_{P(m),i}} \cdot \frac{p_P}{p_i^{sat}} \cdot x_{E,i} \cdot \exp\left[\frac{-v_i (p_F - p_i^{sat})}{RT}\right] \quad (3.13)$$

The exponential term is close to unity (Baker, 2012; Wijmans and Baker, 1995), thus:

$$x_{P(m),i} = \frac{\gamma_{P,i}^V}{\gamma_{P(m),i}} \cdot \frac{p_P}{p_i^{sat}} \cdot x_{P,i} = \frac{\gamma_{P,i}^V}{\gamma_{P(m),i}} \cdot \frac{p_{P,i}}{p_i^{sat}} \quad (3.14)$$

The mass concentration at the feed-side interface is expressed as

$$c_{F(m),i} = \frac{\gamma_{F,i}^L \rho_m}{\gamma_{F(m),i} \rho_F} \cdot c_{F,i} = K_i^L \cdot c_{F,i} \quad (3.15)$$

and at the permeate-side interface:

$$c_{P(m),i} = M_i \rho_m \cdot \frac{\gamma_{P,i}^V p_{P,i}}{\gamma_{P(m),i} p_i^{sat}} = K_i^V p_{P,i} \quad (3.16)$$

where  $M_i$  is the molecular weight of component  $i$  in g/mol, and  $\rho$  is the molar density in mol/cm<sup>3</sup>. The terms  $K_i^L$  and  $K_i^V$  are the liquid and vapor (gas) phase sorption coefficients.

The permeate flux can be written in terms of Fick's law as:

$$J_i = -D_i \frac{dc_i}{dx} \quad (3.17)$$

where  $D_i$  is the diffusion coefficient.

If one substitutes the concentrations from Equations (3.15) and (3.16) into the Equation (3.17), the expression for the membrane flux will become

$$J_i = \frac{D_i (K_i^L c_{F,i} - K_i^V p_{P,i})}{l} \quad (3.18)$$

with  $l$ , the active layer thickness of the membrane.

To show the interconversion between  $K_i^L$  and  $K_i^V$ , a hypothetical vapor-liquid equilibrium at the feed, schematically depicted in Figure 3.14, is usually considered.

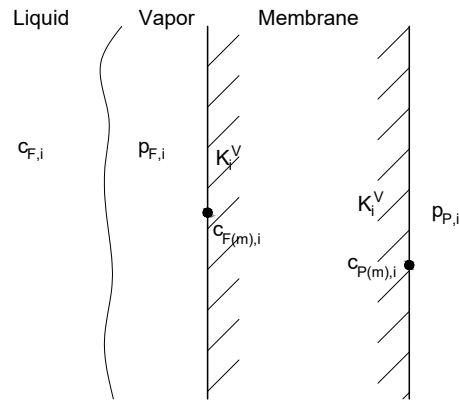


**Figure 3.14:** Hypothetical VLE considered at the feed

We can see from the above Figure how one can interconnect the sorption coefficients using this hypothetical VLE. Thus, considering the existence of a vapor between the feed liquid and the membrane interface, the liquid sorption coefficient,  $K_i^L$  can now be replaced with the vapor sorption coefficient,  $K_i^V$ . Therefore, we can establish the following expression:

$$J_i = \frac{D_i K_i^V (p_{F,i} - p_{P,i})}{l} = \left( \frac{P_i^V}{l} \right) (p_{F,i} - p_{P,i}) \quad (3.19)$$

where  $P_i^V$  is the vapor (gas) permeability coefficient that depends on the vapor phase sorption coefficient and the diffusion coefficient. The Equation (3.19) illustrates the explicit expression of the driving force as the partial vapor pressure across the membrane. This equation was firstly derived by [Kataoka et al. \(1991\)](#) and later, independently, by [Wijmans and Baker \(1995\)](#).

### 3.3.2.2 Reporting the pervaporation data

In 2010, [Baker et al. \(2010\)](#) proposed in their article a way of reporting the pervaporation data that should be preferred over a classical way. The main purpose if this is to simplify the overall understanding and comparison between different experiments on pervaporation and gas permeation. Therefore, all further results of the present Chapter will be reported in the manner described below.

The authors propose to report the pervaporation data in terms of permeabilities/permeances and selectivities rather than in terms of flux and separation factor. In fact, the latter values are not only functions of the intrinsic properties of membrane material, but they also depend on operating conditions (pressure, temperature, feed concentration). In addi-

tion, the diffusivity and sorption also depend on these parameters. The diffusivity usually increases with temperature (Vrentas and Vrentas, 1994), while its dependence on feed concentration relates to the polymer nature (Doghieri and Sarti, 1997). Therefore, it is enough to change the operating conditions, and all the values will change.

In practice, the pervaporation results are often compared with those of gas permeation. As it can be seen from the solution-diffusion equation (Equation (3.19)), the vapor (gas) permeability coefficient,  $P_i^V$  is used. The Equation (3.19) is valid for both pervaporation and gas permeation, so the permeability coefficient remains the same.

In gas permeation, the membrane flux is usually given as molar flux:

$$j_i = J_i \frac{v_i^G}{M_i} \quad (3.20)$$

where  $j_i$  is a molar flux in  $\text{cm}^3(\text{STP})/(\text{cm}^2 \cdot \text{s})$ ,  $v_i^G$  is a molar mass of the ideal gas  $i$  and equals  $22.4 \text{ l}(\text{STP})/\text{mol}$ ,  $M_i$  is a molar mass of the component  $i$ .

According to the solution-diffusion principle, Equation (3.19) can now be written in molar form as:

$$j_i = \frac{D_i \hat{K}_i^V}{l} \Delta p = \frac{D_i \hat{K}_i^V}{l} (p_{E,i} - p_{P,i}) = \frac{\mathcal{P}_i^V}{l} (p_{E,i} - p_{P,i}) \quad (3.21)$$

where  $\mathcal{P}_i^V$  is the permeability term (the same as for gas permeation),  $\Delta p$  is a difference between feed and permeate side partial pressures in cmHg,  $l$  is the membrane active layer thickness.  $D_i$  is the membrane diffusion coefficient in  $\text{cm}^2/\text{s}$ .  $\hat{K}_i^V$  is the molar sorption coefficient of the component  $i$  expressed in  $\text{cm}^3(\text{STP})/(\text{cm}^3 \text{cmHg})$ , being the link between the partial pressure of the component  $i$  in vapor phase and the concentration of  $i$  in the membrane.

The permeability  $\mathcal{P}_i^V$  is commonly reported in Barrers which is expressed as:  $1 \text{ Barrer} = 1 \times 10^{-10} \text{ cm}^3(\text{STP})/(\text{cm}^2 \cdot \text{s} \cdot \text{cmHg})$ .

In case if the membrane thickness is not known, one can use the *permeance* term,  $\mathcal{P}_i^V/l$ , a component flux normalized for driving force. Permeance is reported as gas permeation units (gpu).  $1 \text{ gpu} = 1 \times 10^{-6} \text{ cm}^3(\text{STP})/(\text{cm}^2 \cdot \text{s} \cdot \text{cmHg})$  or  $1.33 \times 10^8 \text{ gpu} = 1 \text{ m}^3\text{m}/(\text{m}^2 \cdot \text{s} \cdot \text{kPa})$ .

To calculate the  $\Delta p$  in the Equation (3.21), one needs to find partial pressures relative to



feed and permeate side, expressed as:

$$\Delta p = p_{F,i} - p_{P,i} = x_{F,i} p_i^{sat} \gamma_i - y_{F,i}^L P_P \quad (3.22)$$

where  $x_{F,i}$  is a mole fraction of the component  $i$  in the feed,  $p_i^{sat}$  is the saturation pressure of the pure component  $i$  at a given feed temperature. The activity coefficient of the component  $i$ ,  $\gamma_{F,i}^L$ , is a very important parameter of the Equation (3.22). It is determined from the hypothetical vapor-liquid equilibria occurring in the feed mixture at given temperature, pressure and composition.

### 3.3.3 Determining the activity coefficients for solution-diffusion model

To determine the permeate-side relative partial pressure, the procedure is straightforward. It is enough to know the permeate-side pressure and permeate composition in vapor phase. These two values are obtained experimentally. However, to calculate the feed-side vapor pressure, one needs to know the activity coefficient. We used the data provided in Chapter 2 which is dedicated to vapor-liquid equilibria.

The activity coefficients were determined from the equilibrium condition (the equality of fugacities in both phases):

$$f_i^L = f_i^V \quad (3.23)$$

where  $f_i^L$  and  $f_i^V$  is the fugacity of the component  $i$  in liquid and vapor phase, respectively.

In all the cases, the fugacity of component  $i$  in vapor phase is calculated as:

$$f_i^V = \phi_i^V P y_i \quad (3.24)$$

For the liquid phase, according to the  $\gamma - \phi$  method:

$$f_i^L = x_i P_i^{sat} \phi_i^{sat} \gamma_i^L \exp\left(\frac{v_i^L (P - P_i^{sat})}{RT}\right) \quad (3.25)$$

and, according to the  $\phi - \phi$  method:

$$f_i^L = \phi_i^L P x_i \Rightarrow \phi_i^L x_i = \phi_i^V y_i \quad (3.26)$$

where  $\phi_i^L$  and  $\phi_i^V$  are the fugacity coefficients of the component  $i$  in liquid and vapor phase,

respectively,  $P_i^{sat}$  is the saturated vapor pressure of the component  $i$ ,  $\phi_i^{sat}$  is the fugacity coefficient of  $i$  at the saturation,  $\gamma_i^L$  is the activity coefficient of  $i$  in the liquid phase. The exponential term is a Poynting factor.

By combining Equations (3.25) and (3.26), we obtain:

$$x_i P_i^{sat} \phi_i^{sat} \gamma_i^L \exp\left(\frac{v_i^L (P - P_i^{sat})}{RT}\right) = \phi_i^V y_i \quad (3.27)$$

Rearranging the previous equation allows to obtain the final expression for activity coefficients calculation:

$$\gamma_i^L = \frac{P \phi_i^V y_i}{P_i^{sat} \phi_i^{sat} x_i} \exp\left(-\frac{v_i^L (P - P_i^{sat})}{RT}\right) \quad (3.28)$$

In order to visualize the activity coefficients, we have plotted them as a function of water molar fraction for 303.15 K, 323.15 K and 343.15 K in the Figure 3.15 below.

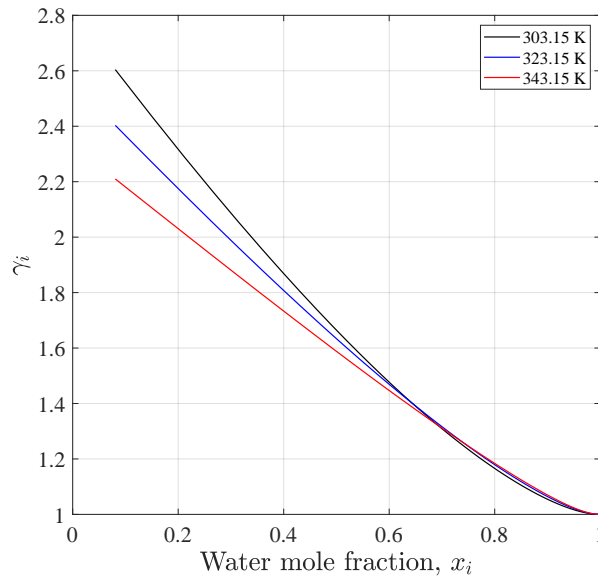


**Figure 3.15:** Water activity coefficients in the liquid ARCACLEAN mixture as a function of molar fraction for 303.15 K, 323.15 K and 343.15 K

Very important conclusions must be taken from the above plot. First of all, as we can see, at  $x_{water} = 0.1$  [mass] (which equals to  $x_{water} = 0.49$  [molar]), the activity coefficients range from 1.6 to almost 1.8, being an additional term for the pervaporation driving force. It means that the feed-side partial vapor pressure becomes almost twice higher, so the activity coefficients are *absolutely not negligible in pervaporation!* Moreover, their influence on driving

force is even higher with lower water content in feed (at the end of dehydration process).

At the same time, the activity coefficients are lower with higher temperature, meaning that at higher temperature the liquid mixture shown less non-ideality. In our case, the temperature effect on the non-ideality becomes inverted after  $x_{water} = 0.7$  molar and as water content in feed goes higher.

## 3.4 Results and discussion

### 3.4.1 Influence of temperature

When mass transfer parameters are driving force normalized, their temperature dependence can be completely different and can not correspond to the mass flux increase/decrease. This fact, concerning the permeance, is illustrated below.

The permeances were determined using the experimental data from Figure 3.9 and the Equation (3.21) for that purpose. The reason of determining permeances and not permeabilities is that the active layer thickness of the 4510-2898 membrane,  $l$ , was not communicated by the supplier (as a part of confidential information) and, thus, was unknown for us.

The procedure of permeances calculation is as follows. First of all, the the respective activity coefficients for each point were determined using the results from Chapter 2 and the Section 3.3.3. Then, using the permeant molar fraction and calculated its saturated pressure at given temperature, the feed-side partial pressure was obtained. It is known from Section 3.2.4.2 that the only component that permeates through the membrane is water. Therefore, the permeate-side partial pressure is equal to the total permeate-side pressure measured experimentally. Finally, the permeances are calculated for each point from the Equation (3.21) and presented graphically in Figure 3.16.

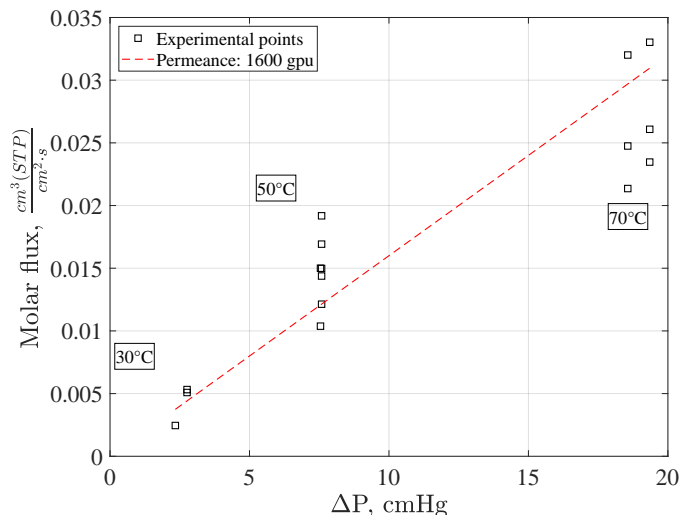


**Figure 3.16:** Experimental data from Figure 3.9 replotted as molar flux over  $\Delta p$  with a fitted value of permeance of 1600 gpu (slope)

Analyzing the obtained results, one can notice that the permeances vary roughly from 1000 to 2600 gpu. This can be explained by the fact that our experimental points are too scattered due to bad reproducibility. In order to check if the permeance is dependent on (or independent of) temperature in our case, a linear function was fitted to the experimental points. A value of 1600 gpu was then obtained as a slope.

An example of how the permeance can change with the temperature was also illustrated by Ray and Ray (2006) and, later, reproduced by Baker et al. (2010) using the solution-diffusion model, for cross-linked and rubber membranes<sup>1</sup>. It was shown, that, for that type of membrane and for temperature ranging from 32 to 52°C, the permeance was changing from 200 to 350 gpu.

Which conclusion can be made from the above Figure? Even if the permeance changes with the temperature, this change appears to be small. The intrinsic permeance depends on diffusivity and sorption. While the diffusivity usually increases with temperature, the sorption usually decreases. In some cases, the sorption changes faster than diffusivity which leads to the decreasing of permeance (Ray and Ray, 2006; Baker et al., 2010). In our case, the change in these values is, apparently, in balance one with another, so the permeance *does not change* with temperature. Figure 3.17 represents the permeances plotted over the feed temperature together with the average value of 1600 gpu. We can see from these two Figures that the permeance can be considered as *independent* of temperature.

<sup>1</sup>Application: dehydration of toluene

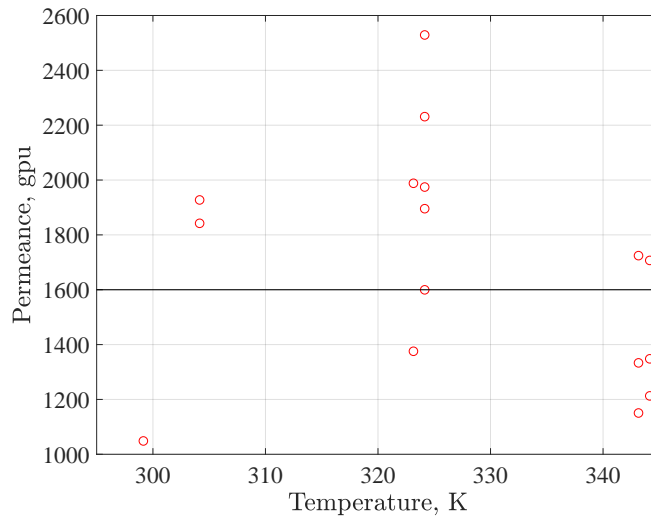


**Figure 3.17:** Calculated permeances for the membrane PERVAP 4510-2898 as a function of temperature. Quasi-stationary regime, water content in feed 10%wt

### 3.4.2 Influence of feed concentration

Let's now proceed to the analysis of mass transfer parameters dependence on initial feed concentration. Figure 3.18 represents the membrane performance in terms of the molar flux over the  $\Delta p$ . Analogically, as the water depletes from the feed, the driving force decreases due to the decreasing of feed-side partial vapor pressure. Finally, that leads to the decrease of the flux.

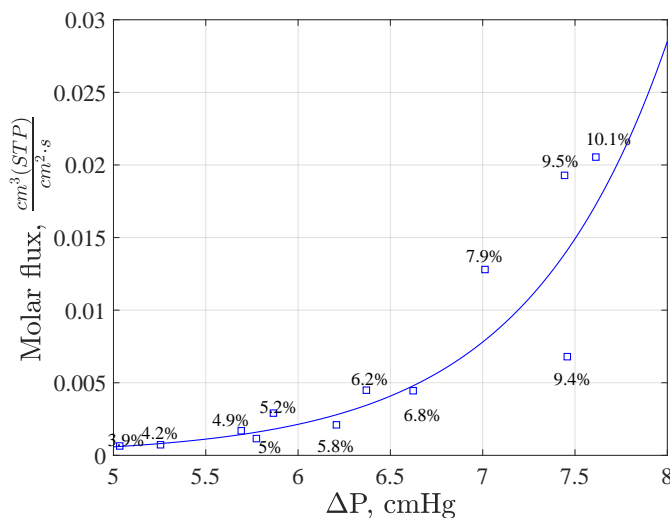


**Figure 3.18:** Molar flux as a function of  $\Delta p$  at 50°C

Concerning the permeance, if we observe how it changes with the initial water concentration in feed, we will see that, contrary to temperature, it is very concentration dependent.

It can be seen from Figure 3.19. When the water concentration is high, the permeance is about 2000 to 3000 gpu. This increase can be due to higher membrane swelling by water, which leads to plasticization. The diffusivity is higher with higher swelling, so does the permeance. At low water concentrations in feed, its permeance drops to 150-200 gpu, although the membrane selectivity still does not change. This fact means, that, probably, even at a very low water concentration in feed, the solvent will not permeate through the membrane, so it can be dehydrated until any level without being lost.

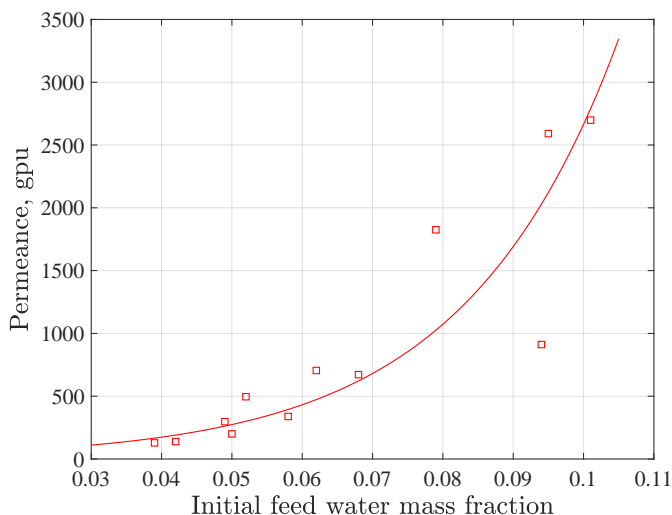


**Figure 3.19:** Evolution of water permeance as a function of initial feed concentration at 50°C

### 3.4.3 Prediction of membrane performance in batch dehydration at different temperatures

In Section 3.2.4.2 the results of the batch solvent dehydration at 323.15 were reported. Once the dependence of mass transfer parameters on operating conditions is established, we can now predict the dehydration of solvent at another temperatures (but at the same permeate-side pressure), using the solution-diffusion model.

The predicted permeate fluxes can be calculated using Equation (3.21). For that, the permeance and the driving force should be known for the desired temperature. To calculate the driving force, one needs to find the feed-side partial vapor pressure at each composition and temperature. It can be done using the NRTL-PR model from Chapter 2 to compute the permeant saturated vapor pressures and activity coefficients for each point. The permeate-side partial vapor pressure should be equal to that of the reference experiment.

Another situation is with the permeance, as in order to calculate it, the diffusion and

sorption coefficients are needed. Nevertheless, some helpful conclusions concerning the permeance can be done from Sections 3.4.1 and 3.4.2. It was shown, that, for the membrane PERVAP 4510-2898, the water permeance was practically independent of temperature and strongly dependent on feed composition. It can be then assumed that the calculated permeances from Figure 3.19 will remain constant for the same concentration at any other temperature.

The batch dehydration was predicted for 303.15 and 343.15 K. The data from Figure 3.10(a) were taken as reference to calculate the permeances for each water concentration in feed. The results, plotted together with the reference 323.15 K curve, are presented in Figure 3.20.

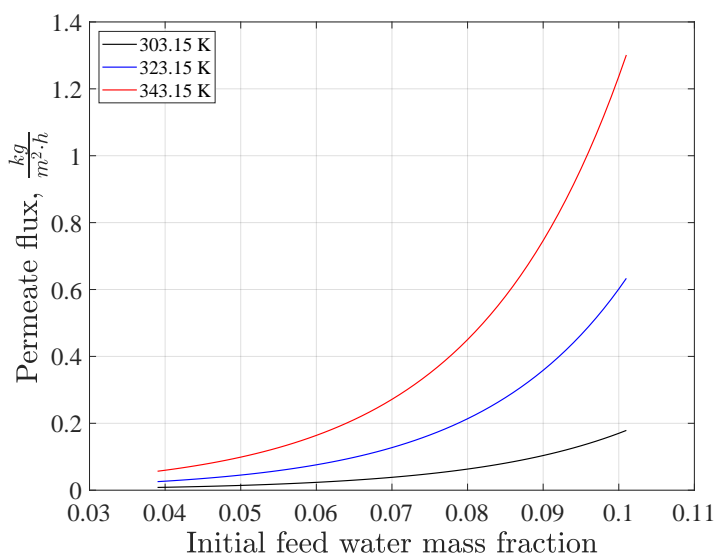


**Figure 3.20:** Prediction of permeate flux in batch dehydration for 303.15 K ad 343.15 K

If compared with the results from Figure 3.9, the predicted permeate flux for 343.15 K looks slightly overestimated at 10% of water in feed. But it still gives a good idea of what permeate fluxes could we achieve when dehydrating the solvent at the temperature of interest. As expected, the highest permeate flux corresponds to the highest temperature. The feed temperature of 343.15 K remains fairly reasonable for the feed liquid to be heated at in a dry cleaning device. For that reason, the 343.15 curve will be used to determine the required membrane surface later in Chapter 4.

### 3.5 Chapter conclusion

Numerous tests that were carried out have proven that the dehydration of the ARCA-CLEAN solvent by pervaporation is feasible. The used commercially available membranes

have demonstrated a very good performance and selectivity. It is important to emphasize that all the used membranes are also available as membrane modules ready-to-use in the industrial pervaporation plants.

Among the tested membranes, the membranes 4510-2898 and 4102-3184 were able to retain 100% of solvent. This is an extremely important result if an application inside a dry cleaning machine is planned, as the solvent losses during the regeneration cycles represent a high part of the operational costs and, thus, should be avoided. The absence of solvent losses can lead to huge economies for the dry cleaning machine operator.

The permeate obtained using the membrane 4100-3239 represented a non-miscible solution. The prevailed permeated solvents are most probably DPnB or/and PnB. It is, of course, possible to analyze the permeate via the GC by firstly diluting the non-miscible samples in a third body (for example, methanol or acetone, as illustrated in Chapter 2) and secondly recalibrating the GC for that type of analysis. However, this membrane was not our priority in this work.

When discussing the membrane performance in terms of permeate flux, one can indicate that the flux order (0.85 to 0.95 kg/m<sup>2</sup>·h) is slightly lower of those generally obtained in pervaporation (for example, the sources [Svang-Ariyaskul et al. \(2006\)](#); [Huang et al. \(2010\)](#); [Baker et al. \(2010\)](#) report the values of permeate flux being between 1 and 1.25 kg/(m<sup>2</sup>·h) in alcohol dehydration). Nevertheless, the membrane module suppliers offer nowadays a wide range of very compact solutions having high membrane surface, which allow to compensate low permeate fluxes and to reach a necessary production level.

It was also shown that determining the activity coefficients is very important in order to correctly characterize the membrane transport. The obtained activity coefficients were ranging from 1.6 to 2.1 meaning a contribution of the order of almost 2 to the driving force.

The mass transfer parameters dependence on operating conditions was studied with the help of the solution-diffusion model. It was shown that the water permeance is practically independent of temperature while the driving force (and, thus, the permeate flux) increases with temperature. In our case, the water permeance was assumed to be only feed concentration dependent. This assumption allowed us to predict the batch dehydration of solvent for 303.15 K and 343.15 K.



The next step of the present study is to design the pervaporation unit that can be integrated into a dry cleaning machine. The key task here will be to determine a membrane surface allowing to achieve the required unit production and performance. This task, as well as the overall unit design, including pumps and heat exchangers, is the subject of the next Chapter.

## Chapter 4

# On the design of the pervaporation unit for solvent dehydration and its integration in the dry cleaning machine

**W**HEN all the necessary data are finally obtained, we now proceed to the design of a pervaporation stage for solvent dehydration in the ARCAFLEX320. During all the steps of design, we intend to keep the system as simpler and compact as possible. We would also like to pay attention that the solvent mixture to dehydrate was considered as already purified from dirt and sludge in the pre-treatment stage. However, the pre-treatment stage development is out of the scope of the present Thesis and is a part of future design and R&D work.

As a first step, we are going to define a starting point for our design by investigating the existing distillation system. We will try to find some common points between the existing and the future systems. Our final goal is to design a system which will perfectly suit the dry cleaning machine with minimum modifications.

Our choice is to design a system to perform the dehydration in *batch* mode. In this mode, the solvent mixture is taken from the feed tank. The retentate coming from the membrane module is returned back to that tank. Such a solution is motivated by the possibility of the retentate recirculation allowing to considerably reduce the membrane effective area. Though the batch pervaporation is usually longer than the continuous one, we do not have any specific time constraint concerning the dehydration.

In the Section [4.1](#), the existing distillation system will be detailed. We intend here to better understand its working principle as well as to determine whether some of the existing

apparatus could be reused in pervaporation or not.

Section 4.2 is completely devoted to the design of the pervaporation stage. The estimation of the main characteristics and parameters will be performed here. Among them, the effective membrane area required, a heat transfer area of the permeate condenser are discussed. The permeate condensing and the vacuum pump choice are discussed as well.

## 4.1 ARCAFLEX320 distillation system

We have started the design of a new regeneration system based on pervaporation by analysing in detail the existing distillation process. The important points to be figured out are:

1. The main energy and water consumers;
2. Equipment that can potentially be reused in pervaporation.

Understanding these points is essential to design an energy efficient and a ready-to-connect pervaporation system.

### 4.1.1 Overview and working principle






The distillation system layout is presented in Figure 4.1. It consists of the following main apparatus: the steam distiller (1), the electric boiler (2) used to generate vapor for distiller heating, the sludge container (3), the auxiliary recovery tank (4), the main and secondary condensers (5) and (6) respectively, the vacuum pump (7), the distillate tank accumulator (8) and the drying recovery tank (9).

A brief description of the distillation stages is the next. After each washing cycle, the solvent is delivered and accumulated in the distiller (1) for the first distillation at 200 mbar in the frame of the *Stage 1* (about 20 cycles). The vapors are condensed in the condenser (5) and the distillate is then passed to the tank (4). The residue in the distiller (1) is distilled once more at 50 mbars in order to eliminate the sludge (*Stage 2*) and the distillate is sent to the solvent tank (not shown in the flowsheet). The residue is evacuated from the distiller to the sludge container (3) and then withdrawn from the system. Then, the solvent is charged in the distiller from the tank (4) for the *Stage 1a* and distilled at 50 mbar. The distillate (78% wt water) is sent back to the tank (4) and then removed as waste. The residue is mixed with the solvent from *Stage 2* in the solvent tank.

CHAPTER 4. ON THE DESIGN OF THE PERVAPORATION UNIT FOR SOLVENT DEHYDRATION AND ITS INTEGRATION IN THE DRY CLEANING MACHINE

POS	NAME
1	STEAM DISTILLER
2	ELECTRIC BOILER
3	SLUDGE CONTAINER
4	ADDITIONAL RECOVERY TANK
5	MAIN CONDENSER
6	VACUUM PUMP CONDENSER
7	VACUUM PUMP
8	DISTILLER TANK ACCUMULATOR
9	TANK DRYING RECOVERY

PIPES DESIGNATION	
	WATER LINE
	SOLVENT LINE
	STEAM LINE
	AIR LINE
	VACUUM LINE

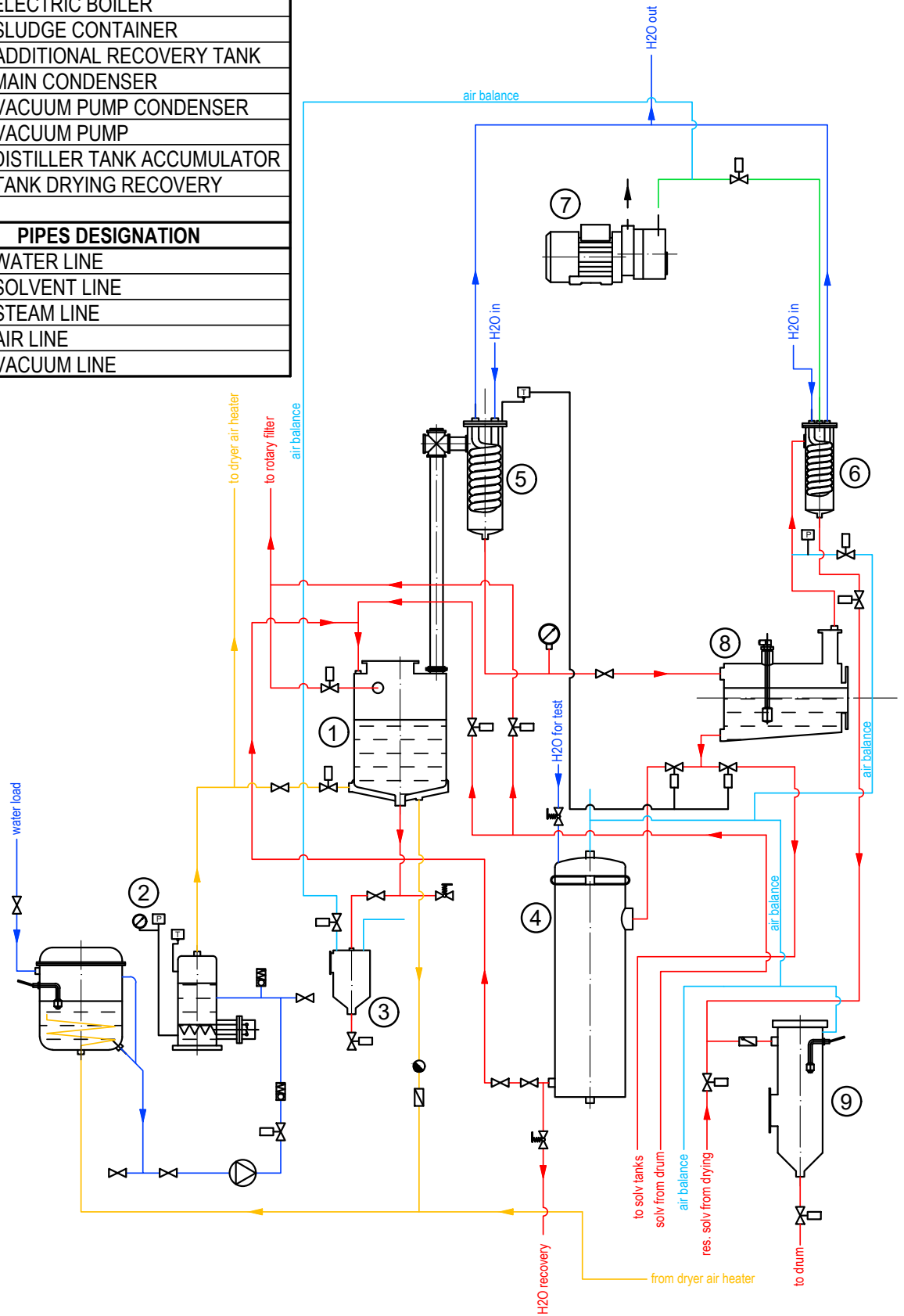


Figure 4.1: Distillation system of the ARCAFLEX320 device

The distillate tank (8) is used to accumulate the distillate and to perform as liquid separator. The distiller (1) is heated by the steam produced in the electric boiler (2). A part of that steam is also used to heat the air in the machine's drum (not shown in the flowsheet) during the garments drying phase. The solvent, evaporated from garments during drying, is condensed and sent to the drying recovery tank (9), from which it is later delivered to the machine's drum. A vacuum in the distillation system is created by the vacuum pump (7). The condenser (6) prevents the liquid suction into the pump.

As it can be seen, the system has two condensers (5) and (6) refrigerated by water from the city network within an open circuit. These devices are, thus, the main water consumers. Respectively, the electricity consumers are the electric boiler (2) (including the water pump) and the vacuum pump (7).

#### 4.1.2 Devices that can be reused

In order to be as optimal as possible while redesigning a system, it is always important to identify such an equipment in the existing system that can be reused in the new one. Generally, this equipment should be present in both previous and new systems and should be compatible with the required operating conditions and performance.

The proposed sketch of the future pervaporation system is presented in Figure 4.2.

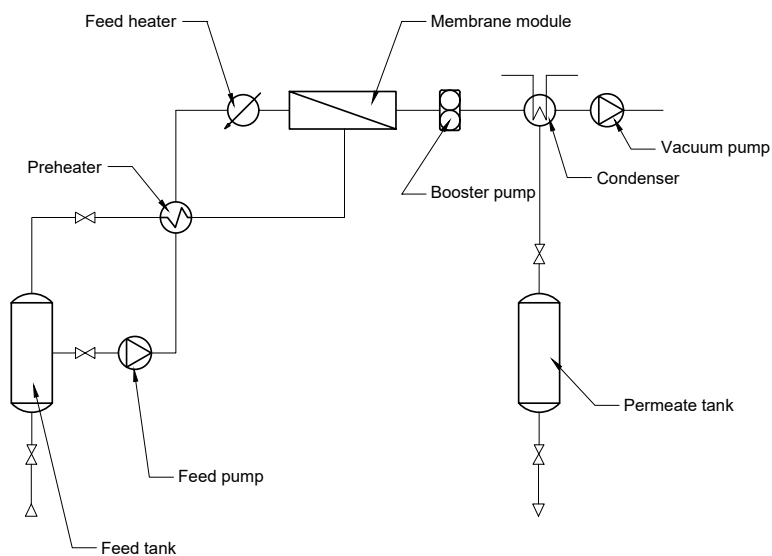


**Figure 4.2:** Initial sketch of the pervaporation dehydration stage

As we can see, both the actual distillation and pervaporation are performed under vac-

uum, so the vacuum pump (7) can probably be reused in pervaporation. However, in pervaporation a much deeper vacuum is used. Therefore, in order to integrate the vacuum pump (7), one needs to be sure that this pump is capable to provide a desired level of vacuum. Moreover, the ability of a vacuum pump to work with saturated or humid vapor is preferable in pervaporation (as it can simplify the system). At the present time, we have no reliable information about the model and performance of the vacuum pump (7) and this point will be clarified in the frame of a future work.

In pervaporation, the feed solution is preheated up to 70°C. The electric heater (2) was used to heat the distiller in the actual system. But when considered with regard to the pervaporation, this device has a drawback that makes it less favourable. As explained before, it generates steam which is then used to heat the feed solution, so the heating is not direct. This scheme means a very high energy consumption. We recommend to use an electric resistance directly to preheat the feed. Compared to steam generator, the resistance can be less energy consuming and more compact (as only one device is used instead of two).

The tank (4) with its volume of 25 liters can be used as a feed vessel, receiving and holding the solvent after the pre-treatment step. The electric resistance can be integrated in the bottom of the tank. The tank can also receive the retentate from recirculation, so that the dehydration can be performed in batch.

Concerning the using of the condenser (5) to condense the permeate vapor, this point is far from being evident. In fact, the condenser should be chosen for every specific application, as its heat exchange area should satisfy the required heat rejection. On the other hand, the condenser (6) can still be used to protect the vacuum pump from liquid suction.

### 4.1.3 Process constraints

There are some constraints and limitations that could be encountered while integrating the pervaporation for solvent dehydration. First of all, it is the duration of dehydration process. Current distillation takes 65 minutes. In case of pervaporation, we do not have a strict constraint in time. It mostly depends on the economic and practical aspects that will be discussed later in this Section.

As illustrated in Chapter 3, pervaporation has much lower production rate than distillation. The highest obtained permeate flux was less than  $1 \text{ kg}/(\text{m}^2 \cdot \text{h})$  at 70°C. To increase that parameter, it is possible to raise the feed temperature to higher values. At the same time,

increasing the feed temperature leads to higher energy expenses, which should be avoided. Moreover, the 65 minutes constraint will not be satisfied by that way. Therefore, the desired production rate is usually reached by increasing the membrane effective area. This will be described in further Sections.

As the dehydration system is a part of the whole dry cleaning machine assembly, one should not neglect the compactness factor. The ARCAFLEX320 gabarit dimensions are presented in Figure 4.3. It is highly preferable to respect those dimensions and take into account that both pre-treatment and dehydration systems should fit together in one assembly. It means that the dehydration system should be as compact as possible.

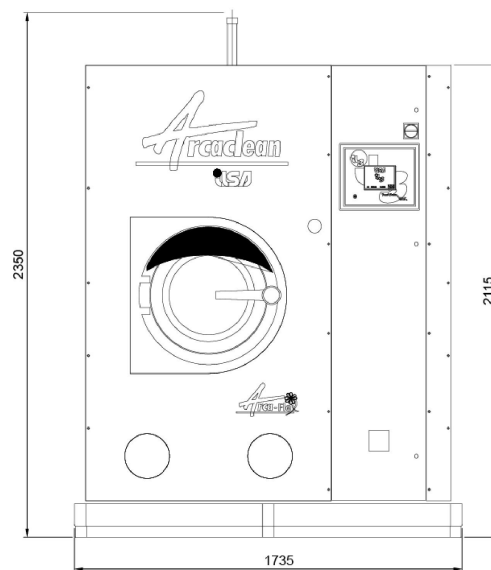


**Figure 4.3:** ARCAFLEX320 gabarit dimensions with solvent tank:  
 $W = 1735 \text{ mm}$ ;  $D = 1600 \text{ mm}$ ;  $H = 2113 \text{ mm}$

## 4.2 Design of the pervaporation unit

### 4.2.1 Membrane module

When choosing the membrane module, several conditions should be satisfied. In our case, we should know:

1. The desired process duration;
2. The feed solution temperature;
3. The feed solution mass/volume;

4. The initial feed water content;
5. The final water content in mixture (the final dehydration point).

These data are necessary to determine the appropriate effective membrane area. In other words, the problem can be reformulated as follows:

"Which membrane area is needed to dehydrate  $X$  liters of solvent mixture from  $Y_1\%$  wt to  $Y_2\%$  wt of water during  $Z$  minutes, knowing that the feed solution temperature is  $N^\circ\text{C}$ ?"

The initial data for calculations are presented in Table 4.1. The value for feed temperature was taken according to the results obtained in Chapter 3. The final water content in solvent recommended by *INNOVACLEAN* is about 1% wt.

**Table 4.1:** Initial data for membrane effective area calculation

Feed volume, l	Initial water content, %wt	Final water content, %wt	Process duration, min	Feed temperature, °C
20	10	≈1	65	70

Generally, in batch pervaporation, the membrane area,  $S$ , is related to the permeate flux<sup>1</sup>,  $J$ , as:

$$\frac{dm}{d\tau} = -SJ(m, \tau) \quad (4.1)$$

Thus, the required membrane area is found as:

$$S = -\frac{1}{\Delta\tau} \int_{m_{in}}^{m_{fn}} \frac{dm}{J(m, \tau)} \quad (4.2)$$

where  $\tau$  is the process time,  $m$  is the permeant mass in feed. The permeant (water) mass in feed is variable because the process is performed in batch and the retentate is recirculated to the feed. For these calculations we have used the predicted permeate flux data at  $70^\circ\text{C}$  from Figure 4.4.

---

<sup>1</sup>And  $J = f(m, \tau)$



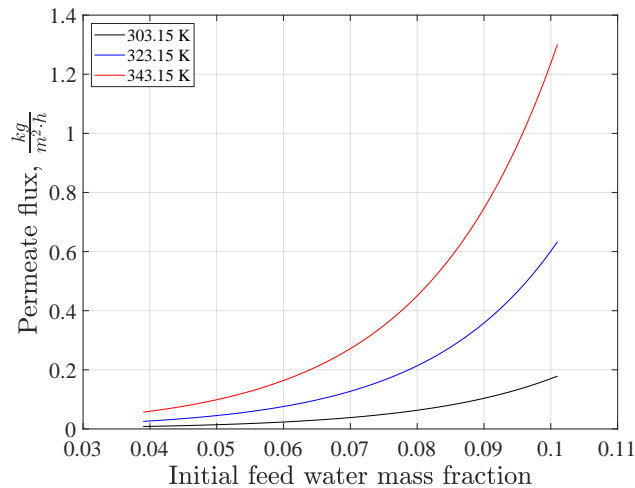


**Figure 4.4:** Prediction of permeate flux in batch dehydration for 303.15 K ad 343.15 K

The calculations were performed in order to determine the dependency of the membrane area on process time and final water content in solvent. Figure 4.5(a) represents the membrane area required to achieve different final water mass fractions during 65 minutes. The results for  $x_{fin} = 0.021$  and  $x_{fin} = 0.016$  are presented more precisely in Figure 4.5(b) as a function of process duration.

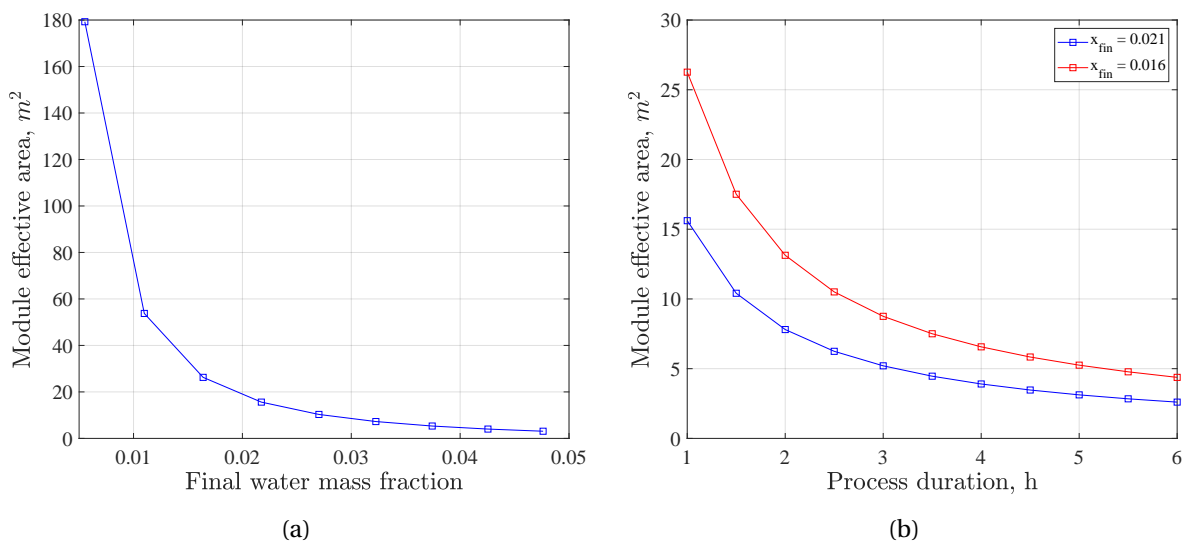


**Figure 4.5:** Membrane effective area as a function of: a) final water mass fraction ( $\tau = 65$  min); b) process duration

It can be seen from this Figure that, in order to dehydrate the solvent until 1.6%wt of water during 65 minutes, a membrane area of about 25 m<sup>2</sup> is required. Consequently, the membrane area can be reduced (and sometimes considerably!) by increasing either process duration or  $x_{fin}$

Finding the most optimal economic solution needs a deeper discussion with *INNOVA-CLEAN*. For the further design, the "most expensive" case, *i. e.* a module of 25 m<sup>2</sup> will be considered.

Another point to discuss concerns the configuration of the chosen module. As stated before, the main requirements for a module are its compactness and price.

There exist different module configurations for pervaporation. The membrane area of 25 m<sup>2</sup> remains relatively high, but it possible to be reduced by increasing the process duration. We have found the *spiral wound* modules the most attractive due to their high compactness and ability to contain large membrane areas. Nowadays, some membrane manufacturers in EU, for example *PERVATECH* (Netherlands), propose spiral wound modules for pervaporation having a wide range of membrane areas. According to our last exchange with *DeltaMem* (Switzerland), it is possible to order a module with a required membrane material and area.

Unfortunately, we have no clear information about the price of membrane modules at the present time. Even if the prices per square meter of membrane reduce every year, they remain relatively expensive. We are currently in contact with membrane modules manufacturer, however, we have not get any information concerning the exact module's price yet.

## 4.2.2 Vacuum system

The vacuum system is essential in pervaporation as it provides the driving force for the process. The vacuum is achieved by the vacuum pump installed on the downstream of membrane module.

The vacuum pump should be powerful enough to create as deeper vacuum as possible. Analogically to heat exchangers, there are several requirements that is preferable to respect towards a vacuum pump:

1. Limit vacuum: <1 Torr;
2. Low energy consumption;
3. Compactness;
4. Price;
5. Preferably:

Another property of vacuum pumps that can be useful in pervaporation is the capability to work with saturated vapors. In case if some non-condensed (for some reasons) residual permeate will be present in the suction line, it can be pumped off without any risk to the pump. Dry or liquid ring vacuum pumps are a good choice. Otherwise, it is always possible to use a pump protection, for example, a secondary condenser, but in this case we have to deal with an additional water consumer.

A common issue of the industrial pervaporation systems is that a desired vacuum level on the downstream of membrane module is often hard to reach. In fact, the downstream pressure will be imposed by the permeate condensation. In the laboratory scale units, the permeate is condensed immediately in the liquid nitrogen trap, so the pressure inside the trap remains extremely low. In the industrial scale, the permeate is condensed at much higher condensation pressures influencing the whole low-pressure side of the unit. This limitation can be overcome by installing a booster-type pump right after the membrane module to keep the downstream pressure as lower as possible to get the desired driving force.

### **4.2.3 Permeate condenser**

The main difference between the laboratory scale and industrial scale pervaporation is in the way how the permeate vapors are condensed. In laboratory scale, a cold trap immersed in liquid nitrogen is used in most of the cases. In industrial applications, it is not possible for practical reasons. Therefore, the permeate vapor is needed to be condensed using classical heat exchangers.

The main requirements towards a heat exchanger for our application were formulated as follows:

1. Ability to work under vacuum;
2. Total permeate condensing;
3. High heat transfer coefficients;
4. Low thermal resistance;
5. Compactness;
6. Price.

There exist three main types of condensers: shell and tube, air cooled and plate condensers. Among these types, the plate heat exchangers have the highest heat transfer coefficients and the lowest  $\Delta T$  between streams. Moreover, they are very compact due to high packing of heat exchange surfaces (plates). For the present pervaporation system, a *brazed plate* heat exchanger was chosen as a condenser. In this Section, a calculation procedure for condenser thermal design will be described.

The design of a heat exchanger starts by definition of the input parameters such as the condensing temperature and pressure,  $T_{cond}$  and  $P_{cond}$ , the nature of heat transfer medium and its temperature,  $T_2^{in}$  the permeate vapor flow,  $D_1$ . The result of the condenser design is the required heat transfer area. Using this value, a commercially available heat exchanger is then chosen. The input parameters used in our calculations are presented in Table 4.2. It was assumed that the water will be used as heat transfer medium, cooled in a chiller at 10°C. The permeate flow rate was assumed to be 3 kg/h basing on the amount of water that should be eliminated from feed. The transfer medium  $\Delta T$  in plate heat exchangers is usually assumed to be 4÷6°C.

**Table 4.2:** Initial data for condenser design

$T_{cond}$ , °C	$P_{cond}$ , mbar	$T_2^{in}$ , °C	$T_2^{out}$ , °C	$D_1$ , kg/h	Permeate	Heat transfer medium
20	23	10	16	3	water	water

The thermophysical properties of streams were calculated using the CoolProp library for MATLAB and gathered in Table 4.3. Here,  $\nu$  is a cinematic viscosity,  $\rho$  is a density,  $\lambda$  is a thermal conductivity and Pr is a Prandtl number. The indices (1) and (2) correspond to the permeate and transfer medium stream, respectively.

**Table 4.3:** Thermophysical properties of streams

Stream	$\nu$ , m <sup>2</sup> /s	$\rho$ , kg/m <sup>3</sup>	$\lambda$ , W/(m·K)	Pr
(1)	$1.0035 \cdot 10^{-6}$	998.16	0.598	7.0092
(2)	$1.2012 \cdot 10^{-6}$	999.38	0.585	8.6014

For the thermal design the following geometry characteristics of plates were taken (Chiumak, 2007): channel cross-section area,  $f_{ch} = 0.00064$  m<sup>2</sup>; hydraulic diameter of channel,  $d_{ch} = 0.004$  m; channel length,  $L = 4.37$  m; plate thickness,  $\delta_p = 0.0005$  m; plate thermal conductivity,  $\lambda_p = 16$  W/(m·K).

The specific heat of condensing is calculated from the condensing process as:

$$q_{cond} = h_1^{in} - h_1^{out}, \quad \left[ \frac{J}{kg} \right] \quad (4.3)$$

with  $h_1^{in} = 2.53 \cdot 10^6$  J/kg, the enthalpy of permeate in the inlet of condenser,  $h_1^{out} = 8.39 \cdot 10^4$  J/kg, the enthalpy of condensed permeate in the outlet of condenser.

The condenser heat duty is equal to:

$$Q_{cond} = q_{cond} \cdot D_1, \quad [W] \quad (4.4)$$

The transfer medium mass flow,  $G_2$ , is found from the heat balance equation:

$$G_2 = \frac{Q_{cond}}{C_{p2}(T_2^{out} - T_2^{in})}, \quad \left[ \frac{kg}{s} \right] \quad (4.5)$$

with  $C_{p2} = 4.19 \cdot 10^3$  J/(kg·K), the transfer medium specific heat.

The logarithmic mean temperature difference is obtained from the expression:

$$LMTD = \frac{T_2^{out} - T_2^{in}}{\ln \frac{T_{cond} - T_2^{in}}{T_{cond} - T_2^{out}}} \quad (4.6)$$

The transfer medium average velocity,  $\omega_2$ , is firstly assumed to be 0.6 m/s (Chiumak, 2007). Then, the number of parallel channels in a plate package is determined:

$$z = \frac{G_2}{\omega_2 \cdot \rho_2 \cdot f_{ch}} \quad (4.7)$$

Then, the value of  $\omega_2$  is corrected:

$$\omega_2 = \frac{G_2}{z \cdot \rho_2 \cdot f_{ch}}, \quad \left[ \frac{m}{s} \right] \quad (4.8)$$

Using the obtained values, the Reynolds number for heat transfer medium is found as:

$$Re_2 = \frac{\omega_2 \cdot d_{ch}}{\nu_2} = 423 \quad (4.9)$$

The transfer medium-side Nusselt number for laminar flow is:

$$Nu_2 = 1.4 \cdot \left[ \frac{Re_2 \cdot d_{ch}}{L} \right]^{0.4} \cdot Pr^{0.33} \cdot 1.05 \quad (4.10)$$

The heat transfer coefficient on the transfer medium side is defined as:

$$\alpha_2 = \frac{\text{Nu}_2 \cdot \lambda_2}{d_{ch}}, \quad \left[ \frac{W}{m^2 \cdot K} \right] \quad (4.11)$$

The heat transfer coefficient at the permeate condensation in channels, without taking into account the vapor velocity correction term, is equal to:

$$\alpha_1 = 1.15 \cdot \left( \frac{(h_1^{in} - h_1^{out}) \cdot \rho_1^2 \cdot \lambda_1^3 \cdot g}{\mu_1 \cdot L \cdot \theta_0} \right)^{0.25}, \quad \left[ \frac{W}{m^2 \cdot K} \right] \quad (4.12)$$

where  $\mu_1 = 0.0010$  Pa·s, the dynamic viscosity of permeate at  $T_{cond}$ ,  $\theta_0 = T_{cond} - T_w$ , the difference between condensing temperature and plate wall temperature at the permeate side, and  $g = 9.81$  m/s<sup>2</sup>.

The heat flow density is defined for each stream as:

1. For the transfer medium side:

$$q_{F2} = \frac{LMTD}{\frac{1}{\alpha_2} + \frac{\delta_p}{\lambda_p} + R_{ls}}, \quad \left[ \frac{W}{m^2} \right] \quad (4.13)$$

2. For the permeate side:

$$q_{F1} = 1.15 \cdot \left( \frac{(h_1^{in} - h_1^{out}) \cdot \rho_1^2 \cdot \lambda_1^3 \cdot g}{\mu_1 \cdot L} \right)^{0.25} \cdot \theta_0^{0.75}, \quad \left[ \frac{W}{m^2} \right] \quad (4.14)$$

with  $R_{ls} = 5.7 \cdot 10^{-5}$  W/(m·K), the thermal resistance of the limescale (in case of the condenser fouling and scaling).

The final value of the heat flow density,  $q_F$ , is determined graphically. To do that, two functions,  $q_{F2} = f(LMTD)$  and  $q_{F1} = f(\theta_0)$ , are plotted within the same coordinates. The first function is plotted starting from  $LMTD = 0$ . To plot the second function, one should guess several values of  $\theta_0$  and calculate the corresponding heat flow densities using the Equation (4.14). The intersection of two functions corresponds to the final heat flow density of system. The graph is presented in Figure 4.6.

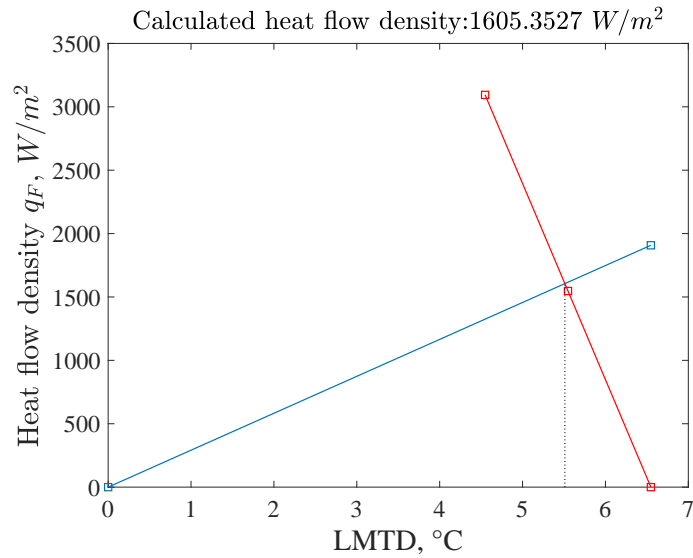


**Figure 4.6:** Plot of functions  $q_{F2} = f(LMTD)$  (—) and  $q_{F1} = f(\theta_0)$  (—)

Finally, the required heat transfer area is calculated as follows:

$$F = \frac{Q_{cond}}{q_F}, \quad [m^2] \quad (4.15)$$

which, in our case equals to  $1.2736 \text{ m}^2$ . The heat of condensation is 2.044 kW.

According to the above obtained heat transfer area, an attractive solution can be a K050, a compact and light brazed plate heat exchanger from KAORI (Taiwan). It is shown in Figure 4.7 and has the following characteristics:

- Heat transfer area:  $1.326 \text{ m}^2$ ;
- Number of plates: 52;
- Size: H = 306 mm, W = 106 mm; D = 134 mm;
- Weight: 7 kg;

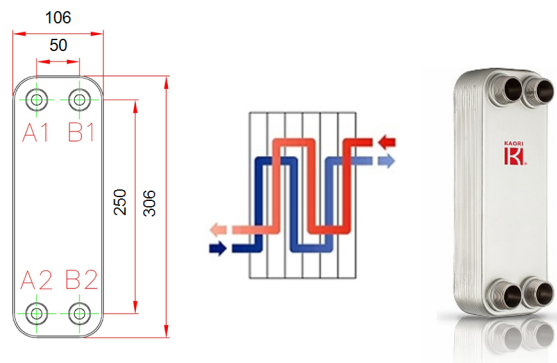


**Figure 4.7:** KAORI K050 brazed plate heat exchanger

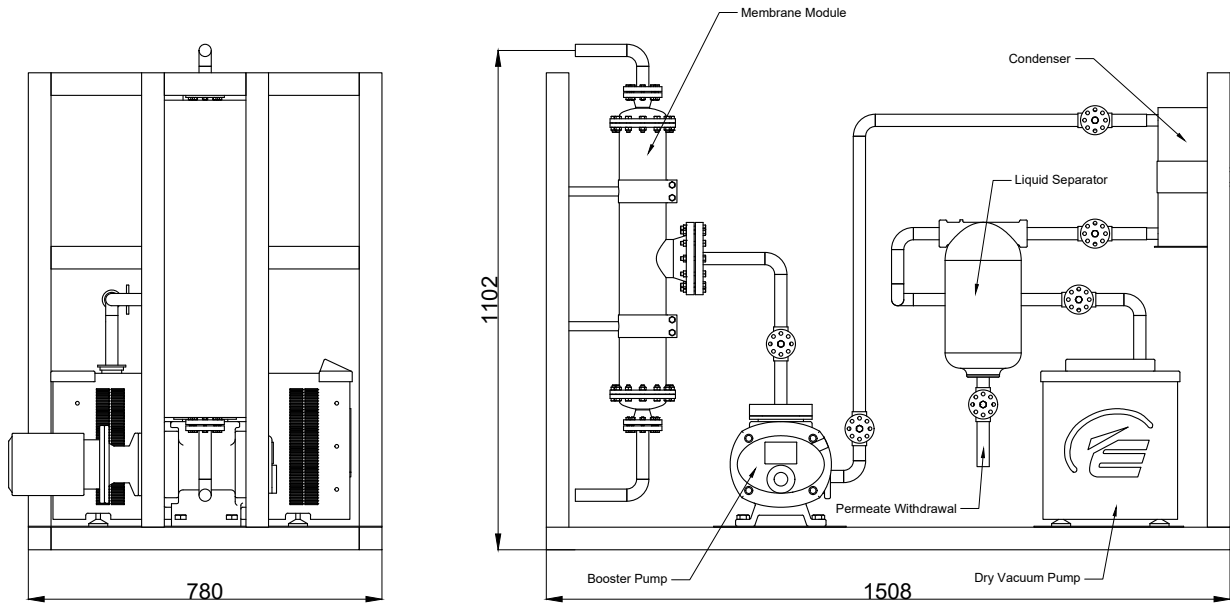
#### 4.2.4 System layout

Basing on the previously made calculations, a preliminary pervaporation system layout is proposed, as shown in Figure 4.8. It is composed of the spiral-wound membrane module, a dry vacuum pump, a permeate brazed plate condenser and a liquid separator. The booster pump, installed between the membrane module and the condenser, allows to maintain the pressure in the module as lower as possible. The membrane module is to be connected to the pre-heater on one side and to the feed tank (for retentate recirculation) on the other side.

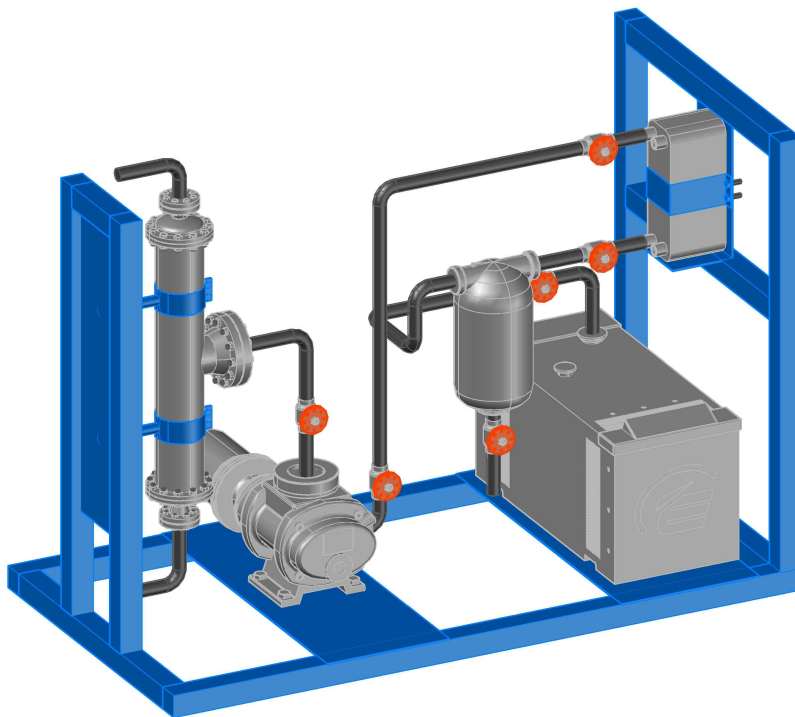
The advantage of such a scheme lays in its simplicity of mounting. Due to its compactness, the unit fits perfectly to the existing ARCAFLEX320 machine.

In order to simplify the system even more, another scheme can be proposed. Indeed, the idea is based on the fact that our permeate consists of the pure water that can be directly evacuated in the atmosphere in the vapor phase. In this case, the permeate condensing is not necessary anymore, so that the condenser, the liquid separator and the booster pump can be taken away from the system and the main vacuum pump will be connected to the membrane module's downstream. This approach has, however, some restrictions. Firstly, the vacuum pump should be able to work with saturated vapors. The second issue is the establishing of the desired vacuum, as the pump will have to evacuate constantly forming vapors. For that reason, the required driving force will be difficult (and, probably, impossible) to achieve.





(a)



(b)

**Figure 4.8:** Proposed pervaporation system layout: a) drawing with dimensions; b) 3D model

### 4.2.5 Operational costs estimation and comparison with distillation

The last task in the pervaporation system design is to estimate its probable cost in terms of energy and water consumption. The estimated values are then compared to those of the currently used distillation.

To calculate the annual process cost, we have taken the dehydration of the 20 liters of solvent mixture with 10%wt per cycle. It was also taken that 1500 cycles are performed yearly. The water and energy consumption per cycle data for distillation was provided by *Arcane Industries*. For pervaporation, an electric pre-heater with an internal resistance was considered. The feed temperature is meant to be 70°C. Along with this, the EDWARDS nXL200i dry vacuum pump and SHINKO AMB-D booster vacuum pump were considered as main and secondary pumps, respectively. The average pumps consumption was taken from their technical sheets, according to the vacuum level they create. For this cost estimation, the pre-treatment system was not taken into account.

The water consumption of the permeate condenser is calculated as described in Section 4.2.3, so the annual cost was estimated according to this consumption and considering the open water cycle. However, as a part of future design, the water for condenser can be refrigerated in a heat pump which is currently used in ARCAFLEX320 for garments drying in the drum. In that approach, the water cycle will be closed, reducing the water consumption and, thus, the annual operating cost.

The prices of water and electricity were considered to be current average values in France:

- Water: 3.5 €/m<sup>3</sup>;
- Electricity: 0.075 €/kWe.

The annual cost comparison chart is presented in Figure 4.9.

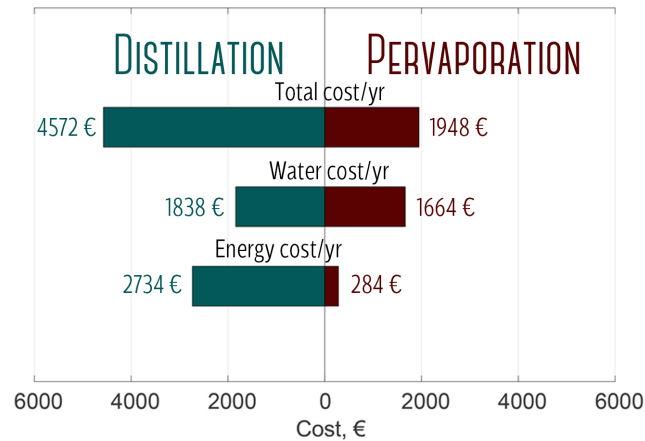


**Figure 4.9:** Comparison of dehydration by distillation and pervaporation in terms of annual costs for 20 liters of solvent mixture with 10%wt of water per cycle (1500 cycles/year)

Thus, according to Figure 4.9, we estimate more than 50% of economy in the annual perspective. This economy can be achieved principally due to considerably reduced energy consumption in pervaporation compared to the current distillation. Concerning the water consumption for means of permeate condensing, it was estimated to be almost equal to that of distillation.

### 4.3 Chapter conclusion

In this Chapter, the pervaporation system for solvent dehydration aiming to replace the distillation in the current generation of ARCAFLEX320 machines was designed. We propose to use a unit based on one (or multiple) spiral-wound membrane modules for the sake of compactness. The required membrane area was estimated for a 65 minutes cycles dehydration of 10%wt of water in feed at 70°C and with the final water content of 1.6%wt. The obtained value for the membrane area is about 20 to 25 m<sup>2</sup>.

To condense the permeate vapor, a brazed plate heat exchanger was proposed. This type of heat exchanger was chosen due to its heat transfer properties (namely, higher heat transfer coefficients, lower  $\Delta T$  between streams), as well as price and compact size. The required heat exchange area was estimated as 1.326 m<sup>2</sup> to reject 2.044 kW of heat from permeate.

The proposed system has two pumps. The main vacuum pump will be used to provide the vacuum in the system, particularly, in the condenser and before. The purpose of the

booster pump is to create as deeper vacuum as possible right on the membrane downstream to achieve the best process driving force. The scheme without permeate condensing was proposed as an alternative solution in order to reduce the system complexity and costs to minimum. In this case, the unit is only equipped by the membrane module and one vacuum pump, and the permeate vapors are evacuated directly to the atmosphere. As explained in Section 4.2.4, this scheme has significant drawbacks in terms of providing the required driving force.

Finally, the proposed unit was compared with the existing distillation in terms of operational costs in the annual perspective. The results have shown that the proposed unit can be more than 2 times less expensive in water/electricity consumption, giving a much better separation quality with no solvent loss.



# Conclusions and directions for future research

## Thesis conclusions

**A**MONG the alternative dehydration processes capable to replace the distillation in dry cleaning machines, the pervaporation is the most promising one as it offers highly favourable conditions for solvent dehydration. Using two of studied poly(vinyl)alcohol cross-linked membranes, we have obtained a perfect water selectivity and a permeate which contained only pure water. The permeate fluxes ranging from 0.85 to 0.95 kg/(m<sup>2</sup>s) were obtained at 10%wt of water in feed and at 70°C (membrane PERVAP4510, the most favourable one). These values are in agreement with those of literature. The other membranes have shown either lower flux (PERVAP4102) or separation efficiency (PERVAP4100, had the solvent permeating through it).

It is very important to understand the mixture of interest in terms of thermodynamics in order to design a pervaporation process. To do that, we have performed an exhaustive experimental and theoretical study of the ARCACLEAN + water mixture. The experimental vapor pressures of pure compounds and mixtures were obtained. It was found out that the solvent mixture is miscible with water regardless of water content. A high non-ideality of this mixture appears to be more present at low water concentrations. Considering the pure components that form the ARCACLEAN solvent, the DPM, DPnB and PnB, these compounds have relatively large molecules and very low vapor pressures. The DPnB and PnB, when mixed with water, form partially miscible mixtures, while as the DPM is fully miscible at all water concentrations.

For thermodynamic modelling of our pure compounds and mixtures, the critical properties of DPM, DPnB and PnB were required. Unfortunately, these properties have not been published yet. Therefore, they were firstly estimated using the Wilson and Jasperson group

contribution method and then adjusted more to improve the representation of the pure compounds by means of the Peng-Robinson cubic EoS.

A fully predictive NRTL-PR thermodynamic model was used to represent the phase equilibria occurring in binary and quaternary mixtures formed from DPM, DPnB, PnB and water. A new functional group, "-O-" (ethers), was added to the model's parameters matrix and its molecular interaction parameters were estimated by fitting to an experimental data set of 16 mixtures containing the same group, as well as the other groups presented in mixture (paraffins, alcohols and water). The modelling results were validated using the previously measured phase equilibria data for pure compounds and mixtures. The results demonstrate a very good representation of the experimental points by the NRTL-PR model. One of the advantages of the NRTL-PR model is that it is based on the Peng-Robinson EoS making it suitable for both vapor-liquid (VLE) and liquid-liquid (LLE) calculations. However, we still had some issues related to very low vapor pressures of our components, which are sometimes hard to represent precisely using an equation of state initially designed for medium and high pressures (occurring in hydrocarbon mixtures). This issue was fixed by adding the DPM + water VLE data to the data set during group interaction parameters estimation. Of course, after this manipulation, one cannot say anymore that the phase equilibria for our binary mixtures were fully predicted. Nevertheless, the quaternary mixtures were completely predicted using the obtained molecular interaction parameters.

Using the NRTL-PR model, we were able to estimate the water activity coefficients in liquid phase. This was one of the most important milestones of the present work, as the activity coefficient is a term included in the pervaporation driving force<sup>2</sup>. Many authors usually neglect this extremely important parameter making their systems independent of their non-ideality. However, we have illustrated that, in our case, the activity coefficients were ranging from 1.6 to 2.1 meaning the contribution to driving force of the order of 2, which can in no case be neglected.

The pervaporation results were then interpreted using the solution-diffusion model, taking into account the obtained activity coefficients. This approach, describing the transport of species through the dense membrane layer, has indicated that the water permeance is independent of temperature but is decreased with lower water concentrations in feed solution.

Concerning the design of the pervaporation stage which will be integrated to the existing

---

<sup>2</sup>when described by the solution-diffusion model

dry cleaning machine, we have estimated the membrane area we need to dehydrate the solvent. As a first approach and for all the estimations, we kept our dehydration process within the same time constraints as the original distillation, 65 minutes, but, at the same time, tried to achieve a deeper dehydration (almost 1%wt of water instead of 4%wt obtained currently in distillation). The water content in feed was taken as 10%wt (approximately close to the value of the real machine) and the feed temperature was taken as 70°C in order to have higher permeate flux. In the above given conditions, the estimated values for the membrane area are from 20 to 25 m<sup>2</sup>. Of course, this value can be reduced either by increasing the process duration or increasing the final water content. The optimal value for membrane area (and even module configuration) will be discussed in the frame of the future work, as it requires more aspects to be taken into account (for instance, economical aspect). Nevertheless, the EU membrane market proposes nowadays a wide range of membrane modules with different configuration and membrane area. At the present time, we have not enough information concerning the module's pricing, but we are currently in contact with membrane manufacturers and are going to get the pricing information very soon.

Another point concerns the condensing of permeate. In this context, we have proposed to use plate heat exchangers as the most compact and efficient ones from the point of view of heat transfer. The required heat transfer area was estimated as 1.32 m<sup>2</sup>. The condenser was designed in a manner to condense the permeate at reasonable temperature and pressure. For the sake of simplicity, we have taken the transfer medium (water) coming with a  $T_{in} = 10^{\circ}\text{C}$ . Having taken into account the  $\Delta T = 10^{\circ}\text{C}$  usually required for condensing, we obtain a condensing temperature  $T_{cond} = 20^{\circ}\text{C}$  and a respective condensing pressure  $P_{cond} = 20$  mbar. In order to achieve the 10°C of the transfer medium, it is needed to be cooled in a chiller. In the future, we are going to examine the possibility of using for this purpose the heat pump installed in the ARCAFLEX320 and currently used for garments drying. This heat pump can probably even be used to preheat the feed liquid.

In spite of the wide range of available vacuum pumps in the market, their choice remains a point to discuss with *INNOVACLEAN* in the future. In this work, we intended to provide only general recommendations concerning vacuum pumps. For instance, we have concluded that it would be judicious to add a booster pump to the system in order to keep very low pressure on the permeate side of the membrane. The advantage of such pumps is also their capacity of working with humid vapors, thus, without requiring a protection from liquid suction. Also, dry and liquid ring vacuum pumps can be an appropriate choice for the main pump. Also, as a part of the future work, it is planned to reduce the complexity of the



system and probably even to study a possibility of a direct permeate evacuation without its condensing. This can reduce the costs and complexity in a considerable way.

As it was demonstrated in Chapter 4, dehydrating the solvent by means of pervaporation can be much cheaper than doing it using the current distillation. More than 50% of economy can be achieved principally due to lower electricity demand for mixture heating. Along with that, pervaporation allows to avoid all the eventual solvent losses, keeping the initial ARCA-CLEAN formula and reducing the necessity of refilling the solvent to almost zero.

### **Short-term perspectives**

One of the most important tasks for the research continuation lies in development of the solvent pre-treatment step in order to get rid of fibers, dirt and colorants. This task was out of the topic of the present Thesis, so the solvent was considered already pre-treated before reaching the dehydration stage. But in reality, the pre-treatment is of high importance because it avoids the fouling of the expensive membrane module. We expect the pre-treatment system to be the following: the fibers and dirt are proposed to be eliminated using the mechanical filters, while the colorants can be removed by means of adsorption, using the activated carbons cartridges, for example. This layout includes only simple and affordable procedures. The filters are easy to clean and replace from time to time, and the cartridges can also be regenerated.

As stated previously, we intend to make our unit the most simple and compact possible, so we would like to reinforce our interest towards the system without permeate condensing. This can be achieved by implementing the sweep gas pervaporation. Investigating this technique is one of our preferences for the future research, as it can provide considerable benefits in both, compactness and cost.

Finally, as a logical continuation, we intend to protect the intellectual property by establishing a patent including all the above processes and procedures. The patenting is already ongoing and will be finalised as soon as the pre-treatment process will be developed.

## Long-term perspectives

In the frame of the long-term perspectives, we plan to do a more in-depth research concerning different directions.

First of all, a more thorough work is interesting to be done in order to improve the thermodynamic tool that was developed. First of all, more experimental points could be obtained for binary and quaternary mixtures, describing their vapor pressures as a function of composition more precisely. It is highly preferable to obtain the measured critical parameters for pure compounds and improve their representation by the Peng-Robinson EoS.

The representation of mixtures could be more improved by enriching the experimental data set used to estimate the interaction parameters for the group "-O-" and including the data for mixtures of very low pressures that were difficult to find before. Also, we are going to make our best effort to integrate our results into PROSIM and provide the conditions to describe the glycol ethers using the NRTL-PR model as a part of this very powerful process simulation tool.

Concerning the pervaporation itself, a lot of fundamental research can be done in the future. It could be useful to do an advanced study of the adsorption and transport of the solvent inside the membrane. The phenomena of concentration and temperature polarization are to be investigated as well. Valuable results can be obtained by firstly developing a flow model with taking the above phenomena into consideration and then applying it study the flows occurring in the industrial membrane modules. The effects of the temperature and concentration polarization become more visible during the scale-up. Further attention should also be paid on the diffusivity and the sorption parameters as well as their dependence on feed temperature and concentration.

In addition to the above directions, it is necessary to study the membrane ageing in order to determine the life duration of the membrane module. This point was yet partially studied. The influence of the solvent on membrane active layer was verified by soaking the membrane samples into the solvent at different temperatures during a period of several months. For that purpose, the solvent before and after regeneration was used in order to understand the influence of sludge on the membrane. It was finally shown that the membrane structure remained completely the same after soaking (at least during the period of experiment) in both clean and dirty solvent at ambient and high temperatures (70 and 80°C). Another positive point is the fact that the solvent does not permeate through the membrane, which

prevents transformations inside the polymer structure. Of course, these results, even being encouraging, should absolutely be confirmed in a much longer time perspective.

# Bibliography

- Aburabie, J. and Peinemann, K.-V. (2017). Crosslinked poly (ether block amide) composite membranes for organic solvent nanofiltration applications. *Journal of Membrane Science*, 523:264–272. [Cited on page 36.]
- Agilent (2002). Fundamentals of Gas chromatography. Courtesy of Agilent Technologies Inc. [Cited on page 97.]
- Ahlers, J. and Gmehling, J. (2002). Development of a universal group contribution equation of state III. Prediction of vapor– liquid equilibria, excess enthalpies, and activity coefficients at infinite dilution with the VTPR model. *Industrial & Engineering Chemistry Research*, 41(23):5890–5899. [Cited on page 69.]
- Ambrose, D. and Walton, J. (1989). Vapour pressures up to their critical temperatures of normal alkanes and 1-alkanols. *Pure and Applied Chemistry*, 61(8):1395–1403. [Cited on page 58.]
- Aminabhavi, T. M., Naidu, B. V. K., Sridhar, S., and Rangarajan, R. (2005). Pervaporation separation of water-isopropanol mixtures using polymeric membranes: Modeling and simulation aspects. *Journal of applied polymer science*, 95(5):1143–1153. [Cited on page 91.]
- Baker, R. W. (2012). *Membrane technology and applications*. John Wiley & Sons. [Cited on pages 19, 105, 107, and 108.]
- Baker, R. W., Wijmans, J., and Huang, Y. (2010). Permeability, permeance and selectivity: A preferred way of reporting pervaporation performance data. *Journal of Membrane Science*, 348(1-2):346–352. [Cited on pages 110, 115, and 119.]
- Ballweg, A., Brüscke, H., Schneider, W., Tusel, G., Bøddeker, K., and Wenzlaff, A. (1982). Pervaporation membranes, an economical method to replace conventional dehydration and rectification columns in ethanol distilleries. In *Proceedings of the Fifth International Alcohol Fuel Technology Symposium, Auckland, New Zealand, (May, 1982)*, pages 97–106. [Cited on page 88.]

- BASF (2014a). Solvenon® DPnB. *Technical Leaflet*. [Cited on pages 26 and 40.]
- BASF (2014b). Solvenon® PnB. *Technical Leaflet*. [Cited on pages 26 and 40.]
- BASF (2017). Solvenon® DPM. *Technical Leaflet*. [Cited on pages 18, 26, 40, 50, and 51.]
- Basile, A., Figoli, A., and Khayet, M. (2015). *Pervaporation, vapour permeation and membrane distillation: principles and applications*. Elsevier. [Cited on pages 105 and 106.]
- Bausa, J. and Marquardt, W. (2001). Detailed modeling of stationary and transient mass transfer across pervaporation membranes. *AIChE journal*, 47(6):1318–1332. [Cited on page 106.]
- Beery, K. E. and Ladisch, M. R. (2001). Adsorption of water from liquid-phase ethanol- water mixtures at room temperature using starch-based adsorbents. *Industrial & engineering chemistry research*, 40(9):2112–2115. [Cited on page 33.]
- Belabbaci, A., Ahmed, N. C.-B., Mokbel, I., and Negadi, L. (2010). Investigation of the isothermal (vapour+ liquid) equilibria of aqueous 2-amino-2-methyl-1-propanol (AMP), N-benzylethanolamine, or 3-dimethylamino-1-propanol solutions at several temperatures. *The Journal of Chemical Thermodynamics*, 42(9):1158–1162. [Cited on page 41.]
- Ben Soltane, H. (2014). *Approche compréhensive de la perméation en nanofiltration organique par des membranes denses de type polyuréthane et poly-diméthysiloxane : application au fractionnement de solutions diluées*. PhD thesis, Université de Lorraine. [Cited on page 36.]
- Binning, R. and James, F. (1958). Permeation. a new commercial separation tool. *Petroleum Refiner*, 39(214). [Cited on page 88.]
- Binning, R., Lee, R., Jennings, J., and Martin, E. (1961). Separation of liquid mixtures by permeation. *Industrial & Engineering Chemistry*, 53(1):45–50. [Cited on page 88.]
- Bouzina, Z., Mokbel, I., Negadi, A., Jose, J., and Negadi, L. (2016). Phase equilibrium measurements and thermodynamic modeling of aqueous solutions of polyamines CO<sub>2</sub> absorbents: 3-aminopropylmethylamine, 3-aminopropyldimethylamine and N, N-diethyl 1, 3-propanediamine at temperatures from 273 K to 363 K. *The Journal of Chemical Thermodynamics*, 92:43–54. [Cited on page 41.]
- Chiavone-Filho, O., Proust, P., and Rasmussen, P. (1993). Vapor-liquid equilibria for glycol ether + water systems. *Journal of Chemical and Engineering Data*, 38(1):128–131. [Cited on page 74.]

- Chiumak, I. (2007). *Handbook of the refrigeration installations design*. Odessa. Druk, 3rd edition. [Cited on pages [131](#) and [132](#).]
- Choudhury, J., Ghosh, P., and Guha, B. (1985). Separation of ethanol from ethanol-water mixture by reverse osmosis. *Biotechnology and bioengineering*, 27(7):1081–1084. [Cited on page [34](#).]
- Chung, T.-S., Jiang, L. Y., Li, Y., and Kulprathipanja, S. (2007). Mixed matrix membranes (mmms) comprising organic polymers with dispersed inorganic fillers for gas separation. *Progress in polymer science*, 32(4):483–507. [Cited on page [91](#).]
- Constantinou, L. and Gani, R. (1994). New group contribution method for estimating properties of pure compounds. *AIChE Journal*, 40(10):1697–1710. [Cited on pages [22](#), [56](#), [57](#), and [163](#).]
- Crawshaw, J. P. and Hills, J. H. (1990). Sorption of ethanol and water by starchy materials. *Industrial & engineering chemistry research*, 29(2):307–309. [Cited on page [34](#).]
- Cripwell, J. T., Schwarz, C. E., and Burger, A. J. (2016). Vapor–Liquid Equilibria Measurements for Di-n-Propyl Ether and Butyl Ethyl Ether with n-Heptane. *Journal of Chemical & Engineering Data*, 62(1):204–209. [Cited on page [74](#).]
- Darvishmanesh, S., Firoozpour, L., Vanneste, J., Luis, P., Degève, J., and Van der Bruggen, B. (2011). Performance of solvent resistant nanofiltration membranes for purification of residual solvent in the pharmaceutical industry: experiments and simulation. *Green Chemistry*, 13(12):3476–3483. [Cited on page [36](#).]
- Doghieri, F. and Sarti, G. (1997). Solubility, diffusivity, and mobility of n-pentane and ethanol in poly (1-trimethylsilyl-1-propyne). *Journal of Polymer Science Part B: Polymer Physics*, 35(14):2245–2258. [Cited on page [111](#).]
- Dong, Y., Zhang, L., Shen, J., Song, M., and Chen, H. (2006). Preparation of poly (vinyl alcohol)-sodium alginate hollow-fiber composite membranes and pervaporation dehydration characterization of aqueous alcohol mixtures. *Desalination*, 193(1-3):202–210. [Cited on page [86](#).]
- Drioli, E., Criscuoli, A., and Curcio, E. (2011). *Membrane contactors: fundamentals, applications and potentialities*, volume 11. Elsevier. [Cited on pages [19](#) and [86](#).]
- Elbaccouch, M. M. and Elliott, J. R. (2001). High-Pressure Vapor-Liquid Equilibrium for Dimethyl Ether + 2-Propanol and Dimethyl Ether + 2-Propanol + Water. *Journal of Chemical & Engineering Data*, 46(3):675–678. [Cited on page [74](#).]

- EPA (1994). Chemicals in the Environment: Perchloroethylene. U. S. Environmental Protection Agency, Office of Pollution Prevention and Toxics, Retrieved on 2007/08/15. [Cited on page 25.]
- EPA (2011). EPA Releases Final Health Assessment for TCE. Accessed 2011/09/28. [Cited on page 25.]
- Escandell, J., Neau, E., and Nicolas, C. (2011). A new formulation of the predictive NRTL-PR model in terms of kij mixing rules. Extension of the group contributions for the modeling of hydrocarbons in the presence of associating compounds. *Fluid Phase Equilibria*, 301(1):80–97. [Cited on page 69.]
- Figoli, A., Santoro, S., Galiano, F., and Basile, A. (2015). Pervaporation membranes: preparation, characterization, and application. In *Pervaporation, vapour permeation and membrane distillation*, pages 19–63. Elsevier. [Cited on page 88.]
- Gallego-Lizon, T., Ho, Y. S., and dos Santos, L. F. (2002). Comparative study of commercially available polymeric and microporous silica membranes for the dehydration of IPA/water mixtures by pervaporation/vapour permeation. *Desalination*, 149(1-3):3. [Cited on page 91.]
- George, S. C. and Thomas, S. (2001). Transport phenomena through polymeric systems. *Progress in Polymer science*, 26(6):985–1017. [Cited on pages 19 and 106.]
- Ghoreyshi, S., Farhadpour, F., and Soltanieh, M. (2002). Multicomponent transport across nonporous polymeric membranes. *Desalination*, 144(1-3):93–101. [Cited on page 106.]
- Goh, P. and Ismail, A. (2018). A review on inorganic membranes for desalination and wastewater treatment. *Desalination*, 434:60–80. [Cited on page 90.]
- Goloborodkina, R., Beregovykh, V., Babich, S., Timofeev, V., and Lvov, S. (1981). Vapor-liquid balance in the systems diethyl-ether-acetone, diethyl-ether-hexane, diethyl-ether-methanol at atmospheric-pressure. *Khim. Farm. Zh.*, 15(9):79–83. [Cited on page 74.]
- Gravelle, S., Yoshida, H., Joly, L., Ybert, C., and Bocquet, L. (2016). Carbon membranes for efficient water-ethanol separation. *The Journal of chemical physics*, 145(12):124708. [Cited on page 35.]
- Guichardon, P. and Dimitrov, O. (2018). Ecoconception machine nettoyage à sec - volet énergie. Technical report, M2P2 UMR 7340 for SAS Innovaclean. [Cited on page 29.]
- Hansen, H. K., Rasmussen, P., and Fredenslund, A. (1991). Vapor-liquid equilibria by UNI-FAC group contribution. 5. Revision and extension. *Industrial & Engineering Chemistry Research*, 30:2352–2355. [Cited on page 67.]

- Hatami, T., Rahimi, M., and Vera, J. (2011). On the compatibility between vapor pressure data and the critical constants: Use of the van der Waals family of cubic equations of state to study the cases of 2-methoxyethanol and 2-ethoxyethanol. *Fluid Phase Equilibria*, 303(2):201–204. [Cited on page 64.]
- Heidemann, R. A. and Kokal, S. L. (1990). Combined excess free energy models and equations of state. *Fluid Phase Equilibria*, 56:17–37. [Cited on page 69.]
- Heisler, E., Hunter, A. S., Siciliano, J., and Treadway, R. (1956). Solute and temperature effects in the pervaporation of aqueous alcoholic solutions. *Science*, 124(3211):77–79. [Cited on page 88.]
- Hu, X. and Xie, W. (2001). Fixed-bed adsorption and fluidized-bed regeneration for breaking the azeotrope of ethanol and water. *Separation Science and Technology*, 36(1):125–136. [Cited on page 34.]
- Huang, H.-J., Ramaswamy, S., Tschirner, U. W., and Ramarao, B. (2008). A review of separation technologies in current and future biorefineries. *Separation and purification technology*, 62(1):1–21. [Cited on page 33.]
- Huang, Y., Ly, J., Nguyen, D., and Baker, R. W. (2010). Ethanol dehydration using hydrophobic and hydrophilic polymer membranes. *Industrial & Engineering Chemistry Research*, 49(23):12067–12073. [Cited on page 119.]
- Huron, M. J. and Vidal, J. (1979). New mixing rules in simple equations of state for representing vapour-liquid equilibria of strongly non-ideal mixtures. *Fluid Phase Equilibria*, 3(4):255–271. [Cited on pages 12, 68, 70, 71, and 161.]
- Husain, S. and Koros, W. J. (2007). Mixed matrix hollow fiber membranes made with modified HSSZ-13 zeolite in polyetherimide polymer matrix for gas separation. *Journal of Membrane Science*, 288(1-2):195–207. [Cited on page 91.]
- INRS (2013). Fiche d'aide à la Substitution de Produit Cancérogène - Perchloroéthylène. INRS. [Cited on page 25.]
- Jaubert, J.-N. and Mutelet, F. (2004). VLE predictions with the Peng–Robinson equation of state and temperature dependent  $k_{ij}$  calculated through a group contribution method. *Fluid Phase Equilibria*, 224(2):285. [Cited on page 69.]
- Joback, K. G. (1984). *A unified approach to physical property estimation using multivariate statistical techniques*. PhD thesis, Massachusetts Institute of Technology. [Cited on pages 22, 56, and 164.]



- Kalyani, S., Smitha, B., Sridhar, S., and Krishnaiah, A. (2008). Pervaporation separation of ethanol–water mixtures through sodium alginate membranes. *Desalination*, 229(1-3):68–81. [Cited on page 89.]
- Kataoka, T., Tsuru, T., Nakao, S.-i., and Kimura, S. (1991). Permeation equations developed for prediction of membrane performance in pervaporation, vapor permeation and reverse osmosis based on the solution-diffusion model. *Journal of chemical engineering of Japan*, 24(3):326–333. [Cited on page 110.]
- Kober, P. A. (1917). Pervaporation, perstillation and percrystallization. *Journal of the American Chemical Society*, 39(5):944–948. [Cited on page 88.]
- Kontogeorgis, G. M. and Vlamos, P. M. (2000). An interpretation of the behavior of EoS/G<sup>E</sup> models for asymmetric systems. *Chemical Engineering Science*, 55(13):2351–2358. [Cited on page 69.]
- Koops, G. and Smolders, C. (1991). Estimation and evaluation of polymeric materials for pervaporation membranes. In *Pervaporation membrane separation processes*, pages 253–278. Elsevier Amsterdam. [Cited on page 89.]
- Ku, H.-C. and Tu, C.-H. (2006). Vapor–liquid equilibria for binary and ternary mixtures of diisopropyl ether, ethanol, and 2, 2, 4-trimethylpentane at 101.3 kPa. *Fluid phase equilibria*, 248(2):197–205. [Cited on page 74.]
- Kuila, S. B. and Ray, S. K. (2014). Dehydration of dioxane by pervaporation using filled blend membranes of polyvinyl alcohol and sodium alginate. *Carbohydrate polymers*, 101:1154–1165. [Cited on page 89.]
- Li, Y., Guan, H.-M., Chung, T.-S., and Kulprathipanja, S. (2006). Effects of novel silane modification of zeolite surface on polymer chain rigidification and partial pore blockage in polyethersulfone (pes)–zeolite a mixed matrix membranes. *Journal of Membrane Science*, 275(1-2):17–28. [Cited on page 91.]
- Lietz, S., Yang, J.-L., Bosch, E., Sandler, J. K., Zhang, Z., and Altstädt, V. (2007). Improvement of the mechanical properties and creep resistance of sbs block copolymers by nanoclay fillers. *Macromolecular Materials and Engineering*, 292(1):23–32. [Cited on page 89.]
- Lim, S. K., Goh, K., Bae, T.-H., and Wang, R. (2017). Polymer-based membranes for solvent-resistant nanofiltration: A review. *Chinese journal of chemical engineering*, 25(11):1653–1675. [Cited on page 36.]

- Lipnizki, F. and Trägårdh, G. (2001). Modelling of pervaporation: models to analyze and predict the mass transport in pervaporation. *Separation and Purification Methods*, 30(1):49–125. [Cited on page 107.]
- Lonsdale, H., Merten, U., and Riley, R. (1965). Transport properties of cellulose acetate osmotic membranes. *Journal of Applied Polymer Science*, 9(4):1341–1362. [Cited on page 106.]
- Lopes, G. H. (2014). *On the coupling of membrane transport to hydrodynamics and bulk mass transfer in reverse osmosis: numerical modeling and experimental studies*. PhD thesis, Ecole Centrale de Marseille. [Cited on page 35.]
- Luis, P. and Van der Bruggen, B. (2015). Pervaporation modeling: State of the art and future trends. In *Pervaporation, Vapour Permeation and Membrane Distillation*, pages 87–106. Elsevier. [Cited on pages 104 and 105.]
- Lydersen, A. (1955). Estimation of critical properties of organic compounds. *Univ. Wisconsin Coll. Eng., Eng. Exp. Stn. Rep. 3*. [Cited on page 56.]
- Mahesh, K. S. (1992). Pervaporation: An overview. *Online Chemical Engineering Information*. <http://www.cheresources.com/pervaporation.pdf>. [Cited on page 86.]
- Mahi, M. R., Bouzina, Z., Mokbel, I., Negadi, A., Goutaudier, C., Jose, J., and Negadi, L. (2019). Vapour-liquid equilibria, enthalpy of vaporisation, and excess Gibbs energies of binary mixtures of 3, 3-diamino-N-methyldipropylamine (DNM)(or N, N, N', N'', N''-pentamethyldiethylenetriamine (PMDETA))+ water. *The Journal of Chemical Thermodynamics*, 128:251–258. [Cited on page 41.]
- Marina, J. and Tassios, D. P. (1973). Prediction of ternary liquid-liquid equilibrium from binary data. *Industrial & Engineering Chemistry Process Design and Development*, 12(3):271–274. [Cited on page 67.]
- Marrero-Morejón, J. and Pardillo-Fontdevila, E. (1999). Estimation of pure compound properties using group-interaction contributions. *AIChE journal*, 45(3):615–621. [Cited on page 56.]
- Meares, P. (1966). On the mechanism of desalination by reversed osmotic flow through cellulose acetate membranes. *European Polymer Journal*, 2(3):241–254. [Cited on page 105.]
- Michelsen, M. L. (1990). A modified Huron-Vidal mixing rule for cubic equations of state. *Fluid Phase Equilibria*, 60(1-2):213–219. [Cited on pages 12, 69, 70, 71, and 161.]

- Mokbel, I. (1993). *Mesure des tensions de vapeur entre 10<sup>-3</sup> et 1400 mmHg par la méthode statique : amélioration d'un appareil de mesure existant : étude de composés purs et de deux systèmes binaires*. PhD thesis, Université Lyon 1, Chimie analytique. [Cited on pages 41 and 43.]
- Mollerup, J. (1986). A note on the derivation of mixing rules from excess Gibbs energy models. *Fluid Phase Equilibria*, 25(3):323–327. [Cited on page 69.]
- Moulik, S., Nazia, S., Vani, B., and Sridhar, S. (2016). Pervaporation separation of acetic acid/water mixtures through sodium alginate/polyaniline polyion complex membrane. *Separation and Purification Technology*, 170:30–39. [Cited on page 89.]
- Mulder, J. (2012). *Basic principles of membrane technology*. Springer Science & Business Media. [Cited on page 35.]
- Naidu, B. V. K., Rao, K. K., and Aminabhavi, T. M. (2005). Pervaporation separation of water+ 1, 4-dioxane and water+ tetrahydrofuran mixtures using sodium alginate and its blend membranes with hydroxyethylcellulose—a comparative study. *Journal of membrane science*, 260(1-2):131–141. [Cited on page 91.]
- Nayak, C. A. and Rastogi, N. K. (2010). Forward osmosis for the concentration of anthocyanin from garcinia indica choisy. *Separation and Purification Technology*, 71(2):144–151. [Cited on page 36.]
- Neau, E., Escandell, J., and Nicolas, C. (2010a). Modeling of Highly Nonideal Systems: 1. A Generalized Version of the NRTL Equation for the Description of Low-Pressure Equilibria. *Industrial & Engineering Chemistry Research*, 49(16):7580. [Cited on pages 66 and 68.]
- Neau, E., Escandell, J., and Nicolas, C. (2010b). Modeling of Highly Nonideal Systems: 2. Prediction of High Pressure Phase Equilibria with the Group Contribution NRTL-PR EoS. *Industrial & Engineering Chemistry Research*, 49(16):7589. [Cited on pages 66, 69, 72, and 73.]
- Neau, E., Escandell, J., and Raspo, I. (2011). A generalized reference state at constant volume for the prediction of phase equilibria from low pressure model parameters: Application to size-asymmetric systems and to the Wong-Sandler mixing rule. *Chemical Engineering Science*, 66:4148–4156. [Cited on pages 12, 71, 72, and 162.]
- Neau, E., Hernández-Garduza, O., Escandell, J., Nicolas, C., and Raspo, I. (2009a). The Soave, Twu and Boston–Mathias alpha functions in cubic equations of state: Part I. Theoretical analysis of their variations according to temperature. *Fluid Phase Equilibria*, 276:87–93. [Cited on page 54.]

- Neau, E., Neau, E., Nicolas, C., and Avaullée, L. (2018). Extension of the group contribution NRTL-PRA EoS for the modeling of mixtures containing light gases and alcohols with water and salts. *Fluid Phase Equilibria*, 458:194. [Cited on page 73.]
- Neau, E., Raspo, I., Escandell, J., Nicolas, C., and Hernández-Garduza, O. (2009b). The Soave, Twu and Boston–Mathias alpha functions in cubic equations of state. Part II. Modeling of thermodynamic properties of pure compounds. *Fluid Phase Equilibria*, 276:156–64. [Cited on pages 54, 55, and 63.]
- Nigiz, F. U., Dogan, H., and Hilmioglu, N. D. (2012). Pervaporation of ethanol/water mixtures using clinoptilolite and 4a filled sodium alginate membranes. *Desalination*, 300:24–31. [Cited on page 89.]
- Park, S.-J., Han, K.-J., and Gmehling, J. (2007). Vapor - Liquid Equilibria and  $H^E$  for Binary Systems of Dimethyl Ether (DME) with  $C_1$ -  $C_4$  Alkan-1-ols at 323.15 K and Liquid - Liquid Equilibria for Ternary System of DME + Methanol + Water at 313.15 K. *Journal of Chemical & Engineering Data*, 52(1):230–234. [Cited on page 74.]
- Paul, D. R. (1976). The solution-diffusion model for swollen membranes. *Separation and Purification Methods*, 5(1):33–50. [Cited on page 105.]
- Paul, D. R. and Kemp, D. (1973). The diffusion time lag in polymer membranes containing adsorptive fillers. In *Journal of Polymer Science: Polymer Symposia*, volume 41, pages 79–93. Wiley Online Library. [Cited on page 90.]
- Peneloux, A., Abdoul, W., and Rauzy, E. (1989). Excess functions and equations of state. *Fluid Phase Equilibria*, 47(2-3):115–132. [Cited on pages 12, 69, 71, and 162.]
- Peneloux, A., Rauzy, E., and Fréze, R. (1982). A consistent correction for Redlich-Kwong-Soave volumes. *Fluid Phase Equilibria*, 8(1):7–23. [Cited on page 55.]
- Peng, D.-Y. and Robinson, D. B. (1976). A New Two-Constant Equation of State. *Industrial & Engineering Chemistry Fundamentals*, 15(1):59. [Cited on page 54.]
- Phuntsho, S., Vigneswaran, S., Kandasamy, J., Hong, S., Lee, S., and Shon, H. K. (2012). Influence of temperature and temperature difference in the performance of forward osmosis desalination process. *Journal of membrane science*, 415:734–744. [Cited on page 36.]
- Pitzer, K. S. (1955). The volumetric and thermodynamic properties of fluids. I. Theoretical basis and virial coefficients. *Journal of the American Chemical Society*, 77(13):3427–3433. [Cited on page 58.]

- Poling, B. E., Prausnitz, J. M., O'connell, J. P., et al. (2001). *The properties of gases and liquids*, volume 5. Mcgraw-hill New York. [Cited on pages 56, 57, 64, 67, and 77.]
- Qiu, J. and Peinemann, K. (2006). Gas transport properties of novel mixed matrix membranes with the organic filler trimethylsilyl-glucose. *Desalination*, 199(1-3):113–114. [Cited on page 91.]
- Rackett, H. G. (1971). Calculation of the bubble-point volumes of hydrocarbon mixtures. *Journal of Chemical & Engineering Data*, 16(3):308–310. [Not cited.]
- Rao, K. S. V. K., Subha, M. C. S., Sairam, M., Mallikarjuna, N. N., and Aminabhavi, T. M. (2006). Blend membranes of chitosan and poly(vinyl alcohol) in pervaporation dehydration of isopropanol and tetrahydrofuran. *Journal of Applied Polymer Science*, 103(3):1918. [Cited on page 91.]
- Rautenbach, R. (1988). Dehydration of multicomponent organic systems by a reverse osmosis pervaporation-hybrid process - module-, process design and economics. *Desalination*, 70(1):445–453. [Cited on page 92.]
- Ray, S. and Ray, S. (2006). Separation of organic mixtures by pervaporation using crosslinked and filled rubber membranes. *Journal of membrane science*, 285(1-2):108–119. [Cited on page 115.]
- Renon, H. and Prausnitz, J. M. (1968). Local compositions in thermodynamic excess functions for liquid mixtures. *AIChE journal*, 14(1):135–144. [Cited on page 67.]
- Robinson, D. B. and Peng, D.-Y. (1978). *The characterization of the heptanes and heavier fractions for the GPA Peng-Robinson programs*. Gas processors association. [Cited on page 54.]
- Sandler, S. I. (2017). *Chemical, biochemical, and engineering thermodynamics*. John Wiley & Sons, 5th edition. [Cited on page 41.]
- Sarraute, S., Mokbel, I., Gomes, M. F. C., Majer, V., and Jose, J. (2008). Atmosphere/water partition of halocyclohexanes from vapour pressure and solubility data. *Atmospheric Environment*, 42(19):4724–4734. [Cited on page 41.]
- Segura, H., Galindo, G., Reich, R., Wisniak, J., and Loras, S. (2002). Isobaric vapor-liquid equilibria and densities for the system methyl 1, 1-dimethylethyl ether + 2-propanol. *Physics and Chemistry of Liquids*, 40(3):277–294. [Cited on page 74.]
- Shawaqfeh, A. T. (2010). Isobaric Vapor-liquid equilibrium for the binary system Diisopropylether + Isopropanol at 95 kPa. *Afinidad*, 67(549). [Cited on page 74.]

- She, Q., Jin, X., and Tang, C. Y. (2012). Osmotic power production from salinity gradient resource by pressure retarded osmosis: effects of operating conditions and reverse solute diffusion. *Journal of Membrane Science*, 401:262–273. [Cited on page 36.]
- Signer, R., Arm, H., and Daenicker, H. (1969). Dampfdrücke, Dichten, thermodynamische Mischfunktionen und Brechungsindices der binären Systeme Wasser-Tetrahydrofuran und Wasser-Diäthyläther bei 25°. *Helv. Chim. Acta*, 52:2347–2351. [Cited on page 74.]
- Sikdar, S. K., Burckle, J. O., Dutta, B. K., Figoli, A., and Drioli, E. (2013). Method for fabrication of elastomeric asymmetric membranes from hydrophobic polymers. US Patent 8,518,263. [Cited on page 89.]
- Soave, G. (1972). Equilibrium constants from a modified Redlich-Kwong equation of state. *Chemical Engineering Science*, 27(6):1197–1203. [Cited on page 54.]
- Sommer, S. and Melin, T. (2005). Performance evaluation of microporous inorganic membranes in the dehydration of industrial solvents. *Chemical Engineering and Processing: Process Intensification*, 44(10):1138–1156. [Cited on page 36.]
- Sourirajan, S. et al. (1970). *Reverse osmosis*. London, UK: Logos Press Ltd. [Cited on page 105.]
- Spencer, C. F. and Danner, R. P. (1972). Improved equation for prediction of saturated liquid density. *Journal of Chemical & Engineering Data*, 17(2):236–241. [Cited on page 55.]
- Spencer, C. F. and Danner, R. P. (1973). Prediction of bubble-point density of mixtures. *Journal of Chemical & Engineering Data*, 18(2):230–234. [Cited on page 55.]
- Suzuki, H. (1987). Composite membrane having a surface layer of an ultrathin film of cage-shaped zeolite and processes for production thereof. US Patent 4,699,892. [Cited on page 90.]
- Svang-Ariyaskul, A., Huang, R., Douglas, P., Pal, R., Feng, X., Chen, P., and Liu, L. (2006). Blended chitosan and polyvinyl alcohol membranes for the pervaporation dehydration of isopropanol. *Journal of Membrane Science*, 280(1-2):815–823. [Cited on page 119.]
- Van Hoof, V., Dotremont, C., and Buekenhoudt, A. (2006). Performance of mitsui naa type zeolite membranes for the dehydration of organic solvents in comparison with commercial polymeric pervaporation membranes. *Separation and purification technology*, 48(3):304–309. [Cited on page 90.]
- Vandezande, P., Gevers, L. E., and Vankelecom, I. F. (2008). Solvent resistant nanofiltration: separating on a molecular level. *Chemical Society Reviews*, 37(2):365–405. [Cited on page 35.]

- Vane, L. M. and Alvarez, F. R. (2005). Vibrating pervaporation modules: Effect of module design on performance. *Journal of membrane science*, 255(1-2):213–224. [Cited on page 106.]
- Verhoeve, L. A. (1970). System 2-isopropoxypropane-2-propanol-water. *Journal of Chemical and Engineering Data*, 15(2):222–226. [Cited on page 74.]
- Vidal, J. (1978). Mixing rules and excess properties in cubic equations of state. *Chemical Engineering Science*, 33(6):787–791. [Cited on page 68.]
- Vijayaraghavan, S., Deshpande, P., and Kuloor, N. (1966). Isobaric vapour-liquid equilibrium. *Indian Chem. Eng.*, 40(12):12–14. [Cited on page 74.]
- Vijayaraghavan, S., Deshpande, P., and Kuloor, N. R. (1967). Vapor-liquid equilibrium data for the systems diisopropyl ether-n-heptane and diisopropyl ether-carbon tetrachloride at medium pressures. *Journal of Chemical and Engineering Data*, 12(1):15–16. [Cited on page 74.]
- Voutsas, E., Louli, V., Boukouvalas, C., Magoulas, K., and Tassios, D. (2006). Thermodynamic property calculations with the universal mixing rule for EoS/ $G^E$  models: Results with the Peng–Robinson EoS and a UNIFAC model. *Fluid Phase Equilibria*, 241(1-2):216–228. [Cited on page 69.]
- Vrentas, J. and Vrentas, C. M. (1994). Solvent self-diffusion in glassy polymer-solvent systems. *Macromolecules*, 27(20):5570–5576. [Cited on page 111.]
- Wan, Y., Wu, H., Yu, A., and Wen, D. (2006). Biodegradable polylactide/chitosan blend membranes. *Biomacromolecules*, 7(4):1362–1372. [Cited on page 89.]
- Watson, J., Zhang, G., and Payne, P. (1992). The diffusion mechanism in silicone rubber. *Journal of membrane science*, 73(1):55–71. [Cited on page 89.]
- Wee, S.-L., Tye, C.-T., and Bhatia, S. (2008). Membrane separation process—pervaporation through zeolite membrane. *Separation and Purification Technology*, 63(3):500–516. [Cited on page 90.]
- Wijmans, J. G. and Baker, R. W. (1995). The solution-diffusion model: a review. *Journal of membrane science*, 107(1-2):1–21. [Cited on pages 19, 106, 107, 108, and 110.]
- Wilson, G. and Jasperson, L. (1996). Critical constants  $t_c$ ,  $p_c$ , estimation based on zero, first and second order methods. In *Proceedings of the AIChE Spring Meeting*. [Cited on pages 21, 22, 56, 59, and 163.]

- Xia, S., Dong, X., Zhu, Y., Wei, W., Xiangli, F., and Jin, W. (2011). Dehydration of ethyl acetate–water mixtures using PVA/ceramic composite pervaporation membrane. *Separation and Purification Technology*, 77(1):53. [Cited on page 92.]
- Xie, Z., Hoang, M., Duong, T., Ng, D., Dao, B., and Gray, S. (2011). Sol–gel derived poly (vinyl alcohol)/maleic acid/silica hybrid membrane for desalination by pervaporation. *Journal of Membrane Science*, 383(1-2):96–103. [Cited on page 89.]
- Yamada, T. and Gunn, R. D. (1973). Saturated liquid molar volumes. Rackett equation. *Journal of Chemical & Engineering Data*, 18(2):234. [Cited on page 55.]
- Yasuda, H. and Peterlin, A. (1973). Diffusive and bulk flow transport in polymers. *Journal of Applied Polymer Science*, 17(2):433–442. [Cited on page 105.]
- Yaws, C. L. (2008). *Thermophysical properties of chemicals and hydrocarbons*. William Andrew. [Cited on page 64.]
- Yoshikawa, M., Ogata, N., and Shimidzu, T. (1986). Polymer membrane as a reaction field. iii.: Effect of membrane polarity on selective separation of a water—ethanol binary mixture through synthetic polymer membranes. *Journal of membrane science*, 26(1):107–113. [Cited on page 89.]
- Zhang, L., Yu, P., and Luo, Y. (2007). Dehydration of caprolactam–water mixtures through cross-linked PVA composite pervaporation membranes. *Journal of Membrane Science*, 306(1-2):93. [Cited on pages 91 and 103.]
- Zhang, S., Zou, Y., Wei, T., Mu, C., Liu, X., and Tong, Z. (2017). Pervaporation dehydration of binary and ternary mixtures of n-butyl acetate, n-butanol and water using PVA-CS blended membranes. *Separation and Purification Technology*, 173:314. [Cited on page 103.]
- Zhang, X., Ning, Z., Wang, D. K., and da Costa, J. C. D. (2013). A novel ethanol dehydration process by forward osmosis. *Chemical engineering journal*, 232:397–404. [Cited on page 36.]
- Zhao, S., Zou, L., Tang, C. Y., and Mulcahy, D. (2012). Recent developments in forward osmosis: opportunities and challenges. *Journal of membrane science*, 396:1–21. [Cited on page 36.]





# Appendix A

## Literature reference states and expressions for $g^E$

### A.1 Zero pressure reference state (Michelsen, 1990)

$$\frac{g^E}{RT} = C \left[ -\alpha + \sum_i x_i \alpha_i \right] + \sum_i x_i \ln \frac{b_i}{b}, \quad C = 0.53 \quad (\text{A.1})$$

with the following  $\alpha^M$  function:

$$\alpha^M = \alpha - \sum_i x_i \alpha_i = -\frac{1}{C} \left[ \frac{g^E}{RT} - \sum_i x_i \ln \frac{b_i}{b} \right] \quad (\text{A.2})$$

### A.2 Infinite pressure reference state (Huron and Vidal, 1979)

$$\frac{g^E}{RT} = C \left[ -\alpha + \sum_i x_i \alpha_i \right], \quad C = 0.623 \quad (\text{A.3})$$

with the following  $\alpha^M$  function:

$$\alpha^M = \alpha - \sum_i x_i \alpha_i = -\frac{1}{C} \left[ \frac{g^E}{RT} \right] \quad (\text{A.4})$$

### A.3 Constant packing fraction (Peneloux et al., 1989)

$$g^E = g_{comb}^E + g_{res}^E \quad (\text{A.5})$$

with the following  $\alpha^M$  function:

$$\alpha^M = \alpha - \sum_i x_i \alpha_i = -\frac{1}{C} \left[ \frac{g_{res}^E}{RT} \right], \quad C = 1.00 \quad (\text{A.6})$$

### A.4 Generalized reference state at constant volume (Neau et al., 2011)

$$\frac{g^E}{RT} = C \left[ -\alpha + \sum_i x_i \alpha_i \right] + \sum_i x_i \ln \frac{r_i}{r}, \quad C = 0.56 \quad (\text{A.7})$$

with the following  $\alpha^M$  function:

$$\alpha^M = \alpha - \sum_i x_i \alpha_i = -\frac{1}{C} \left[ \frac{g^E}{RT} - \sum_i x_i \ln \frac{r_i}{r} \right] \quad (\text{A.8})$$

## Appendix B

# Pure compounds group contribution parameters for the estimation of critical properties

**Table B.1:** *Constantinou and Gani (1994)* group contributions used in Equations (2.16) and (2.17) for DPnB and PnB

<b>First Order Contributions</b>		
<b>Group</b>	$\Delta tc1k$	$\Delta pc1k$
CH3	1,6781	0,0199
CH2	3,492	0,0106
CH2O	6,0723	0,0151
CH	4,033	0,0013
OH	9,7292	0,0051
<b>Second Order Contributions</b>		
<b>Group</b>	$\Delta tc2j$	$\Delta pc2j$
CHOH	2,8035	0,00439

**Table B.2:** *Wilson and Jasperson (1996)* group contributions used in Equations (2.18) to (2.20) for DPM, DPnB and PnB

<b>First Order Contributions</b>		
<b>Atom</b>	$\Delta tc$	$\Delta pc$
C	0,008532	0,72983
H	0,002793	0,1266
O	0,020341	0,4336
<b>Second Order Contributions</b>		
<b>Group</b>	$\Delta tcj$	$\Delta pcj$
-OH, C5 or more	0,010	0,000

APPENDIX B. PURE COMPOUNDS GROUP CONTRIBUTION PARAMETERS FOR THE  
ESTIMATION OF CRITICAL PROPERTIES

---

**Table B.3:** *Joback (1984) group contributions used in Equations (2.14) and (2.15) for PnB*

<b>Group</b>	<b>tck</b>	<b>pck</b>
CH3	0,0141	-0,012
CH2	0,0189	0,000
CH	0,0164	0,002
OH	0,0741	0,0112

## **Appendix C**

**Measured experimental vapor pressures  
and VLE data for pure compounds, binary  
and quaternary mixtures**

## C.1 Pure compounds

**Table C.1:** Experimental vapor pressure data and pressures calculated with Equation (2.4) for DPM, DPnB and PnB

$T_{\text{exp}}[\text{K}]$	$P_{\text{exp}}[\text{Pa}]$	$P_{\text{calc}}[\text{Pa}]$	$\delta P/P, \%$
DPM ( $\Delta H_{\text{vap}}/R = -6848.560, C = 26.706$ )			
283,15	12,414	12,507	0,746
293,15	28,330	28,538	0,731
303,15	61,226	61,666	0,718
313,15	125,964	126,853	0,705
323,15	247,837	249,556	0,694
333,15	468,209	471,407	0,683
343,15	852,337	858,073	0,673
353,15	1499,852	1509,807	0,664
363,15	2558,400	2575,158	0,655
DPnB ( $\Delta H_{\text{vap}}/R = -6455.711, C = 24.058$ )			
283,15	3,520	3,524	0,132
293,15	7,661	7,670	0,115
303,15	15,840	15,856	0,100
313,15	31,268	31,296	0,088
323,15	59,178	59,225	0,078
333,15	107,793	107,868	0,070
343,15	189,599	189,719	0,063
353,15	322,994	323,181	0,058
363,15	534,332	534,617	0,053
PnB ( $\Delta H_{\text{vap}}/R = -7100.00, C = 28.75$ )			
283,15	39,447	39,659	0,538
293,15	92,788	93,299	0,551
303,15	206,283	207,444	0,563
313,15	435,790	438,291	0,574
323,15	878,995	884,133	0,585
333,15	1699,822	1709,927	0,595
343,15	3163,202	3182,305	0,604
353,15	5682,967	5717,793	0,613
363,15	9885,757	9947,172	0,621

## C.2 Aqueous binary mixtures

**Table C.2:** Measured isothermal VLE and VLLE data of the  $H_2O+DPM$ ,  $H_2O+DPnB$  and  $H_2O+PnB$  at 283.15÷363.15 K

Temperature [K]	$H_2O(1)+DPM(2)$		$H_2O(1)+DPnB(2)$		$H_2O(1)+PnB(2)$	
	$x_1$	$P_{\text{tot}} [\text{Pa}]$	$x_1$	$P_{\text{tot}} [\text{Pa}]$	$x_1$	$P_{\text{tot}} [\text{Pa}]$
283,15	0,000	12,366	0,000	3,520	0,000	39,447
	0,110	296,703	0,210	840,097	0,217	1149,584

APPENDIX C. MEASURED EXPERIMENTAL VAPOR PRESSURES AND VLE DATA FOR  
PURE COMPOUNDS, BINARY AND QUATERNARY MIXTURES

**Table C.2:** Measured isothermal VLE and VLLE data of the  $H_2O+DPM$ ,  $H_2O+DPnB$  and  $H_2O+PnB$  at 283.15÷363.15 K (Continued)

Temperature [K]	$H_2O(1)+DPM(2)$		$H_2O(1)+DPnB(2)$		$H_2O(1)+PnB(2)$	
	$x_1$	$P_{tot}$ [Pa]	$x_1$	$P_{tot}$ [Pa]	$x_1$	$P_{tot}$ [Pa]
293,15	0,276	570,718	0,461	1224,566	0,427	1246,134
	0,468	821,697	0,720	1213,124	0,693	1214,888
	0,654	969,110	0,851	1229,809	0,841	1283,570
	0,841	1064,926	0,997	1276,743	0,997	1243,413
	1,000	1255,406	1,000	1255,406	1,000	1255,406
	0,000	28,218	0,000	7,661	0,000	92,788
	0,110	575,418	0,210	1586,443	0,217	2126,634
	0,276	1104,041	0,461	2307,919	0,427	2370,585
	0,468	1559,771	0,720	2283,733	0,693	2323,426
	0,654	1867,732	0,851	2308,389	0,841	2417,798
303,15	0,841	2034,668	0,997	2379,262	0,997	2344,697
	1,000	2344,041	1,000	2344,041	1,000	2344,041
	0,000	60,979	0,000	15,840	0,000	206,283
	0,110	1068,236	0,210	2872,792	0,217	3777,634
	0,276	2044,762	0,461	4171,577	0,427	4322,354
	0,468	2838,219	0,720	4123,443	0,693	4257,395
	0,654	3447,126	0,851	4156,601	0,841	4367,947
	0,841	3724,926	0,997	4255,450	0,997	4240,177
	1,000	4200,057	1,000	4200,057	1,000	4200,057
	0,000	125,447	0,000	31,268	0,000	435,790
313,15	0,110	1906,300	0,210	5008,573	0,217	6468,600
	0,276	3640,875	0,461	7260,407	0,427	7584,455
	0,468	4970,802	0,720	7169,441	0,693	7505,176
	0,654	6117,890	0,851	7208,652	0,841	7598,539
	0,841	6560,980	0,997	7333,683	0,997	7383,264
	1,000	7250,505	1,000	7250,505	1,000	7250,505
	0,000	246,800	0,000	59,178	0,000	878,995
	0,110	3282,070	0,210	8436,896	0,217	10713,804
	0,276	6255,489	0,461	12210,319	0,427	12853,294
	0,468	8408,994	0,720	12046,001	0,693	12774,365
323,15	0,654	10479,176	0,851	12082,887	0,841	12773,239
	0,841	11158,447	0,997	12219,945	0,997	12422,401
	1,000	12100,582	1,000	12100,582	1,000	12100,582
	0,000	466,237	0,000	107,793	0,000	1699,822



APPENDIX C. MEASURED EXPERIMENTAL VAPOR PRESSURES AND VLE DATA FOR  
PURE COMPOUNDS, BINARY AND QUATERNARY MIXTURES

**Table C.2:** Measured isothermal VLE and VLLE data of the  $H_2O+DPM$ ,  $H_2O+DPnB$  and  $H_2O+PnB$  at 283.15÷363.15 K (Continued)

Temperature [K]	$H_2O(1)+DPM(2)$		$H_2O(1)+DPnB(2)$		$H_2O(1)+PnB(2)$	
	$x_1$	$P_{tot}$ [Pa]	$x_1$	$P_{tot}$ [Pa]	$x_1$	$P_{tot}$ [Pa]
343,15	0,110	5469,400	0,210	13773,866	0,217	17215,587
	0,276	10404,129	0,461	19903,967	0,427	21103,358
	0,468	13783,358	0,720	19618,762	0,693	21059,664
	0,654	17378,800	0,851	19634,551	0,841	20812,787
	0,841	18382,015	0,997	19747,139	0,997	20258,059
	1,000	19583,514	1,000	19583,514	1,000	19583,514
	0,000	848,706	0,000	189,599	0,000	3163,202
	0,110	8847,600	0,210	21853,549	0,217	26908,832
	0,276	16798,600	0,461	31534,341	0,427	33661,857
	0,468	21951,200	0,720	31056,619	0,693	33721,700
353,15	0,654	27984,000	0,851	31015,738	0,841	32961,095
	0,841	29413,500	0,997	31030,646	0,997	32107,843
	1,000	30816,900	1,000	30816,889	1,000	30816,889
	0,000	1493,390	0,000	322,994	0,000	5682,967
	0,110	13926,400	0,210	33778,089	0,217	41009,318
	0,276	26397,100	0,461	48675,463	0,427	52292,589
	0,468	34049,800	0,720	47900,432	0,693	52576,104
	0,654	43861,400	0,851	47741,728	0,841	50858,670
	0,841	45828,900	0,997	47529,267	0,997	49578,917
	1,000	47264,600	1,000	47264,602	1,000	47264,602
363,15	0,000	2547,273	0,000	534,332	0,000	9885,757
	0,110	21380,800	0,210	72137,424	0,217	61065,012
	0,276	40460,357	0,461	73359,030	0,427	79287,826
	0,468	51555,087	0,720	72137,424	0,693	79991,673
	0,654	67066,645	0,851	71762,567	0,841	76622,181
	0,841	69682,695	0,997	71110,447	0,997	74746,580
	1,000	70803,290	1,000	70803,290	1,000	70803,290

### C.3 Organic binary mixtures

APPENDIX C. MEASURED EXPERIMENTAL VAPOR PRESSURES AND VLE DATA FOR  
PURE COMPOUNDS, BINARY AND QUATERNARY MIXTURES

**Table C.3:** Measured isothermal VLE data of the PnB+DPM, DPM+DPnB and  
PnB+DPnB at 283.15÷363.15 K

Temperature [K]	PnB(1)+DPM(2)		DPM(1)+DPnB(2)		PnB(1)+DPnB(2)	
	$x_1$	$P_{tot}$ [Pa]	$x_1$	$P_{tot}$ [Pa]	$x_1$	$P_{tot}$ [Pa]
283.15	0,000	12,366	0,000	3,520	0,000	3,520
	0,160	16,799	0,160	5,758	0,160	11,394
	0,334	26,831	0,336	7,033	0,330	20,711
	0,489	29,831	0,496	7,780	0,493	33,044
	0,667	53,117	0,666	8,558	0,665	44,098
	0,837	47,149	0,836	10,435	0,838	65,180
	0,985	63,822	1,000	12,366	1,000	39,447
	1,000	39,447				
293.15	0,000	28,218	0,000	7,661	0,000	7,661
	0,160	37,691	0,160	12,541	0,160	24,222
	0,334	57,999	0,336	15,791	0,330	43,212
	0,489	65,324	0,496	17,635	0,493	67,981
	0,667	107,422	0,666	19,748	0,665	89,604
	0,837	99,717	0,836	24,012	0,838	135,998
	0,985	133,498	1,000	28,218	1,000	92,788
	1,000	92,788				
303.15	0,000	60,979	0,000	15,840	0,000	15,840
	0,160	80,172	0,160	25,948	0,160	48,994
	0,334	119,158	0,336	33,612	0,330	85,886
	0,489	135,841	0,496	37,871	0,493	133,411
	0,667	207,383	0,666	43,126	0,665	173,750
	0,837	200,725	0,836	52,299	0,838	270,320
	0,985	265,972	1,000	60,979	1,000	206,283
	1,000	206,283				
313.15	0,000	125,447	0,000	31,268	0,000	31,268
	0,160	162,509	0,160	51,252	0,160	94,739
	0,334	233,805	0,336	68,176	0,330	163,379
	0,489	269,574	0,496	77,454	0,493	250,784
	0,667	383,889	0,666	89,594	0,665	322,963
	0,837	386,393	0,836	108,384	0,838	514,244
	0,985	507,080	1,000	125,447	1,000	435,790
	1,000	435,790				
323.15	0,000	246,806	0,000	59,178	0,000	59,178
	0,160	315,311	0,160	97,056	0,160	175,872

APPENDIX C. MEASURED EXPERIMENTAL VAPOR PRESSURES AND VLE DATA FOR PURE COMPOUNDS, BINARY AND QUATERNARY MIXTURES

**Table C.3:** Measured isothermal VLE data of the PnB+DPM, DPM+DPnB and PnB+DPnB at 283.15÷363.15 K (Continued)

Temperature [K]	PnB(1)+DPM(2)		DPM(1)+DPnB(2)		PnB(1)+DPnB(2)	
	$x_1$	$P_{tot}$ [Pa]	$x_1$	$P_{tot}$ [Pa]	$x_1$	$P_{tot}$ [Pa]
333.15	0,334	440,016	0,336	132,361	0,330	298,664
	0,489	512,748	0,496	151,545	0,493	453,358
	0,667	684,050	0,666	177,897	0,665	577,723
	0,837	714,254	0,836	214,712	0,838	940,102
	0,985	928,909	1,000	246,806	1,000	878,995
	1,000	878,995				
	0,000	466,237	0,000	107,793	0,000	107,793
	0,160	587,922	0,160	176,881	0,160	314,581
	0,334	797,255	0,336	246,939	0,330	526,552
	0,489	938,354	0,496	284,801	0,493	790,944
343.15	0,667	1177,359	0,666	338,979	0,665	997,983
	0,837	1272,502	0,836	408,248	0,838	1657,491
	0,985	1640,921	1,000	466,237	1,000	1699,822
	1,000	1699,822				
	0,000	848,706	0,000	189,599	0,000	189,599
	0,160	1057,135	0,160	311,279	0,160	543,940
	0,334	1395,343	0,336	444,256	0,330	898,147
	0,489	1657,803	0,496	515,908	0,493	1335,867
	0,667	1963,294	0,666	622,098	0,665	1669,900
	0,837	2192,030	0,836	747,698	0,838	2827,311
353.15	0,985	2804,137	1,000	848,706	1,000	3163,202
	1,000	3163,202				
	0,000	1493,394	0,000	322,994	0,000	322,994
	0,160	1838,698	0,160	530,537	0,160	911,801
	0,334	2365,909	0,336	773,097	0,330	1486,346
	0,489	2835,965	0,496	903,627	0,493	2190,230
	0,667	3180,424	0,666	1103,091	0,665	2713,916
	0,837	3661,493	0,836	1323,258	0,838	4679,092
	0,985	4648,701	1,000	1493,394	1,000	5682,967
	1,000	5682,967				
363.15	0,000	2547,273	0,000	534,332	0,000	534,322
	0,160	3102,071	0,160	878,070	0,160	1485,573
	0,334	3896,600	0,336	1304,918	0,330	2392,456
	0,489	4710,073	0,496	1534,620	0,493	3494,544

APPENDIX C. MEASURED EXPERIMENTAL VAPOR PRESSURES AND VLE DATA FOR  
PURE COMPOUNDS, BINARY AND QUATERNARY MIXTURES

**Table C.3:** Measured isothermal VLE data of the PnB+DPM, DPM+DPnB and PnB+DPnB at 283.15÷363.15 K (Continued)

Temperature [K]	PnB(1)+DPM(2)		DPM(1)+DPnB(2)		PnB(1)+DPnB(2)	
	$x_1$	$P_{tot}$ [Pa]	$x_1$	$P_{tot}$ [Pa]	$x_1$	$P_{tot}$ [Pa]
	0,667	5017,029	0,666	1895,239	0,665	4294,246
	0,837	5945,644	0,836	2269,392	0,838	7531,824
	0,985	7495,032	1,000	2547,273	1,000	9885,757
	1,000	9885,757				

## C.4 Quaternary mixtures

**Table C.4:** Measured isothermal VLE data of the quaternary system Water + ARCA-CLEAN at 283.15÷363.15 K

Temperature [K]	H <sub>2</sub> O(1) + DPM(2) + DPnB(3) + PnB(4)				
	$x_1$	$x_2$	$x_3$	$x_4$	$P_{tot}$ [Pa]
283,15	0,000	0,634	0,247	0,119	18,049
	0,226	0,491	0,191	0,092	560,429
	0,326	0,428	0,166	0,080	737,326
	0,384	0,391	0,152	0,073	855,614
	0,474	0,334	0,130	0,062	912,770
	1,000	0,000	0,000	0,000	1255,406
293,15	0,000	0,634	0,247	0,119	40,098
	0,226	0,491	0,191	0,092	1086,18852
	0,326	0,428	0,166	0,080	1454,427
	0,384	0,391	0,152	0,073	1645,986
	0,474	0,334	0,130	0,062	1744,804
	1,000	0,000	0,000	0,000	2344,041
303,15	0,000	0,634	0,247	0,119	84,515
	0,226	0,491	0,191	0,092	2015,255
	0,326	0,428	0,166	0,080	2743,214
	0,384	0,391	0,152	0,073	3032,689
	0,474	0,334	0,130	0,062	3195,712
	1,000	0,000	0,000	0,000	4200,057
313,15	0,000	0,634	0,247	0,119	169,849
	0,226	0,491	0,191	0,092	3594,275
	0,326	0,428	0,166	0,080	4968,530

APPENDIX C. MEASURED EXPERIMENTAL VAPOR PRESSURES AND VLE DATA FOR  
PURE COMPOUNDS, BINARY AND QUATERNARY MIXTURES

**Table C.4:** Measured isothermal VLE data of the quaternary system Water + ARCA-CLEAN at 283.15÷363.15 K (Continued)

Temperature [K]	<b>H<sub>2</sub>O(1) + DPM(2) + DPnB(3) + PnB(4)</b>				
	$x_1$	$x_2$	$x_3$	$x_4$	$P_{tot}$ [Pa]
323,15	0,384	0,391	0,152	0,073	5373,772
	0,474	0,334	0,130	0,062	5631,226
	1,000	0,000	0,000	0,000	7250,50529
	0,000	0,634	0,247	0,119	326,912
	0,226	0,491	0,191	0,092	6185,012
	0,326	0,428	0,166	0,080	8674,217
	0,384	0,391	0,152	0,073	9190,808
	0,474	0,334	0,130	0,062	9581,006
333,15	1,000	0,000	0,000	0,000	12100,582
	0,000	0,634	0,247	0,119	604,961
	0,226	0,491	0,191	0,092	10301,9222
	0,326	0,428	0,166	0,080	14645,511
	0,384	0,391	0,152	0,073	15220,748
	0,474	0,334	0,130	0,062	15789,307
	1,000	0,000	0,000	0,000	19583,514
	0,000	0,634	0,247	0,119	1080,053
343,15	0,226	0,491	0,191	0,092	16656,420
	0,326	0,428	0,166	0,080	23983,952
	0,384	0,391	0,152	0,073	24476,5059
	0,474	0,334	0,130	0,062	25273,788
	1,000	0,000	0,000	0,000	30816,889
	0,000	0,634	0,247	0,119	1865,980
	0,226	0,491	0,191	0,092	26207,633
	0,326	0,428	0,166	0,080	38194,887
353,15	0,384	0,391	0,152	0,073	38315,867
	0,474	0,334	0,130	0,062	39391,909
	1,000	0,000	0,000	0,000	47264,6019
	0,000	0,634	0,247	0,119	3128,176
	0,226	0,491	0,191	0,092	40219,150
	0,326	0,428	0,166	0,080	59287,096
	0,384	0,391	0,152	0,073	58517,930
	0,474	0,334	0,130	0,062	59914,096
363,15	1,000	0,000	0,000	0,000	70803,290

# Appendix D

## GC setup and operating conditions used in Chapter 2

In this Appendix, we present the operating parameters and setup of the GC device used during each analysis phase of Chapter 2. All the device parameters described below were obtained experimentally according to the recommendations of equipment supplier.

**Phase 1** During this phase, the samples of *aqueous* mixtures ( $\text{H}_2\text{O}+\text{DPM}$ ,  $\text{H}_2\text{O}+\text{DPnB}$ ,  $\text{H}_2\text{O}+\text{PnB}$ ) were analysed. The device setup was as follows:

1. **Carrier gas:**  $\text{H}_2$
2. **Column:** Restek Rt-Q-BOND
  - Non-polar based on 100% divinyl benzene;
  - Ref.: 19743,  $l = 15 \text{ m}$ ,  $\varnothing_{in} = 0.32 \text{ mm}$ ,  $\delta_{film} = 10 \mu\text{m}$ ;
  - $T_{max} = 300^\circ\text{C}$ ;
  - $P = 3.84 \text{ psi}$ ;
  - Flow rate:  $1.5 \text{ mL/min}$ ;
  - Average velocity:  $44 \text{ cm/sec}$
3. **Injector:** Automatic
  - Volume per injection:  $1 \mu\text{L}$ ;
  - Split ratio: 20;
  - Split flow rate:  $29.9 \text{ mL/min}$ ;

- $T = 250^{\circ}\text{C}$ ;
- $P = 3.84 \text{ psi}$ ;
- Total flow rate:  $39.5 \text{ mL/min}$ ;

4. **Oven:** Programmed mode (Oven Ramp)

- $T_{oven}$  :  $150^{\circ}\text{C}$  during  $2 \text{ min}$   $\rightarrow$  heating up to  $270^{\circ}\text{C}$  ( $\Delta = 40^{\circ}\text{C/min}$ )  $\rightarrow$   $270^{\circ}\text{C}$  during  $10 \text{ min}$ ;
- Analysis duration:  $15 \text{ min}$ ;
- $T_{max} = 280^{\circ}\text{C}$ ;

5. **Detector:** TCD

- $T_{det}$  :  $250^{\circ}\text{C}$ ;
- Reference flow rate:  $20 \text{ mL/min}$ ;

6. **Solvent used to dilute the samples:** High purity acetone

**Phase 2** The Phase 2 correspond to the analysis of samples of *organic* mixtures (DPM+DPnB, DPM+PnB, DPnB+PnB). The device settings used during this phase were as follows:

1. **Carrier gas:**  $\text{H}_2$

2. **Column:** Agilent HP-5

- Non-polar based on the (5%-Phenyl)-methylpolysiloxane;
- Ref.: 19091J-413,  $l = 30 \text{ m}$ ,  $\varnothing_{in} = 0.32 \text{ mm}$ ,  $\delta_{film} = 0.25 \mu\text{m}$ ;
- $T_{max} = 325 \div 350^{\circ}\text{C}$ ;
- $P = 3.84 \text{ psi}$ ;
- Flow rate:  $1.5 \text{ mL/min}$ ;
- Average velocity:  $44 \text{ cm/sec}$

3. **Injector:** Automatic

- Volume per injection:  $1 \mu\text{L}$ ;
- Split ratio: 13;

- Split flow rate: 19.5 *mL/min*;
- $T = 250^{\circ}\text{C}$ ;
- $P = 4.70 \text{ psi}$ ;
- Total flow rate: 29 *mL/min*;

4. **Oven:** Programmed mode (Oven Ramp)

- $T_{oven}(PnB + DPM)$  : 100°C during 2 *min* → heating up to 120°C ( $\Delta = 10^{\circ}\text{C/min}$ ) → 120°C during 1 *min*;
- $T_{oven}(DPM + DPnB)$  : 100°C during 2 *min* → heating up to 160°C ( $\Delta = 10^{\circ}\text{C/min}$ ) → 160°C during 1 *min*;
- Analysis duration: 5 *min*;
- $T_{max} = 280^{\circ}\text{C}$ ;

5. **Detector:** FID

- $T_{det} : 250^{\circ}\text{C}$ ;
- $H_2$  flow rate: 40 *mL/min*;
- Air flow rate: 400 *mL/min*;

6. **Solvent used to dilute the samples:** High purity methanol

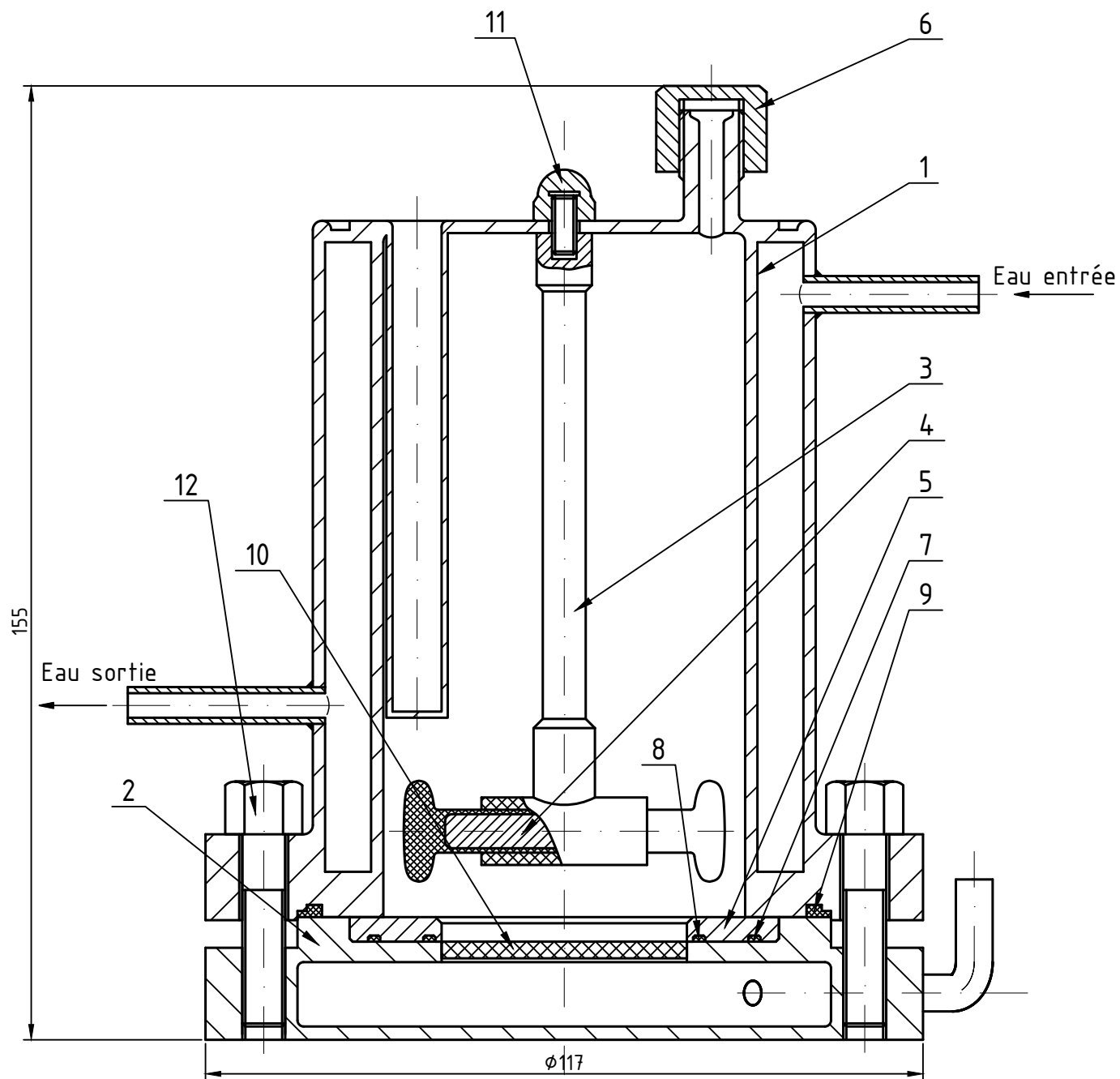




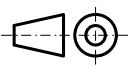
## **Appendix E**

### **Membrane cell used in experiments for the laboratory scale pervaporation**

*See the technical drawing on the next page*



12	6	Vis M7x30		
11	1	Ecrou borgne		
10	1	Support poreux de la membrane		
9	1	Joint d'étanchéité		
8	1	Joint torique $\phi 44$		
7	1	Joint torique $\phi 62$		
6	1	Bouchon		
5	1	Support membrane		
4	1	Agitateur magnetique		
3	1	Axe agitateur		
2	1	Base (partie perméat)		
1	1	Chambre thermostatée		

REP.	NBR.	DESIGNATION	MATIERE	OBS.
Echelle 1:1		M2P2 UMR7340, Centrale Marseille		Nom:
 A4		CELLULE MEMBRANAIRE DE PERVAPORATION		Classe:
Date				00

